University of Texas at El Paso
ScholarWorks@UTEP

Open Access Theses & Dissertations

2015-01-01

Expression And Functional Analysis Of Lipids And Glycolipids From The Mammal-Dwelling Stages Of Trypanosoma Cruzi

Felipe Gazos Lopes
University of Texas at El Paso, fgazos@yahoo.com.br

Follow this and additional works at: https://digitalcommons.utep.edu/open_etd

 Part of the Biochemistry Commons, and the Biology Commons

Recommended Citation

Lopes, Felipe Gazos, "Expression And Functional Analysis Of Lipids And Glycolipids From The Mammal-Dwelling Stages Of Trypanosoma Cruzi" (2015). *Open Access Theses & Dissertations*. 1090.
https://digitalcommons.utep.edu/open_etd/1090

This is brought to you for free and open access by ScholarWorks@UTEP. It has been accepted for inclusion in Open Access Theses & Dissertations by an authorized administrator of ScholarWorks@UTEP. For more information, please contact lweber@utep.edu.

EXPRESSION AND FUNCTIONAL ANALYSIS OF LIPIDS AND GLYCOLIPIDS FROM THE MAMMAL-DWELLING STAGES OF *TRYPANOSOMA CRUZI*

FELIPE GAZOS LOPES

Department of Biological Sciences

APPROVED:

Igor C. Almeida, D.Sc., Chair

Siddhartha Das, Ph.D.

Manuel Miranda-Arango, Ph.D.

Hugues Ouellet, Ph.D.

Katja Michael, Ph.D.

Charles Ambler, Ph.D.

Dean of the Graduate School

Copyright ©

by

Felipe Gazos Lopes

2015

Dedication

I dedicate this dissertation to my wife, Anna Carolina Barbosa

EXPRESSION AND FUNCTIONAL ANALYSIS OF LIPIDS AND GLYCOLIPIDS FROM THE MAMMAL-DWELLING STAGES OF *TRYPANOSOMA CRUZI*

by

FELIPE GAZOS LOPES, M.Sc.

DISSERTATION

Presented to the Faculty of the Graduate School of

The University of Texas at El Paso

in Partial Fulfillment

of the Requirements

for the Degree of

DOCTOR OF PHILOSOPHY

Department of Biological Sciences

THE UNIVERSITY OF TEXAS AT EL PASO

May 2015

ACKNOWLEDGEMENTS

First, I would like to thank my mentor, Dr. Igor Almeida, for all of the support and help he has given me throughout my doctoral studies. I have learned a great deal from him. My committee members Dr.Igor Almeida, Dr.Siddhartha Das, Dr. Katja Michael, Dr. Manuel Miranda-Arango, Dr. German Rosas-Acosta and Dr. Hugues Ouellet have my greatest thanks for their work in making my project one that I have enjoyed pursuing. Special thanks to my wife Anna Carolina Barbosa, my mother Angela Hampshire, my father Ulisses Gazos Lopes, my stepfather Rafael Linden and all of the Hampshire/Carvalho Santos and Gazos Lopes families. Their undying support has had a profound effect on me. The present and former Almeida lab members Ernesto Nakayasu, Alexandre Marques, Luciana Ganiko, Nasim Salloum, Gloria Polanco, Susana Portillo, and Aaron Garcia have been instrumental for my time here at UTEP The Das lab members Tavis Mendez, Trevor Duarte, Atasi De Chatterjee, Christianseoul Salazar, Debashi Roy, and Joaquin De Leon.. Elizabeth Walsh and Renato Aguilera for all of their support helping me achieve my doctoral milestones

Also, I would like to acknowledge NIH-R01 and the RISE program for their financial support.

ABSTRACT

Trypanosoma cruzi is the causative agent of the life-threatening Chagas disease, in which increased platelet aggregation related to myocarditis is observed. Platelet-activating factor (PAF) is a potent intercellular lipid mediator and second messenger that exerts its activity through a PAF-specific receptor (PAFR). Previous data from our group suggested that *T. cruzi* synthesizes a phospholipid with PAF-like activity. The structure of *T. cruzi* PAF-like molecule, however, remains elusive. Here, we have purified and structurally characterized the putative *T. cruzi* PAF-like molecule by electrospray ionization-tandem mass spectrometry (ESI-MS/MS). Our ESI-MS/MS data demonstrated that the *T. cruzi* PAF-like molecule is actually a lysophosphatidylcholine (LPC), namely *sn*-1 C18:1(delta 9)-LPC. Similar to PAF, the platelet-aggregating activity of C18:1-LPC was abrogated by the PAFR antagonist, WEB 2086. Other major LPC species, i.e., C16:0-, C18:0-, and C18:2-LPC, were also characterized in all *T. cruzi* stages. These LPC species, however, failed to induce platelet aggregation. Quantification of *T. cruzi* LPC species by ESI-MS revealed that intracellular amastigote and trypomastigote forms have much higher levels of C18:1-LPC than epimastigote and metacyclic trypomastigote forms. C18:1-LPC was also found to be secreted by the parasite in extracellular vesicles (EV) and an EV-free fraction. A three-dimensional model of PAFR was constructed and a molecular docking study was performed to predict the interactions between the PAFR model and PAF, and each LPC species. Molecular docking data suggested that, contrary to other LPC species analyzed, C18:1-LPC is predicted to interact with the PAFR model in a fashion similar to PAF. Taken together, our data indicate that *T. cruzi* synthesizes a bioactive C18:1-LPC, which aggregates platelets via PAFR. We propose that C18:1-LPC might be an important lipid mediator in the progression of Chagas disease and its biosynthesis could eventually be exploited as a potential target for new therapeutic interventions.

Glycosylphosphatidylinositol (GPI)-anchoring is a protein post-translational modification ubiquitously found in eukaryotes. There is a growing body of evidence showing that protein-free GPIs (or glycoinositolphospholipids, GIPLs) and GPI-anchored proteins (GPI-APs) are involved in host-protozoan interaction processes, such as host-cell adhesion and invasion, and pathogenesis. Here, we used a highly sensitive and unbiased approach that employs liquid chromatography-tandem mass spectrometry (LC-MS^n) for the analysis of the GPIome (GPIomics) of the mammal-dwelling trypomastigote and amastigote stages of *Trypanosoma cruzi*, the causative agent of Chagas disease. This approach allows for the structural characterization of both the lipid and the glycan moieties of GPI-APs and GIPLs. We have identified over 140 GIPL and GPI-AP species from these two parasite forms, most of which had not been described in the literature. In contrast to epimastigote-derived GIPLs (eGIPLs), trypomastigote-derived and amastigote-derived GIPLs (tGIPLs and aGIPLs, respectively) tend to have longer and structurally more diverse glycan moieties. Similar results were observed for trypomastigote-derived and amastigote-derived GPI-APs (tGPI-APs and aGPI-APs, respectively), although tGPI-APs and aGPI-APs tended to be structurally less diverse than their GIPL counterparts. The lipid moieties of tGIPLs are composed mainly of O-alkyl-2-O-acyl-glycerolipids (AAGs), typically with longer fatty acid chains than those of eGIPLs. Conversely, amastigotes tend to have an approximately equal number of GIPLs containing AAG or ceramide moieties. Interestingly, the majority of the lipid moieties of GPI-APs derived from both mammal-dwelling stages of *T. cruzi* contain C18:1- or C18:2- fatty acid substituents. The proteomic analysis of fractions enriched in GPI-APs from the three life-stages of this parasite showed much greater protein diversity in the mammal-dwelling stages than in epimastigotes. The observations made in this study will, hopefully, help us further understand possible structure-function correlations of GPIs and their role during chronic infection.

TABLE OF CONTENTS

LIST OF TABLES

LIST OF FIGURES

1. CHAPTER 1: INTRODUCTION

1.1. Chagas Disease:

Chagas disease (Cd) is one of the major parasitic diseases in the Americas, affecting 8-10 million people worldwide. Cd has a broad spectrum of clinical outcomes, ranging from a complete lack of symptoms to severe disease and, in many cases, death (1-3). The clinical course of the disease includes an acute phase, an indeterminate phase, and a chronic phase. The acute phase is characterized by very high parasitemia and often flu-like symptoms. The indeterminate stage is characterized by a lack of clear manifestations of infection, with patients remaining asymptomatic despite parasite persistence in blood and other tissues. About 20-30% of chronically infected individuals develop cardiovascular disease, which leads to congestive cardiac failure and sudden cardiac death, or develop gastrointestinal (GI) complications, like megacolon or megaesophagus. Some patients may also show both cardiac and GI alterations (1-8). The other 70-80% of these individuals will either remain asymptomatic or develop megaesophagous and/or megacolon syndromes. Both acutely-infected and chronically-infected individuals also commonly exhibit an increase in platelet aggregation, focal ischemia, and myonecrosis (9,10). The damages caused to these individuals during the chronic phase of this disease are irreversible and, in many cases, lead to a lack of productivity (due to patient morbidity) and to premature deaths (usually due to heart disease) (3,11).

In 2006, over 12,500 people died from Cd-related complications, mostly from sudden cardiac arrest (1,2,8). Due to a marked increase in population migration from endemic countries, Cd is becoming a considerable burden to Europe, Australia, Japan, and the USA (4-6). It is estimated that 300,000 individuals infected with *T. cruzi* currently live in the USA, with 30,000-

45,000 of them having developed cardiomyopathy and 315 having already disseminated the disease congenitally (4,5,8).

The etiologic agent of Cd is the protozoan parasite *Trypanosoma cruzi*, which exhibits a complex life-cycle with four distinct developmental stages. These parasites are naturally transmitted by vector insects of the subfamily Triatominae (popularly known as *kissing bugs*), which feed on mammalian blood. Whenever these insects feed on contaminated blood, they ingest non-proliferative, infective bloodstream trypomastigotes, which convert into replicative, noninfective epimastigotes in the vector's midgut. After the blood meal is digested by the vector, the epimastigotes undergo nutritional stress and migrate to the insect's hindgut and transform into non-replicative, infective metacyclic trypomastigote forms. The vector tends to defecate either during or shortly after bloodfeeding, depositing concentrated infective metacyclic forms near the bite wound. These parasites then gain access to the host through injured skin or exposed oral or ocular mucosa, and then proceed to infect any nucleated cell in the body, usually persisting indefinitely in tissues such as the heart and adipose tissue in the form of proliferative intracellular amastigotes. The intracellular amastigotes will multiply in the host-cell cytoplasm, eventually converting into bloodstream trypomastigote forms, which burst out of the host-cells to either infect new surrounding cells or reach the bloodstream to infect other cells in various tissues in the body. Eventually, the cycle is closed when another kissing bug consumes infected blood. *T. cruzi* can also be transmitted orally, congenitally, via blood transfusion, or organ transplantation (**Fig.1**) (1,2,9,12).

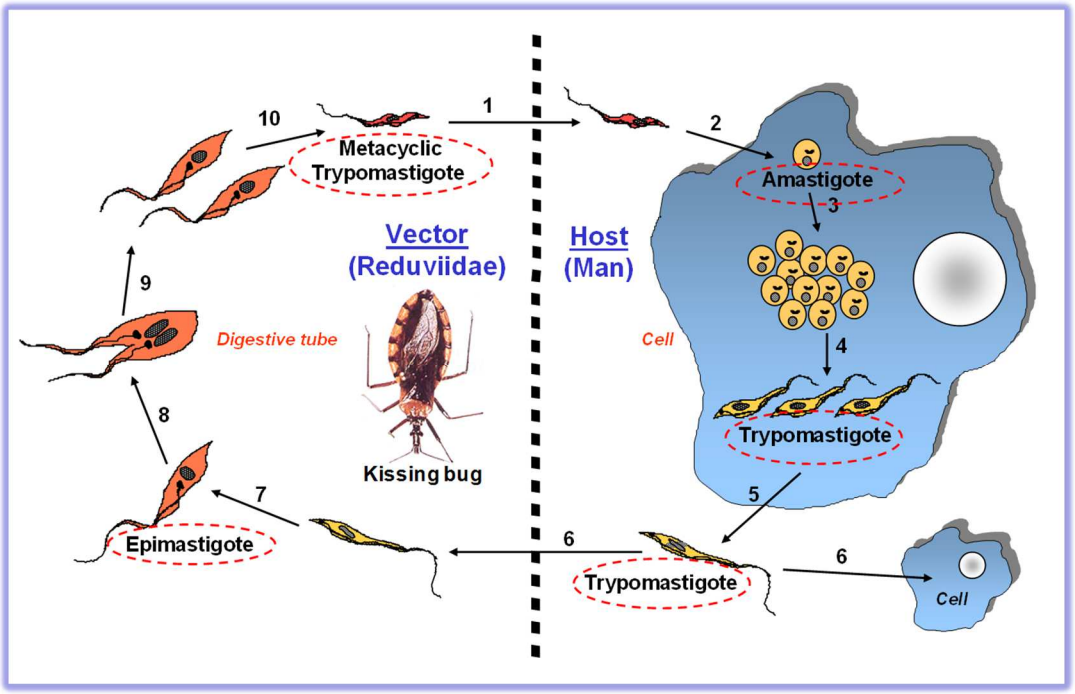

Figure 1.1: The life cycle of *T. cruzi*. **(1)** Metacyclic trypomastigotes **(Metas)** are released with vector droppings shortly after a bloodmeal, where they gain access to the host via injured skin or exposed mucosa. (**2)** Metas quickly infect host cells at the parasite entry site. **(3)** The parasites then transform into the replicative intracellular amastigotes **(ICAs)** form. (**4)** ICAs divide by binary fission in the host-cell cytoplasm and convert into trypomastigote **(TCT)** foms. (**5-6)** TCTs burst out of the host cell and into the bloodstream, where they may either infect new host cells or be ingested by the insect vector during blood-feeding. **(7-8)** Once in the vector digestive tube **TCTs** convert into the replicative epimastigote (**Epi)** forms, which multiply in the insect's midgut. **(9)** As the bloodmeal is digested, Epis will migrate to the vector's hindgut, where they will transform into Metas, continuing the cycle.

Thus far, there are only two drugs (i.e., Nifurtimox and Benznidazole) available for Cd treatment. Both drugs cause moderate to severe side effects (4,7), and neither of them being fully efficacious for patients with chronic Cd (7). Moreover, no vaccines for the prevention and/or treatment of Cd are currently available (1,2). Consequently, there is a great necessity for the development of novel, more efficient therapies for Cd. The **main objective** of this project is to identify and validate potential new molecular targets against *T. cruzi*. To this end, the two molecular parasite targets we will focus in this disseration are **(1) phospholipids**, and **(2) glycosylphosphatidylinositol (GPI)-anchored glycocolipids and glycoproteins**. The rationale for this will be explained in detail in Chapters 2 and 3 of this dissertation.

1.2 Specific aims

Specific aim 1: We aim to better understand the mechanisms behind the increase in platelet aggregation during the acute and chronic stages of Cd.

Platelet-activating factor (PAF) is a potent intercellular lipid mediator and second messenger that exerts its activity through a PAF-specific receptor (PAFR). Previous data from our group suggested that *T. cruzi* synthesizes a phospholipid with PAF-like activity. The structure of *T. cruzi* PAF-like molecule, however, remains elusive. Our **hypothesis** is that *T. cruzi* either synthesizes a bona fide PAF, or a PAF-like molecule, which hadn't been described because of technical limitations involved in the purification and analysis of this type of molecule. Our aim is to purify and characterize the molecule(s) responsible for the PAF-like activity of *T. cruzi* lipid extracts. This aim will be explored in chapter 2 of this dissertation.

Specific aim 2: To carry out the detailed expression GPIomic analysis of the infective mammalian-cell-derived trypomastigote and amastigote forms of *T. cruzi*.

Our laboratory has developed a high-throughput approach for the global analysis of a class of glycolipids known as GPIs, which cover the surface of *T. cruzi* and are required for host-cell infection and modulation of the host imune response against the parasite. This approach (i.e., GPIomics) has only been employed so far for the global analysis of GPIs (GPIome) of the noninfective insect-dwelling (epimastigote) stage of this parasite. Therefore, we plan to apply the same strategy for the analysis of the GPIome of the mammal-dwelling (trypomastigote and amastigote) parasite stages, which are responsible for causing chronic Cd in humans.

Our **hypothesis** is that this method will help us identify new GPI structures and novel GPI biosynthetic pathways that can be exploited for the development of new therapeutic interventions for Cd. This aim will be explored in chapter 3 of this dissertation

The background for each specific aim will be provided in greater detail on the chapter in which that aim is explored.

2. CHAPTER 2: STRUCUTRAL AND FUNCTIONAL ANALYSIS OF A PLATELET-ACTIVATING LYSOPHOSPHATIDYLCHOLINE OF *TRYPANOSOMA CRUZI*

Notice: A significant portion of this chapter was originally published under the same title on the journal "PLoS Neglected Tropical Diseases", 2014 Aug 7;8(8):e3077. doi: 10.1371/journal.pntd.0003077. eCollection 2014. Permission to republish the same content in this chapter was granted by the editors (For more details, please see pages 139-140 of this dissertation).

The original authors of the manuscript are: Felipe Gazos-Lopes, Mauricio M. Oliveira, Lucas V. B. Hoelz, Danielle P. Vieira, Alexandre F. Marques, Ernesto S. Nakayasu, Marta T. Gomes, Nasim G. Salloum, Pedro G. Pascutti, Thaıs Souto-Padron, Robson Q. Monteiro, Angela H. Lopes, Igor C. Almeida.

2.1 Introduction

2.1.1 Lipids: Structure and Function

Lipids comprise of a diverse group of macromolecules, playing several important biological roles, including the formation of the plasma membrane and of subcellular compartments, energy storage, cell signaling, and protein trafficking (13-19). For decades, lipids have been loosely defined as being hydrophobic metabolites that are soluble in solvents, but insoluble in water. This broad definition encompasses several classes of molecules, such as sterols, fatty acids, glycerophospholipids, sphingolipids, isoprenoids, and terpenes, among many

others. Because of the tremendous functional and structural diversity of these molecules, it is not surprising that several different lipid classification schemes have been proposed over the years. In order to avoid ambiguity in the field of lipid biology and other related fields, the International Lipid Classification and Nomenclature Committee (ILCNC) established a revised comprehensive classification and nomenclature system for lipids using well-defined chemical principles. This system was formulated as an expansion of the guidelines established by the International Union of Pure and Applied Chemistry (IUPAC) (20,21). Under this new classification, lipids are defined as "hydrophobic or amphipathic small molecules that may originate entirely or in part by carbanion-based condensations of thioesters and/or by carbocation-based condensation of isoprene units" (20). The new classification system acknowleges 8 lipid categories, namely "Fatty Acyls" (FA), "Glycerolipids" (GL), "Glycerophospholipids" (GP), "Sphingolipids" (SP), "Sterol Lipids" (ST), "Prenol Lipids" (PR), "Saccharolipids" (SL), and "Polyketides" (PK) (**Fig. 2**) (20). We will briefly describe the first six categories on this list, but will not go into detail on the structure and function of SLs and PKs, because to date they have neither been described in mammals or in any trypanosomatid model.

FAs are composed of a saturated or an unsaturated hydrocarbon chain and a terminal carboxyl group. The length of most FAs range from 14 to 26 carbon atoms, and the number of unsaturations found in these molecules usually range from 0 to 6. Derivatives of this basic structure are considered as subclasses within this group. FAs are building blocks to several other lipid categories, such as GLs, GPs, SPs, and cholesterol esters. FAs and their derivatives, such as prostaglandins and leukotrienes, have been described to have important biological activities, such as in inflammation and cell signaling events (22-25).

PRs are synthesized from five-carbon isoprene units (26). These lipids play very diverse biological roles, being precursors to several molecules, such as vitamins A, E and K, and sterols, quinones, and hydroquinones (27-30). Also, PRs and phosphorylated PRs, such as dolichol phosphate, play key roles in the biosynthesis of several classes of glycolipids and glycans, such as glycosylphosphatidylinositols (GPIs) and *N*- and O-glycans, and in the synthesis of the cell walls of several organisms (31-33).

STs consist of cholesterol and its derivatives, as well as other related molecules (usually refered to as "steroids"). They share a four ring core structure, and are important membrane components, helping regulate membrane fluidity (34). They also participate in cell signaling events, play several roles in inflammation, act as hormones, and even play a role in digestion in vertebrates (34-36) .

SPs are a complex family of compounds derived from a sphingoid base, which is a backbone synthesized from the condensation of a serine and a fatty acid-CoA. Of relevance to this dissertation are ceramides (Cers) and inositolphosphoceramides (IPCs), which are *N*-acyl-derivatives of sphingosine. Typically, the amide-linked fatty acids in Cers are saturated or monounsaturated long carbon chains varying in length from 14 to 26 carbon atoms. Their sphingoid backbones usually have 16 to 18 carbons atoms and are either saturated or monounsaturated. IPCs are formed through the addition of a phosphorylinositol headgroup to ceramides via a phosphodiester linkage. These molecules play a plethora of structural and signaling roles, which are beyond the scope of this dissertation (20,37).

GLs mainly include monoacylglycerides (MAGs), diacylglycerides (DAGs), and triacylglycerides (TAGs). These lipids consist of a glycerol backbone to which one or more FAs

may be esterified to its hydroxyl groups (38). Some organisms add fatty alcohols, instead of fatty acids, to the glycerol backbone. TAGs are most commonly known for their role in the storage of cellular energy and from being the main constituents of anima-derived fat, but it has also been shown that several diseases are associated to changes in their metabolism (39,40).

GPs also have a glycerol backbone, but are distinguished from other GLs because of the presence of a functional polar "head group" esterified to either the *sn*-3 position (Eubacteria and Eukarya) or *sn*-1 position (Archea) via a phosphodiester bond. The other two positions may either have a hydroxyl group or may be modified with either a fatty acid or with a fatty alcohol. Based on the composition of the head group, GPS are usually divided into glycerophosphatidic acids (PA), glycerophosphocholines (PC), glycerophosphoethanolamines (PE), glycerophosphoserines (PS), glycerophosphoglycerols (PG), and glycerophosphoinositols (PI). Whenever only either the *sn*-1 or the *sn*-2 positions are esterified, the lipid is reffered to as a "*lyso*-GP". As an example, a GP with only one fatty acid and a phospocholine head group is reffered to as a "*lyso*-PC". GPs are the main components of cell membranes, and participate in several biological processes, such as cell signaling and molecular trafficking (41-43).

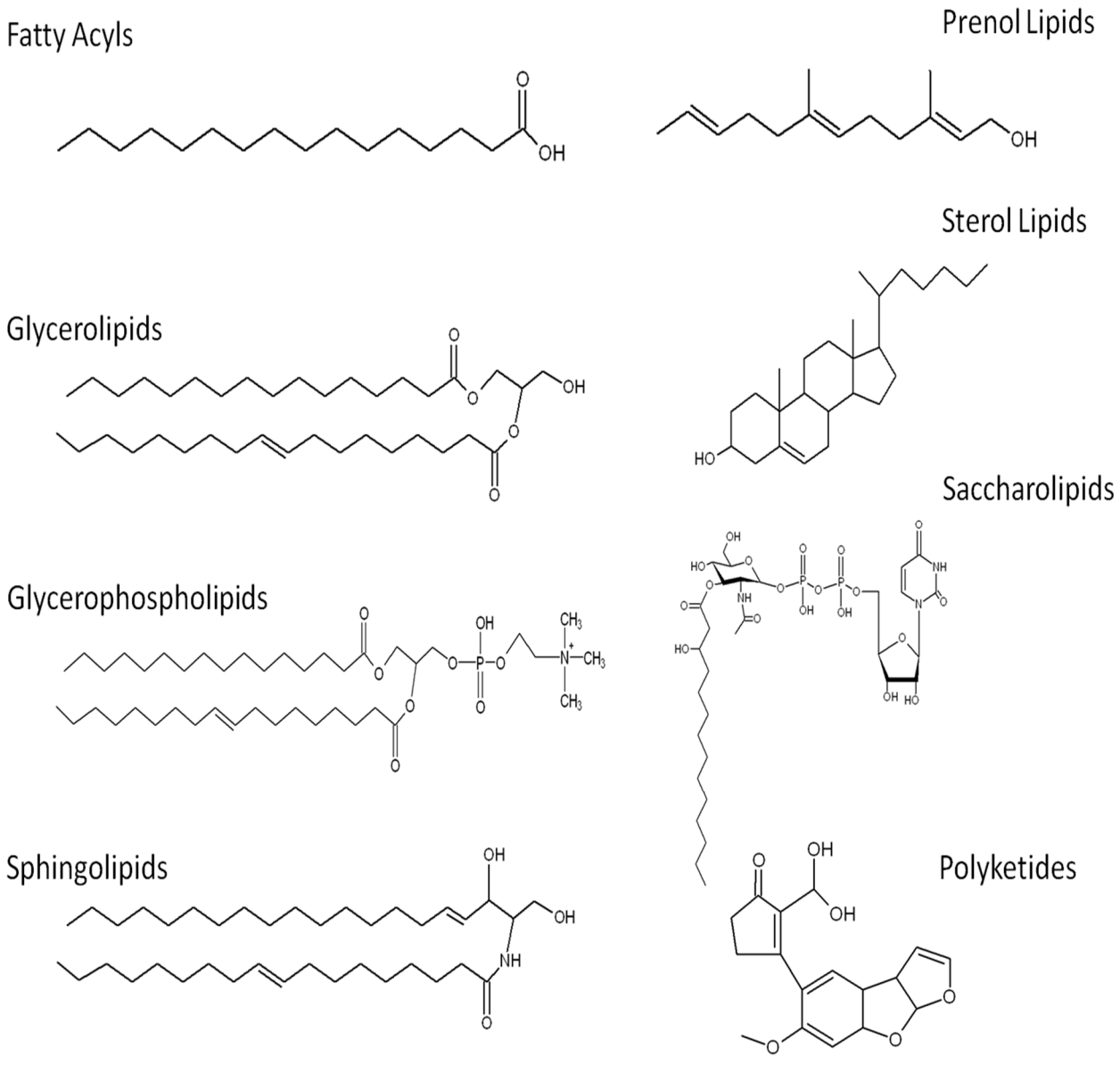

Figure 2: Representative lipids from each of the 8 categories proposed by the new ILCNC system. Figure modified from (20).

2.1.2 - Bioactive lipids in T. cruzi and their role in Chagas disease

In general, lipid mediators (44,45) nd specifically, lysophosphatidylcholine (LPC) (46), have been implicated in experimental models of Cd. LPC is present in the saliva of at least one of the insect vectors of Cd, the hemipteran *Rhodnius prolixus*, where it acts as an anti-hemostatic molecule and immunomodulator of *T. cruzi* infection in a mammalian model ((46), (47), (48)). LPC (1-acyl-2-hydroxy-*sn*-glycero-3-phosphorylcholine) is a major plasma phospholipid of oxidized low-density lipoproteins (Ox-LDL), albumin, and other carrier proteins, being a critical factor in the inflammatory processes and the atherogenic activity of Ox-LDL ((49), (50), (51)). LPC is an intracellular modulator that activates several second messengers, controlling important biological activities, such as cellular proliferation and differentiation, transcription of adhesion molecules and growth factors in endothelial cells, and transportation of fatty acids, choline, and phosphatidylglycerol between tissues (49), (50), (51), (52), (53). The biological activities of LPC are usually mediated by G protein-coupled receptors (GPCRs), such as G2A, GPR4, and the receptors for prostacyclin (IP), thromboxane A2 (TXA2) (TP), and platelet-activating factor (PAF) (PAFR) ((53), (54), (55), (56), (57), (58), (59), (60), (61), (62)). Specifically, LPC species are capable of eliciting different cellular activities depending on the length and degree of unsaturation of its sole acyl-chain ((59), (63), (64)). Trypanosomatid parasites (e.g., *T. brucei*, *Leishmania* spp., and *T. cruzi*) are known to synthesize phosphatidylcholine (PC) and LPC. Over 50% of the total lipids shed to the culture medium by *T. cruzi* were identified as PC and LPC (65). These molecules were also found in *Leishmania* ((66), (67)), African trypanosomes ((68)), and in the malaria parasite, *Plasmodium falciparum* ((69)). To the best of our knowledge, however, the chemical structures of LPC species synthesized by *T. cruzi* have not been defined to date.

Platelet-activating factor (1-*O*-alkyl-2-acetyl-*sn*-glycero-3-phosphocholine; PAF) is structurally very similar to LPC ((70)). PAF exhibits potent biological activity and is synthesized by a wide variety of cells, including neutrophils, platelets, macrophages, and lymphocytes ((71)). PAF induces numerous physiological and pathophysiological effects, such as cellular differentiation, inflammation, and allergy, through the activation of specific GPCRs with seven transmembrane helices ((54), (72)). We have previously shown that *T. cruzi* synthesizes a lipid with platelet-aggregating properties similar to PAF ((73)). Preliminary structural analysis by chemical and enzymatic treatment indicated that the *T. cruzi* PAF-like lipid, metabolically labeled with ^{14}C-acetate, was labile to mild-alkaline or hydrofluoric acid hydrolysis, suggesting a molecule containing a glycerolipid moiety with at least one acyl chain and a phosphate group ((73)). However, the detailed structure of the *T. cruzi* PAF-like lipid remains elusive.

Here, we describe the identification and bioactivity of the as-yet elusive *T. cruzi* PAF-like molecule. We use a novel approach for the enrichment of this and other closely related lysophospholipids, followed by tandem mass spectrometry (MS^n) to provide ample structural information. Moreover, we constructed a 3-D molecular model of PAFR and used molecular docking to predict the interactions of the *T. cruzi* PAF-like molecule and other lysophospholipids with this receptor.

2.2 Materials and Methods

2.2.1 - Ethics statement Heading

Rabbit platelets used in this study were obtained following the guidelines of the Committee for Evaluation of Animal Use for Research of the Federal University of Rio de Janeiro (CAUAP-UFRJ) and the NIH Guide for the Care and Use of Laboratory Animals. The vertebrate animal protocol was approved by CAUAP-UFRJ under registry number IBQM011.

2.2.2 Chemicals

Synthetic C16:0-, C18:0-, C18:1(Δ^9)-, and C22:6-LPC, and C16:0-PAF were purchased from Avanti Polar Lipids (Alabaster, AL). The competitive PAF antagonist WEB 2086 (4-[3-[4-(2-chlorophenyl)-9-methyl-6h-thieno[3,2-f] ((74),(10),(75)) triazolo[4,3-a]diazepin-2-yl]-1-oxopropyl]morpholine) was kindly provided by Dr. H. Heurer from Boehringer Ingelheim (Ingelheim, Germany). Otherwise indicated, all other reagents and solvents used here were of analytical, HPLC, or mass spectrometric grade from Sigma-Aldrich (St. Louis, MO).

2.2.3 *Trypanosoma cruzi* culture

All *T. cruzi* life cycle stages or forms were obtained from the Y strain ((76)). Epimastigote forms (Epis) were maintained by weekly transfers using liver infusion tryptose (LIT) medium ((77)), supplemented with 0.002% hemin and 10% heat-inactivated fetal calf serum (FCS; Hyclone, heat-inactivated at 56°C for 30 min) at 28°C. Metacyclic trypomastigote forms (Metas) were obtained by spontaneous axenic differentiation of Epis at 28°C, followed by their purification using ion-exchange chromatography ((78), (79)). Mammalian tissue culture-derived trypomastigotes (TCTs) were obtained from the supernatants of 5 to 6 days old *T. cruzi*-

infected LLC-MK2 cells (American Type Culture Collection, Rockville, MD), maintained in RPMI-1640 medium supplemented with 2% FCS at 37°C in a 5% humidified CO_2 atmosphere ((80)). Intracellular amastigotes (ICAs) were obtained as described ((81)). Briefly, infected monolayers of LLC-MK2 cells were gently detached by scraping (BD Falcon cell scraper, BD Biosciences) and resuspended in PBS supplemented with 10% FCS. Mammalian cells were disrupted by passage through a 27-gauge needle (BD, Becton and Dickinson & Co.). ICA forms were separated from the cell debris by centrifugation (800× *g* for 5 min at 4°C). The supernatant was then harvested and passed through a DE-52 column and parasites were incubated for 2 h at 37°C in a humidified 5% CO_2 atmosphere, after which the parasites were again passed through a DE-52 column, from which they were harvested and stored. For the viability testing of all parasite forms, cells were resuspended in a Trypan Blue solution and counted in a Neubauer chamber ((82)). In this study, all experiments were performed using parasites that were harvested by centrifugation and washed three times with PBS before use, unless otherwise specified. All parasite forms were counted and then frozen in liquid nitrogen prior to use.

2.2.4 Lipid extraction

Frozen pellets derived from Epis, Metas, ICAs, and TCTs (2×10^9 cells each), were suspended in 1.6-ml ice-cold HPLC-grade water and transferred to 13×100-mm Pyrex culture tubes with polytetrafluoroethylene (PTFE)-lined screw caps. HPLC-grade chloroform and methanol were added to each vial, giving a final ratio of chloroform/methanol/water (C/M/W) of 1:2:0.8 (v/v/v). The samples were mixed vigorously using a vortex for 2 min and then centrifuged for 15 min at 1,800× *g* at room temperature. After centrifugation, the supernatants were transferred to PTFE-lined Pyrex glass test tubes and the pellets were dried under a constant

flow of N_2 stream. The dry pellets were then extracted three times with C/M (2:1, v/v) and twice with C/M/W (1:2:0.8, v/v/v). After extraction, the supernatants were pooled together and dried before being subjected to Folch's partition ((83,84)). To this end, samples were first dissolved in C/M/W (4:2:1.5, v/v/v) and then mixed vigorously for 5 min using a vortex and finally centrifuged for 15 min at 1,800× *g* at room temperature. After centrifugation, the lower (organic) and upper (aqueous) phases were separated in PTFE-lined Pyrex glass test tubes. The Folch lower phase was then washed two times with a freshly prepared upper phase, dried under N_2 steam, and stored at −70°C until use.

2.2.5 Solid-phase extraction (SPE) of phospholipids

Phospholipids derived from the lower phase of the Folch's partition, as described above, were purified from other classes of lipids using a three-step SPE protocol ((85)). Briefly, 100 mg silica gel (Merck, grade 7754, high purity, 70–230 mesh, 60 Å) were packed into borosilicate glass Pasteur pipettes (5 ¾″, Fisher Scientific) using Pyrex glass fiber wool (8-µm pore size, Sigma-Aldrich) as a sieve. The column was sequentially conditioned with 4 ml each methanol, acetone, and chloroform. Dried Folch lower phase samples from all *T. cruzi* life stages were redisolved in 3 ml chloroform and a third of each sample was added to the column. Lipids were sequentially eluted with 4 ml chloroform (neutral lipids), acetone (glycolipids), and methanol (phospholipids and free fatty acids). Each fraction was collected into a 7-ml amber glass vial with PTFE-lined screw top (SUPELCO, Sigma-Aldrich). All samples were immediately dried under a constant flow of N_2 stream and stored at −70°C until use.

2.2.6 *T. cruzi* PAF-like phospholipid enrichment

With the purpose of enriching the putative PAF-like molecule from a complex *T. cruzi* phospholipid mixture, a novel method was developed using perfusion chromatography ((86)). Briefly, fifty microliters of a suspension of 40 mg/ml POROS R1 50 (poly[styrene/divinylbenzene], with similar binding strength as C4 supports) beads (Applied Biosystems, 50-µm diameter) in HPLC-grade n-propanol (Honeywell, Burdick & Jackson, Radnor, PA) were packed into a 200-µl sterile micropipette tip (Axygen, Corning Life Sciences, Union City, CA). Pyrex glass fiber wool (8-µm pore size, Sigma-Aldrich) was used as sieve. The POROS R1 mini-column was washed twice with 100 µl HPLC-grade methanol and then conditioned with an n-propanol/water gradient (from 50% to 0%, in 5% increments). Each step of the gradient was performed with 100 µl solvent, with the exception of the last step (0% n-propanol), which was performed twice with 100 µl HPLC-grade water. Then, either the mixture of lipid standards (100 pmol C16:0-*lyso*-PC (C16:0-LPC), C16:0-*lyso*-PAF (C16:0-LPAF), C16:0-PAF, and C18:0/C18:1-diacyl-PC) or *T. cruzi* phospholipids derived from the SPE procedure were suspended in HPLC-grade water, sonicated for 10 min in a bath sonicator, and added to the column. Both the standards and the phospholipid extracts were eluted using a 0%–50% *n*-propanol gradient in 5% *n*-propanol increments. Each fraction was stored in Axygen 2-ml microcentrifuge tube at −70°C until further use.

2.2.7 Structural characterization of LPC species by tandem electrospray ionization-linear ion trap-mass spectrometry (ESI-LIT-MS)

All fractions derived from the POROS R1 mini-column purification, as well as the fractions obtained prior to this last procedure (namely, the lower Folch and methanol phase),

were dissolved in MS-grade methanol containing 5 mM LiOH, as indicated. Samples were directly injected (at 300 nl/min) by chip-based infusion using a TriVersa NanoMate nanoelectrospray source (Advion, Ithaca, NY), into an LTQXL ESI-linear ion trap-MS (ESI-LIT-MS) (Thermo Fisher Scientific), in positive-ion mode. The source voltage was set at 0.01 kV and current at 0.03 μA; capillary voltage and temperature were 36 V and 150°C, respectively; and tube lens voltage was set at 145 V. Select ions were subjected to sequential tandem fragmentation (MS^n) by collision-induced dissociation (CID). Full-scan (MS) spectra were collected at the 400–1000 *m/z* range. Tandem mass fragmentation was carried out using normalized collision energies of 35, 40, and 45 for MS^2, MS^3, and MS^4, respectively. The resulting spectra were compared to the aforementioned phospholipid standards, as well as to previously described results.

The location of the acyl chain on *T. cruzi* LPC species was determined by MS^2 and M^3 analysis, essentially as described by Hsu et al. ((87)). Briefly, *sn*-1 and *sn*-2 C18:1-LPC regioisomer standards were generated by treatment of 18:1(Δ9-*cis*)-PC (1,2-dioleoyl-*sn*-glycero-3-phosphocholine, catalog # 850375, Avanti Polar Lipids) with either PLA2 (from porcine pancreas, catalog # P6534, Sigma-Aldrich) or PLA1 (from *Thermomyces lanuginosus*, catalog # L3295, Sigma-Aldrich). For PLA1 treatment, one mg of diacyl-PC standards were dried under N2 stream, redisolved in 200 μL of reaction buffer (50 mM Tris-HCl, 2 mM $CaCl_2$, 140 mM NaCl, pH 8.0) and sonicated for 30 min. Afterwards, the samples were incubated at 37°C for 2 h in the presence of 12 units PLA1. The reaction was interrupted by the addition of 1.5 mL chloroform, followed by vortexing for 1 min. The resulting LPC species present in the organic phase of the mixtures were then purified by SPE, following the protocol described above. Finally, LPCs were recovered in the methanolic phase of the SPE column. PLA2 treatment was

performed following the same procedure steps used for PLA1 treatment but using a different reaction buffer (100 mM Tris-HCl, 5 mM $CaCl_2$, 100 mM NaCl, pH 8.0) and 5 units PLA2 ((88)). The purified lipids (methanolic phase of the SPE) were analyzed by ESI-LIT-MS in 100% methanol containing 5 mM LiOH or 5 mM NaCl. The MS analyses were performed as described above. The assignment of the fatty acid position on the LPC (*sn*-1 or *sn*-2) was performed by comparing the fragmentation pattern of standard *sn*-1 and *sn*-2 C18:1-LPCs with *T. cruzi*-derived 18:1-LPC samples.

The position of the double bond on fatty acid substituents was determined by MS4, essentially as described by Hsu et al. ((89)). Briefly, *sn*-1 C18:1(Δ6-*cis*)-LPC and sn-1 C18:1(Δ9-*cis*)-LPC standards were generated by treatment of both 18:1(Δ6-*cis*)-PC (1,2-dipetroselenoyl-*sn*-glycero-3-phosphocholine, catalog # 850374, Avanti Polar Lipids) and 18:1(Δ9-*cis*)-PC (1,2-dioleoyl-*sn*-glycero-3-phosphocholine, catalog # 850375, Avanti Polar Lipids) with PLA2 (from porcine pancreas, catalog # P6534, Sigma-Aldrich), as described above. LPC species were recovered from incubation mixtures and analyzed by ESI-LIT-MS in 100% methanol containing 5 mM LiOH, as described above.

2.2.8 Quantification of *T. cruzi* LPC species

Commercial C10:0-LPC (1-decanoyl-2-hydroxy-*sn*-glycero-3-phosphocholine, catalog # 855375, Avanti Polar Lipids) was used as an internal standard to quantify the most abundant LPC species found in *T. cruzi* samples. Briefly, 18 nmoles of standard C10:0-LPC were added to parasite pellets (7×10^8 cells) shortly before lipid extraction. Lipid extraction was conducted on freshly prepared parasite pellets following the protocol described above. Then, the Folch lower-phase fractions were analyzed by ESI-MS (at the 400–1000 *m/z* range) under the identical MS

conditions used for the characterization of *T. cruzi* LPCs. The amount of each LPC species was calculated using the formula: [*T. cruzi* LPC peak intensity/C10:0-LPC peak intensity]×[concentration of C10:0-LPC (18 pmol/µl)/MRRF], where, MRRF stands for the molar relative response factor of each LPC species to the C10:0-LPC standard. The MRRF was calculated by dividing the intensity of the peak corresponding to a standard LPC (C16:0-LPC, C18:0-LPC, or C18:1-LPC) by the intensity of the peak corresponding to C10:0-LPC (*m/z* 418.5), when all molecules were in equimolar concentrations.

T. cruzi LPC species were also quantified in extracellular vesicles (EV) and EV-free supernatant or conditioned medium (VF) of Epis (eV2, eV16, and eVF) and Metas (mV2, mV16, and mVF), obtained from Epi and Meta pellets (9×10^9 parasites each), as previously described ((90)). C10:0-LPC (*m/z* 418) (18 nmoles per sample) was used as an internal standard. LPC species were extracted from Epi- and Meta-derived EVs, and respective total parasite pellets (ePellet and mPellet) as described above. The Folch lower phase fractions were analyzed by ESI-LIT-MS as above.

2.2.9 Platelet aggregation assay

C16:0-PAF and various synthetic (C16:0-, C18:0-, C18:1-, and C22:6-LPC) or purified (C18:2-LPC) LPC species were tested in a platelet aggregation assay ((91)). Rabbit blood platelets were prepared from blood collected with 5 mM EDTA as anticoagulant, isolated by centrifugation, washed and resuspended in a modified Tyrode's buffer, pH 7.4, containing 2 mM $CaCl_2$, at a final concentration of $3–4\times10^5$ cells/µl in Tyrode's buffer. Platelet aggregation experiments were performed with a Chronolog Aggregometer (Havertown, PA, USA), with monitoring time of 5 min. Rabbit platelets used in this investigation were obtained following the

guidelines for animal experimentation of the USA National Institutes of Health and the experimental protocol received official approval of the Institutional Animal Care and Use Committee, Universidade Federal do Rio de Janeiro.

2.2.10 Comparative modeling

The amino acid sequence of the human PAF receptor (PAFR, UniProtKB ID: P25105) was obtained from ExPASy server ((92)). The region between Asp10-Ser310, part of PAFR sequence that includes all seven-transmembrane domains, was submitted to I-TASSER server, which combines threading and *ab initio* algorithms ((93), (94)). The I-TASSER server, ranked as the best server in recent CASP7 and CASP8 experiments, builds protein models based on multiple-threading alignments by LOMETS program and iterative TASSER program simulations ((95), (94)). In addition, MODELLER v9.10 program ((96), (97)) (http://salilab.org/modeller/) was used to add a disulfide bridge between Cys90-Cys173 and, subsequently, to refine the best I-TASSER model. Thus, the final model was validated using three programs: PROCHECK ((98)) and ERRAT ((99)) both at SAVES server (http://nihserver.mbi.ucla.edu/SAVES_3/) and PROQM ((100)) (available as a server at http://www.bioinfo.ifm.liu.se/services/ProQM/index.php?about=proqm). PROCHECK analyzes the stereochemical quality and ERRAT evaluates the non-bonded atomic interactions in the model structure, while PROQM uses a specific-scoring function for membrane protein, including GPCR, to assess local and global structural quality of the model.

2.2.11 Molecular docking

The ligand structures (C16:0-PAF, C16:0-LPC, C18:0-LPC, C18:1-LPC, and C18:2-LPC) were built in the Spartan'10 software (Wavefunction, Inc., Irvine, CA). The docking of the ligands to the PAFR model binding site was performed using Molegro Virtual Docker (MVD) program (CLC bio, Aarhus, Denmark), which uses a heuristic search algorithm that combines differential evolution with a cavity prediction algorithm. The MolDock scoring function used is based on a modified piecewise linear potential (PLP) with new hydrogen bonding and electrostatic terms included. Full description of the algorithm and its reliability compared to other common docking algorithm has been described ((101)). As no satisfactory cavities were found by cavity prediction algorithm using MVD, His248 (a constituent residue of the binding pocket) was set as center of searching space. The search algorithm MolDock optimizer was used with a minimum of 50 runs and the parameter settings were: population size = 200; maximum iteration = 2000; scaling factor = 0.50; offspring scheme = scheme 1; termination scheme = variance-based; crossover rate = 0.90. Due to the stochastic nature of algorithm search, ten independent simulations per ligand were performed to predict the binding mode. Consequently, the complexes with the lowest interaction energy were evaluated. The interactions between PAFR and each ligand were analyzed using the ligand map algorithm, a standard algorithm in MVD program. The usual threshold values for hydrogen bonds and steric interactions were used. All figures of PAFR modeling and docking were edited using Visual Molecular Dynamics (VMD) program (available for download at http://www.ks.uiuc.edu/Research/vmd/vmd-1.9.1/).

2.3 Results

2.3.1 Enrichment of LPC and PAF from complex mixtures

Previous results from our group strongly indicated that *T. cruzi* synthesizes a phospholipid with platelet-aggregating activity similar to PAF ((73)) Thus far, however, the precise structure of this bioactive parasite-derived molecule remains unknown. Aiming at the enrichment and characterization of the putative *T. cruzi* PAF-like phospholipid from a complex phospholipid mixture, we developed a fractionation protocol, which included solvent extraction and Folch's partition, followed by SPE and perfusion chromatography (**Fig. 3**). Lipid fractions obtained after each step of purification were analyzed by ESI-LIT-MS in positive-ion mode. Total-ion mapping (TIM) for the neutral loss of the trimethylamine group (= 59 a.m.u.) was performed to promptly localize phosphocholine-containing phospholipids of all life-cycle stages of *T. cruzi* (data not shown). ESI-LIT-MS analysis of the Folch lower phase of the four parasite forms (Epi, Meta, ICA, and TCT) showed major phospholipid species at the 700–900 *m/z* range, except for the ICA form (**Fig. 4A**). Tandem MS (MS^n) analysis of these lipid species revealed that, as expected, they were mostly diacyl-PC and sphingomyelin (SM) species (data not shown, to be published elsewhere). In contrast to other parasite forms, ICA is much richer in lipid species at the 500–600 *m/z* range, particularly *m/z* 526, 528, 530, and 574 (**Fig. 4A**). Noteworthy, lithiated singly-charged ion species ($[M+Li]^+$) of synthetic LPAF, LPC, and PAF standards were found at this range of the spectrum (**Fig. S1**, top spectrum). ESI-LIT-MS analysis of SPE-derived fractions of all *T. cruzi* forms revealed a clear enrichment of phosphocholine-containing lipids at the low *m/z* range (400–600), which would indicate an enrichment of potential LPC, LPAF, or PAF molecules. Nevertheless, most samples still contained high amounts of diacyl-PCs and, possibly, SMs (data not shown). Therefore, a novel protocol using POROS R1 beads

was designed to enrich the putative PAF-like molecule, which as we predicted could have a structure similar to PAF, LPAF, or LPC. First, we tested the POROS R1 mini-column with a complex mixture of phospholipid standards containing LPAF, LPC, PAF, and diacyl-PCs. We were able to obtain highly enriched LPAF, LPC, and PAF species in the 20% and 25% n-propanol fractions (**Fig. S1**). Identical conditions were applied for further fractionation of the phospholipids present in the SPE methanolic fraction of all *T. cruzi* forms. The 25%-n-propanol fractions from these parasite stages were then compared by positive-ion mode ESI-LIT-MS, using the same concentration of cells (4×10^5/μl) and flow rate (300 nl/min) (**Fig. 4B**). The ion species at the 700–900 *m/z* range, corresponding to diacyl-PCs and SMs, were noticeably much less abundant in the 25%-*n*-propanol POROS R1 fraction (**Fig. 4B**) than in the Folch lower phase and SPE methanolic fractions (**Fig. 4A** and data not shown), which is in agreement with the observed phospholipid standard results (**Fig. S1**). In contrast, the ion species at the 400–600 *m/z* range were prominently more abundant in the 25%-*n*-propanol POROS R1 fraction than in lower Folch and SPE methanolic fractions (**Fig. 4A, B** and data not shown). In particular, the ion species at *m/z* 526 and 528 were remarkably abundant in the infective TCT form and in the noninfective ICA form. Tandem MS was then performed for the elucidation of the molecular structures of all phosphocholine-containing lysophospholipids at the 400–600 *m/z* range.

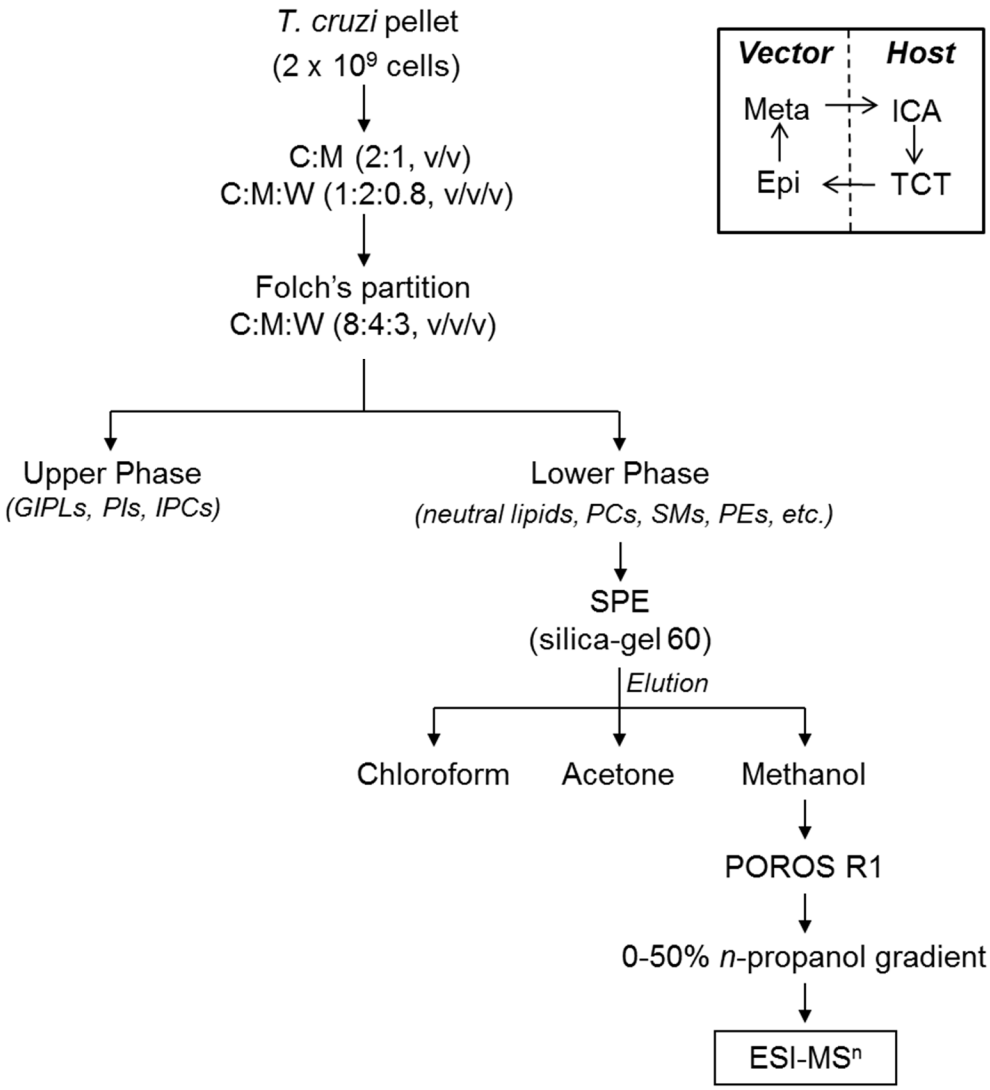

Figure 3: Schematic representation of the methodology used for the enrichment and analysis of the putative T. cruzi PAF-like phospholipid. The total lipid content of the pellets from *T. cruzi* epimastigote (Epi), metacyclic trypomastigote (Meta), tissue culture-derived trypomastigote (TCT), or intracellular amastigote (ICA) forms was extracted with organic solvents followed by Foch's partition. Folch lower-phase samples were fractionated by SPE in a silica gel (60 A˚) column. The different lipid classes were eluted with chloroform (neutral lipids), acetone (glycolipids), and methanol (phospholipids). The latter was further fractionated by perfusion chromatography using POROS R1 50 mini-columns, eluted with a 0%–50% n-propanol gradient. All fractions were diluted in methanol containing 5 mM LiOH and analyzed by MSn. The inset depicts the *T. cruzi* life cycle with the four stages used in this study. Picture taken from Gazos-Lopes et al, 2015, *PLoS neglected tropical diseases* **8**, e3077

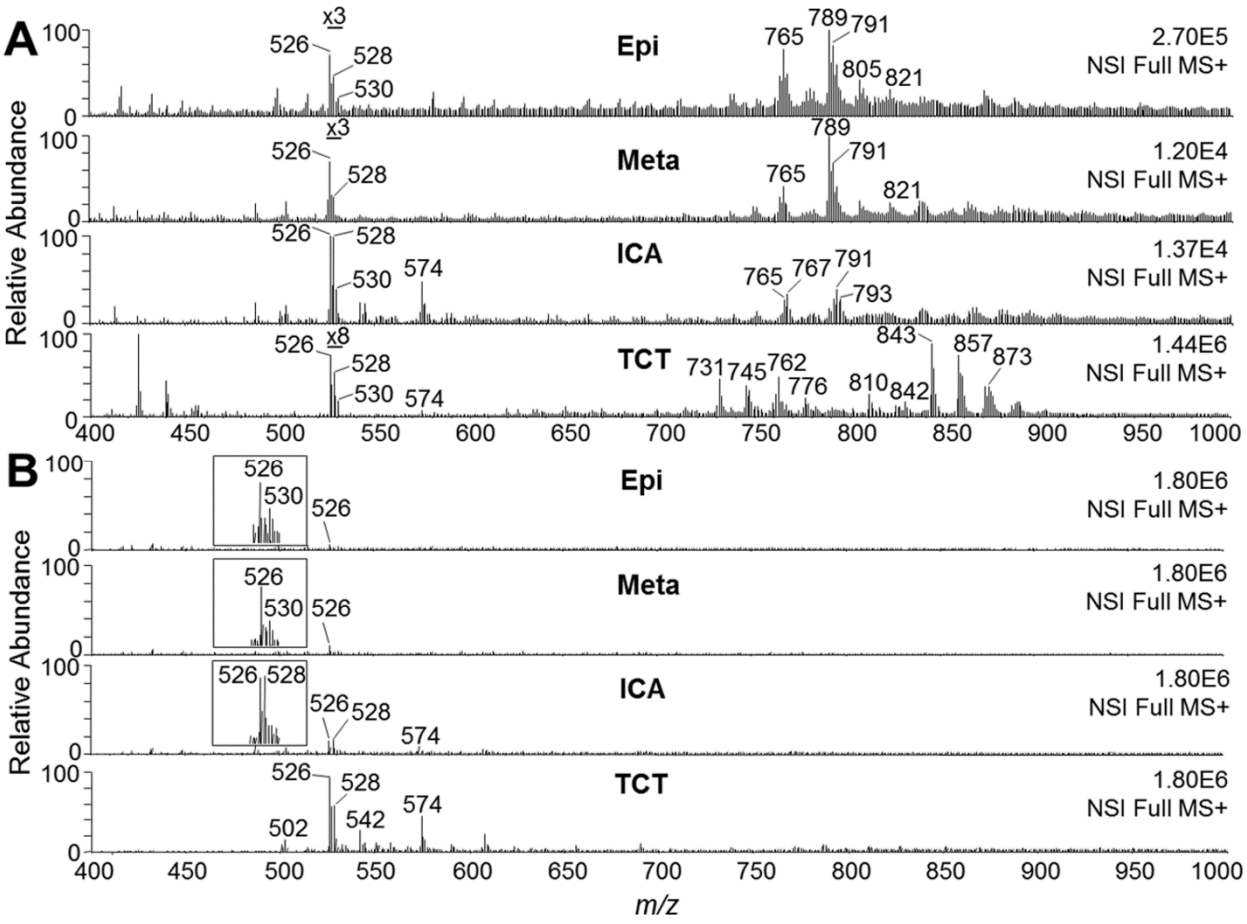

Figure 4: Full ESI-LIT-MS spectra of *T. cruzi* phospholipids.(**A**) MS1 spectra of lipids obtained in the Folch lower phase prior to fractionation. Lipid samples from all *T. cruzi* stages were diluted in methanol containing 5 mM LiOH and analyzed by direct infusion in an LTQXL ESI-LIT-MS (positive-ion mode, MS+). Note that the region of spectrum corresponding to LPAF, LPC, and PAF species in Epi, Meta, and TCT has been magnified for better visualization. (**B**) MS1 spectra of phospholipids obtained by SPE followed by POROS R1 fractionation. Lipids eluted in 25% n-propanol were diluted in methanol containing 5 mM LiOH and analyzed as above. Since the same initial total number of cells (5×10^8) was used for lipid fractionation from each parasite stage, all spectra were normalized. Magnification of the MS range where PAF and LPC species would be found is indicated (insets). Epi, epimastigote; Meta, metacyclic trypomastigote; ICA, intracellular amastigote; TCT, tissue culture-derived trypomastigote.*m/z*, mass to charge ratio. Picture taken from Gazos-Lopes et al, 2015, *PLoS neglected tropical diseases* **8**, e3077.

2.3.2 Structural characterization and quantification of *T. cruzi* lysophospholipid species by tandem MS

The fragmentation pattern of the synthetic C16:0-PAF standard (*m/z* 530) was compared to those of synthetic C18:0- and C18:1-LPC standards (*m/z* 530 and 528, respectively), because certain PAF and LPC species may be isobaric. The assignment of the lysophospholipid species found in the 25%-*n*-propanol POROS R1 fraction of all *T. cruzi* forms was based on the fragmentation pattern of these standards, as well as on previously reported results ((70), (87), (89)). Tandem MS (MS^2) analysis of singly-charged, lithiated C16:0-PAF, C18:0-LPC, and C18:1-LPC ion species gave rise to fragment ions at *m/z* 471, 471, and 469, respectively, corresponding to the neutral loss of 59 a.m.u. (= trimethylamine group). The fragmentation of 16:0-PAF standard, however, also gave rise to a fragment ion at *m/z* 341, consistent with the neutral loss of the whole phosphocholine headgroup along with the lithium adduct (−189 a.m.u.). This fragment could not be detected on either LPC standards (**Fig. S2A**). MS^3Fragmentation of the major ions obtained by MS^2 of C16:0-PAF, C18:0-LPC, and C18:1-LPC (i.e., *m/z* 471, 471, and 469), gave rise to the major non-lithiated ion fragments at *m/z* 341, 341, and 339, respectively, corresponding to the loss of 130 a.m.u. (= ethyl phosphate group+Li) (**Fig. S2B**). In addition, we observed lithiated ion fragments at *m/z* 347, 347, and 345, corresponding to the loss of 124 a.m.u. (= ethyl phosphate group), for C16:0-PAF, C18:0-LPC, and C18:1-LPC, respectively. Interestingly, C18:0-LPC and C18:1-LPC also gave rise to two fragment ions (*m/z* 291 and 289, respectively) that could not be detected in the C16:0-PAF standard. These fragment ions corresponded to the lithiated ($[R_1CO_2H+Li]^+$) stearoyl (*m*/z 291) and oleyl chains (*m*/z 289), after the loss of choline ($N^+(CH_3)_3(CH_2)_2OH$) from the precursor ions *m/z* 427 and

425, respectively (**Fig. S2B**) ((87)). Finally, we carried out MS^4 analysis of the major fragment ion species obtained by MS^3 of C16:0-PAF, C18:0-LPC, and C18:1-LPC standards (*m/z* 341, 341, and 339, respectively) (**Fig. 5**). A complex fragmentation pattern that provided ample structural information for all three standards was observed. In these spectra, it was possible to identify fragment ions generated by the loss of the acetyl group at the *sn*-2 position of C16:0-PAF (*m/z* 281 and 263), and a fragment ion corresponding to the protonated C16:0-alkyl chain (R_1^+) (*m/z* 225). Moreover, a series of fragments resulting from the loss of methylene groups (= 14 a.m.u.) from the PAF C16:0-alkyl chain could also be seen below *m/z* 225. Similar information could be obtained from the C18:0-LPC and C18:1-LPC, where fragment ions derived from the protonated stearoyl (*m/z* 285, 267, and 249) and oleyl (*m/z* 265 and 247) acyl chains at the *sn*-1 position could be identified ((87)). In both cases, a series of fragments corresponding to the loss of methylene units could also be seen below *m/z* 240 (**Fig. 5**). Based on the fragmentation pattern of the standards in MS^2, MS^3, and MS^4, we could assign the different lysophospholipid species of *T. cruzi* enriched in the POROS R1 25%-n-propanol fraction. As observed in **Figs. 5, and S2A,B**, the parent ions at *m/z* 526, 528, and 530 corresponded to C18:2-LPC, C18:1-LPC, and C18:0-LPC, respectively. The lithiated ($[R_1CO_2H+Li]^+$), non-lithiated ($[R_1CO^+]^+$, and dehydrated $[R_1CO^+ - H_2O]^+$) fragment ions of linoleyl (*m*/z 287, 263, and 245), oleyl (*m*/z 289, 265, and 247), and stearoyl (*m*/z 291, 285, 267, and 249) chains, respectively, corroborated our assignments of *T. cruzi* (Tc) *m/z* 526, 528, and 530 as C18:2-, C18:1, and C18:0-LPC (**Figs. 5, and S2A,B**). No detectable traces of C16:0-PAF (isobaric to C18:0 LPC) or any other PAF-like species could be found. The structure and the fragmentation pattern of C16:0-PAF and the major *T. cruzi* LPC species are represented in **Fig. 6**.

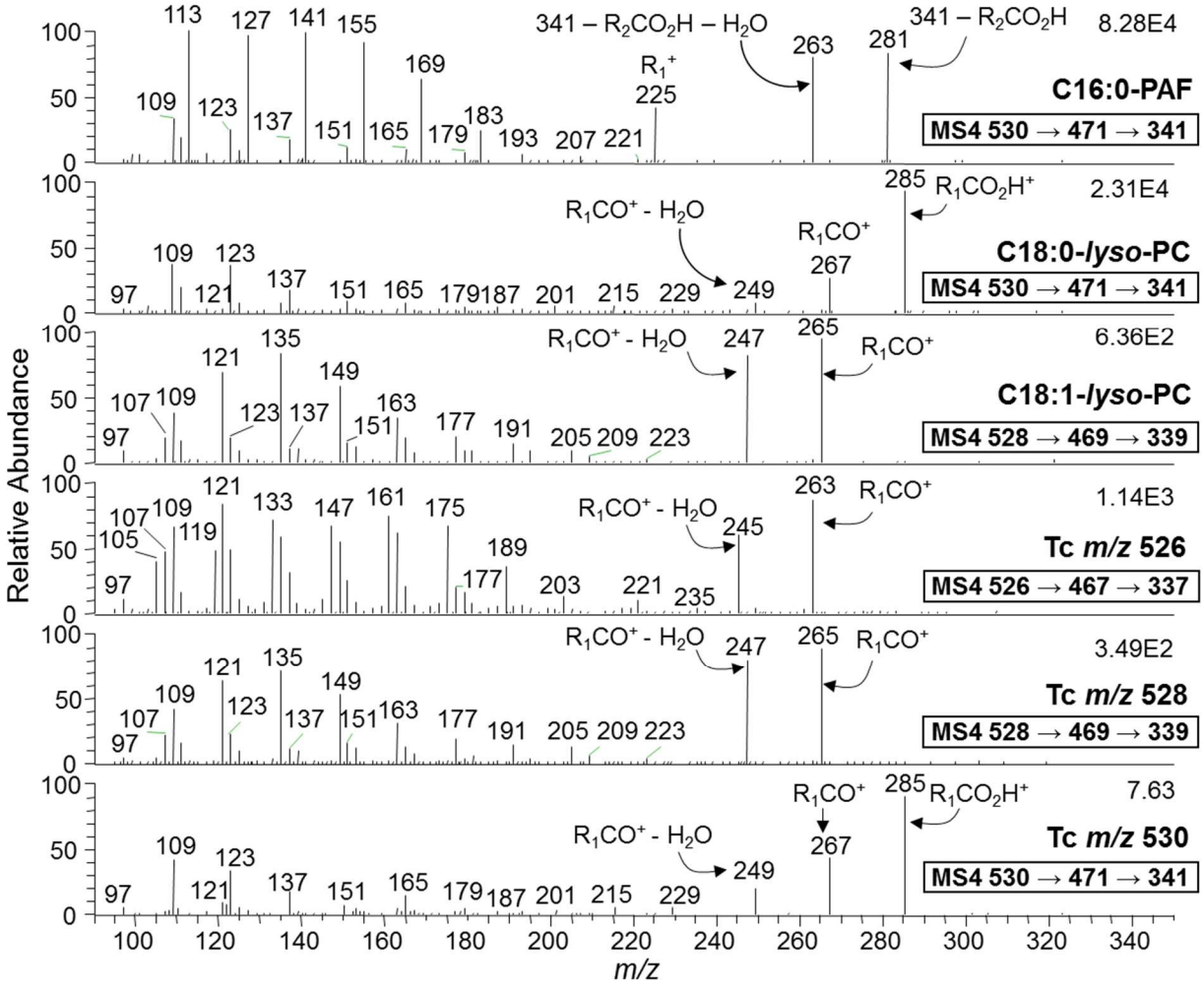

Figure 5: ESI-LIT-MS4 analysis of major *T. cruzi* ion species enriched by POROS R1 fractionation.

Phospholipid standards (C16:0-PAF, C18:0-LPC, and C18:1-LPC) or *T. cruzi* phospholipids from the POROS R1 25% n-propanol fractions were diluted in methanol containing 5 mM LiOH and then infused directly into the LTQXL MS. Fragment ion species resulting from neutral loss of 59 m/z (trimethylamine) from the parent ion at MS2 were selected for MS3 fragmentation (Suppl. Figs. 2A and 2B). Then, ion species resulting from neutral loss of 189 m/z (phosphocholine+Li) from parent ions observed at MS3 were selected for MS4 fragmentation. All spectra shown were obtained from TCT preparation. Identical fragmentation patterns were observed from Epi, Meta, and ICA samples. Picture taken from Gazos-Lopes et al, 2015, *PLoS neglected tropical diseases* **8**, e3077.

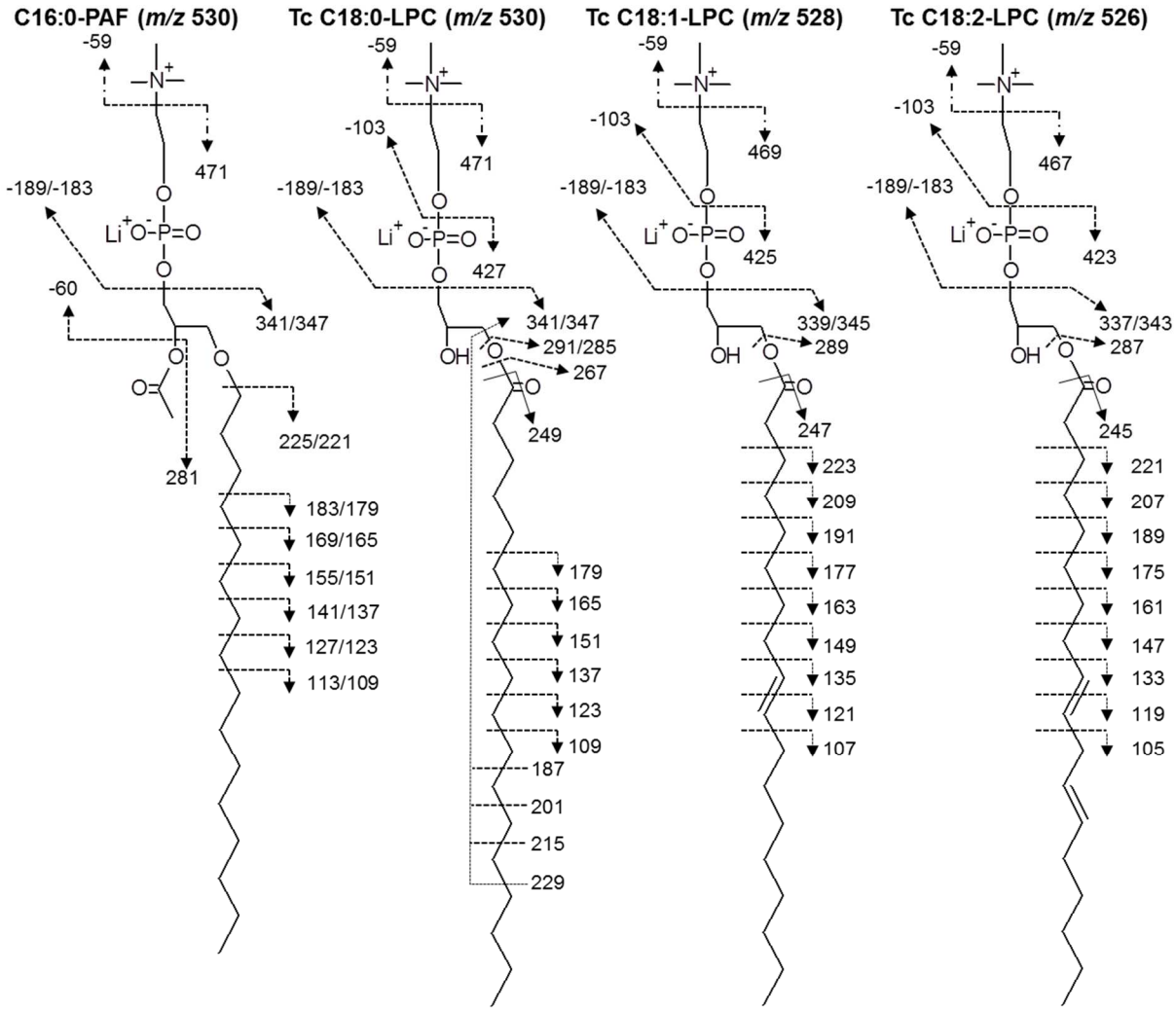

Figure 6: Proposed molecular structures of the three major LPC species of *T. cruzi*.

Fragment ions obtained from the MSn analysis of *T. cruzi* ion species at m/z 530, 528, and 526 are indicated. The tandem fragmentation of C16:0-PAF standard is included as a reference. Picture taken from Gazos-Lopes et al, 2015, *PLoS neglected tropical diseases* **8**, e3077.

The MS^n experiments carried out above, however, could not provide sufficient structural information to determine the position of the fatty acid (*sn*-1 or *sn*-2) and the location of the double bonds on three major LPCs of *T. cruzi*. To address this point, we first generated LPC standards with fatty acids on either the *sn*-1 or *sn*-2 position by treating diacyl-PCs with commercial PLA2 and PLA1, respectively. Following protocols by Hsu et al. ((87)), we were able to determine that the acyl chain in the three major *T. cruzi* LPCs was localized at the *sn*-1 position. In **Figs. S3A,B**, the fragmentation spectra (MS^2 and MS^3) of sodiated and lithiated *sn*-1 C18:1-LPC, *sn*-2 C18:1-LPC, and *T. cruzi* C18:1-LPC (from ICA form) are shown. In agreement with Hsu et al. ((87)), the relative abundance of the sodiated parent ion (*m/z* 544) to the fragment ion (*m/z* 485), corresponding to the loss of trimethylamine (−59 a.m.u), could be used to differentiate between the two possible regioisomers (**Fig. S3A**). Clearly, *T. cruzi* C18:1-LPC showed a fragmentation pattern consistent with an acyl chain located at *sn*-1. This result was corroborated by the fragmentation spectrum of the lithiated *T. cruzi* C18:1-LPC (**Fig. S3B**). In this case, the relative abundance of the fragment ion at *m/z* 425 [M – $N^+(CH_3)_3(CH_2)_2OH+Li^+]^+$ to the ions at *m/z* 339 (M - 189) and *m/z* 345 (M - 183) was used to corroborate the *sn*-1 position of the acyl chain on *T. cruzi* C18:1-LPC. We carried out identical experiments with *T. cruzi* C18:0- and C18:2-LPC and found that both contained the acyl chain at the *sn*-1 position (data not shown).

To address the location of the double bonds in *T. cruzi* C18:1- and C18:2-LPC, we followed the protocols described by Hsu and Turk ((103)). By comparing the MS^4 spectra of Δ^9- and Δ^6-C18:1-LPC standards, we observed noticeably different fragmentation patterns of the acyl chain, especially in the relative abundance of fragment ions $C_{16}H_{31}$ (*m/z* 223), $C_{14}H_{29}$ (*m/z* 197), $C_{14}H_{27}$ (*m/z* 195), $C_{13}H_{27}$ (*m/z* 183), $C_{13}H_{25}$ (*m/z* 181), C_8H_{15} (*m/z* 111), and

C_8H_{13} (*m/z* 109) (**Fig. S3C**). When *T. cruzi* C18:1-LPC (from ICA forms) was analyzed under the same MS conditions, the fragmentation pattern observed was consistent with a Δ^9 double bond (**Fig. S3C**, bottom spectrum). The same type of experiment was conducted with *T. cruzi* C18:2-LPC (from ICA forms) and the resulting fragmentation was consistent with $\Delta^{9,12}$ double bonds (data not shown).

The POROS R1 protocol we have described here also enriched other LPC species, which included C22:6-LPC (*m/z* 574), C22:4-LPC (*m/z* 578), C16:0-LPC (*m/z* 502), and C16:1-LPC (*m/z* 500) that were also characterized by MS^n (**Fig. S4**). Most of these species, except for C22:6-LPC, had very low abundance and, in the case of Epi and Meta forms, could only be seen in the enriched 25%-*n*-propanol POROS R1 fraction. Even for TCT and ICA forms, $MS^3$and MS^4 of the C16:1-, C22:4- and C18:0-LPC species could only be conducted with samples derived from the POROS R1 chromatography. This confirms that indeed this last fractionation step is necessary for the full characterization of low-abundance LPC species from complex phospholipid mixtures of *T. cruzi*. Using the current methodology, however, we were unable to detect any *bona fide* PAF species in any of the four parasite stages analyzed. Even employing the highly specific and sensitive MS approach, selective-ion monitoring (SIM), we could not detect any trace amounts of PAF species in *T. cruzi*. This was true not only for the POROS R1 25% n-propanol fractions, but for all fractions described in this study. Therefore, we surmise that if there were any PAF species in this parasite, the concentration levels would likely be below the detection limit of the MS approaches used in the present study.

After characterizing the different *T. cruzi* LPC species, we proceeded to quantify them using a synthetic C10:0-LPC as an internal standard. These analyses were conducted on freshly prepared parasite pellets to minimize the amount of time that *T. cruzi* phospholipases A1 and

A2 ((104)) could have to act on PCs, leading therefore to an artificial increase in LPC levels. Overall, the lipid profiles of freshly prepared pellets were nearly identical to the profiles of previously frozen pellets of the same parasite forms (**Figs. 4 and 7**, and data not shown). The LPC quantification showed that the amount of C16:0-, C18:0-, C18:1- and C18:2-LPC present in the mammalian-dwelling forms of *T. cruzi* (ICA and TCT) were much higher than in the insect-dwelling (Epi, Meta) forms (**Table 1**). For instance, although the two most abundant LPC species found in all four parasite forms were C18:1- and C18:2-LPC, ICA forms had ~44 and ~35 times more of these species, respectively, than Epis. TCTs also showed very high levels of these lipids, having approx. 16–17 times more C18:1- and C18:2 LPC than Epis (**Table 1**). Interestingly, TCTs also contained the highest levels of C16:0-LPC, which has been shown to have immunosuppressant activities in the context of *T. cruzi* infection ((46)).

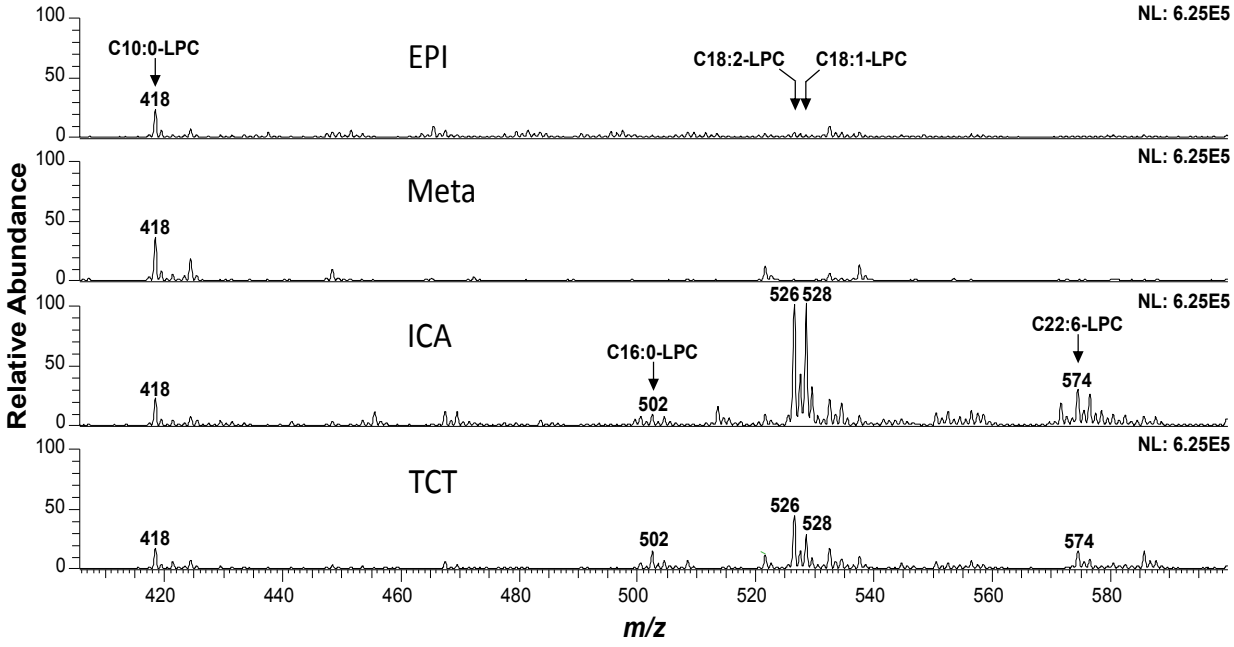

Figure 7: Quantification of LPC species in different life-cycle stages of *T. cruzi*.

C10:0-LPC (m/z 418) was used as an internal standard for quantification of the most abundant *T. cruzi* LPC species. C10:0-LPC (18 nmoles) was added to all fresh parasite pellets prior to lipid extraction with C:M (2:1, v/v) and C:M:W (1:2:0.8, v/v/v), followed by Folch's partition. The Folch lower phase was analyzed by ESI-LIT-MS^n. LPC species are indicated in the spectra. Epi, epimastigote; Meta, metacyclic trypomastigote; ICA, intracellular amastigote; TCT, tissue culture-derived trypomastigote. Picture taken from Gazos-Lopes et al, 2015, *PLoS neglected tropical diseases* **8**, e3077.

Table 1. C18:2-, C18:1-, C18:0- and C16:0-LPC content in different life-cycle stages of *T. cruzi.*

LPC species	Picomoles of LPC per 10^6 cells	LPC amount (mol^{-17}) per parasite[a, b]	Number of LPC molecules per parasite[c]	Parasite surface area (μm^2)[d]	Number of LPC molecules per μm^2[e]	LPC ratio (in regard to Epi)[f]
C18:2-LPC (*m/z* 526.4)						
Epi	1.4	0.15	0.90×10^6	63	0.14×10^5	1.0
Meta	0.6	0.05	0.32×10^6	24	0.13×10^5	0.4
ICA	**48.6**	5.10	**29.20×10^6**	15	**19.47×10^5**	**34.7**
TCT	**24.2**	2.55	**14.60×10^6**	13	**11.23×10^5**	**17.3**
C18:1-LPC (*m/z* 528.4)						
Epi	1.1	0.11	0.66×10^6	63	0.10×10^5	1.0
Meta	0.4	0.05	0.26×10^6	24	0.11×10^5	0.4
ICA	**48.7**	5.00	**30.00×10^6**	15	**20.00×10^5**	**44.3**
TCT	**17.0**	1.75	**10.50×10^6**	13	8.08×10^5	**15.5**
C18:0-LPC (*m/z* 530.4)						
Epi	0.4	0.04	0.24×10^6	63	0.04×10^5	1.0
Meta	0.7	0.07	0.40×10^6	24	0.17×10^5	1.8
ICA	**18.4**	1.72	**10.32×10^6**	15	6.88×10^5	**46.0**
TCT	4.9	0.50	2.70×10^6	13	2.08×10^5	**12.2**
C16:0-LPC (*m/z* 502.5)						
Epi	**n/a[g]**	**n/a**	**n/a**	63	**n/a**	**n/a**
Meta	**n/a**	**n/a**	**n/a**	24	**n/a**	**n/a**
ICA	3.9	0.40	2.40×10^6	15	1.60×10^5	**n/a**
TCT	**7.9**	0.78	4.45×10^6	13	3.42×10^5	**n/a**

[a]The molar relative response factors (MRRF) of C10:0-LPC and LPC standards were used to calculate the amount of each LPC molecular species in Folch lower-phase fractions of *T. cruzi*.
[b]The number of parasites was determined before lipid extraction by counting live parasites in a hemocytometer. Values are means of three determinations. The standard deviation in all cases was <15%.
[c]Determined by multiplying the number of moles by the Avogadro's constant.
[d]Estimated based on the parasite's length and diameter as determined by scanning electron microscopy, and assuming that each parasite is cylindrical, as previous described [103].
[e]Obtained by dividing the number of LPC molecules per cell by the surface area of each parasite form.
[f]Obtained by dividing the amount of picomoles of LPC per 10^6 cells of each parasite form (column 1) by the values obtained for Epi.
[g]Not analyzed due to absence or trace amounts of the compound.
doi:10.1371/journal.pntd.0003077.t001

Taken from Gazos-Lopes et al, 2015, *PLoS neglected tropical diseases* **8**, e3077.

To assess whether *T. cruzi* is also able to secrete LPC species to the extracellular milieu, we analyzed extracellular vesicles (EVs) and EV-free supernatant or conditioned medium (VF) of Epi and Meta forms, obtained as described ((90)). Epi and Meta forms secrete two types of EVs, namely V2 and V16, which are vesicles obtained after 2 h and 16 h of ultracentrifugation (at 100,000×g), respectively. In both stages, V2 are larger vesicles resembling ectosomes (130–140 nm), whereas V16 are smaller vesicles resembling exosomes (70–90 nm). The final vesicle-free supernatant (VF) in both stages is virtually devoid of EVs ((90)). As shown in **Table S1 and Fig. S5**, although Epis have higher amounts of C18:1- and C18:2-LPC than Metas in the total parasite pellet, the latter secrete much higher amounts of these phospholipids in the EV-free conditioned medium (mVF). Metas secrete 1.9 pmol of C18:1-LPC per 10^6 cells in mVF and an additional 0.5 pmol associated with mV2 fraction. Similar values were found for C18:2-LPC in mVF and mV2 (**Table S1**). In comparison, Epis only secrete trace amounts of both LPCs in eV2. In our analyses, however, we were only able to detect trace amounts of C16:0-LPC in the V2, V16, and VF fractions of Epis and Metas (data not shown). Taken together, our data strongly indicate that C18:1-LPC, C18:2-LPC, and eventually other LPCs could actively be secreted by Metas during the early stages of the infection. Moreover, LPCs secreted by these parasites could contribute to the overall LPC pool in the plasma, saturating the lipid carrier proteins, and eventually activating PAF receptors. Most importantly, the relative concentration of C18:1-LPC could even be higher in the infected tissues, due to the continuous secretion of this phospholipid, associated or not with parasite EVs. Owing to the technical difficulty in obtaining enough parasites for preparation of EVs from TCTs or ICAs, we have not been able to conduct the same kind of quantification in these mammal-dwelling stages.

2.3.3 Effect of LPC species on the aggregation of rabbit platelets

Since we were unable to detect any PAF species in any of the four parasite stages analyzed, we hypothesized that the PAF-like molecule could be one or more of the lysophospholipids structurally characterized here. This assumption is also based on previous reports that certain LPC species seem to activate the PAFR ((57), (105)). Moreover, purification of sufficient amounts of each *T. cruzi* LPC species for the bioassay (i.e., platelet aggregation) was not feasible. Therefore, we carried out the platelet aggregation assays using synthetic (C16:0-, C18:0-, C18:1-, and C22:6-LPC, at 1, 10, 100, and 1000 μM) or purified (C18:2-LPC) LPC species, and synthetic C16:0-PAF (at 1 μM; positive control). In a set of experiments platelets were pre-incubated for 30 min in the presence of 10 μM WEB 2086. As seen in **Fig. 8**, C16:0-LPC, C18:0-LPC, and C18:2-LPC failed to aggregate platelets at 10 μM, or at any other concentrations used (data not shown). Interestingly, C18:1-LPC was able to aggregate rabbit platelets at 10 and 100 μM (**Fig. 8**), but unlike PAF, failed to perform this activity at 1 μM (data not shown). WEB 2086 completely abolished platelet aggregation induced by C16:0-PAF and C18:1-LPC (at final concentrations of 1 μM and 100 μM, respectively) (**Fig. 8**). We were aware of the fact that depending upon the acyl chain length and degree of unsaturation, high concentrations (>30 μM) of LPCs could act as strong detergent and promote cell lysis ((63)). Therefore, in our platelet aggregation assays, we used all LPCs at a maximal 10 μM concentration, except for C18:1-LPC, which was also tested at 100 μM. We did not observe platelet lysis up to 10 μM of any LPC tested, or even at 100 μM of C18:1-LPC

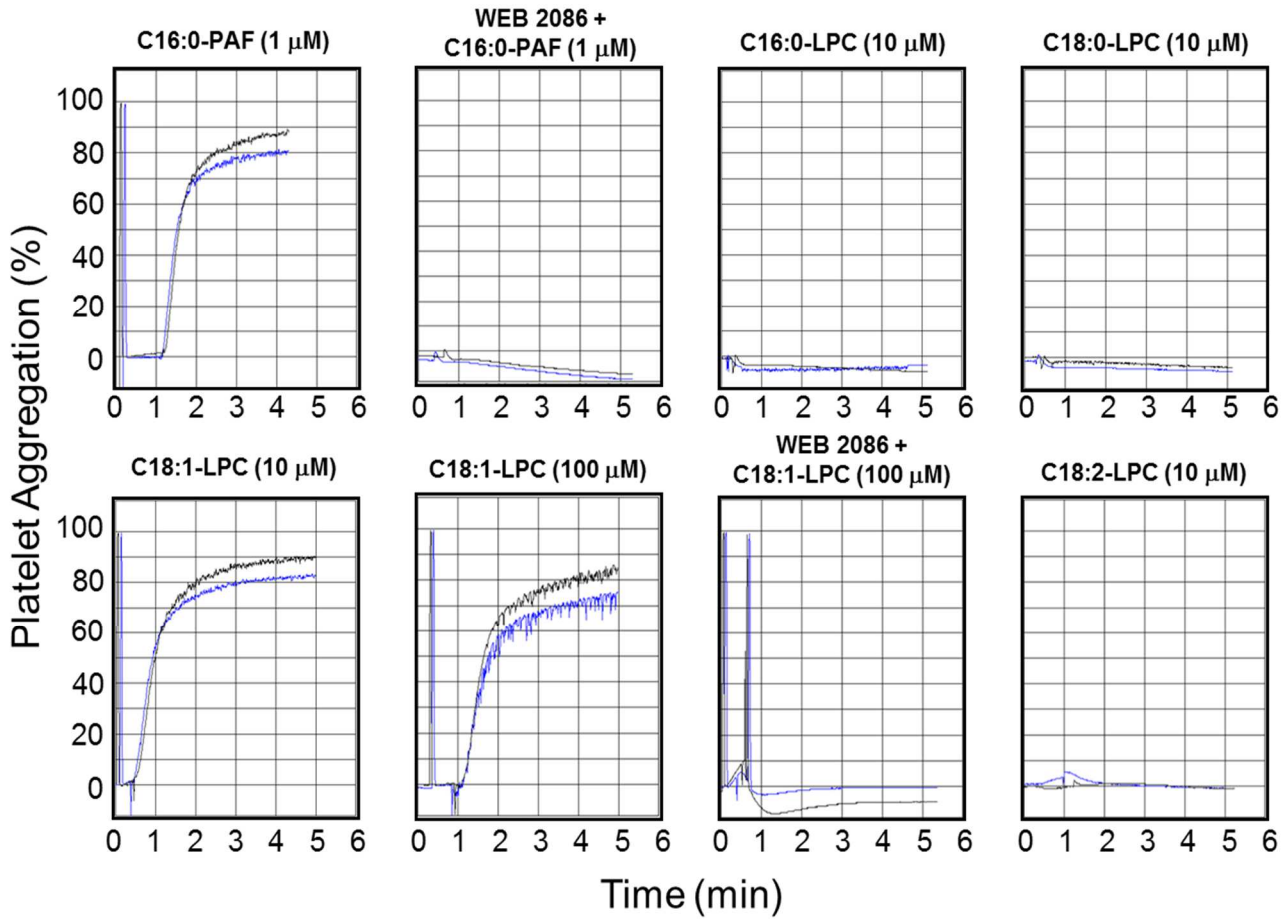

Figure 8: Activity of C16:0-PAF and different *T. cruzi* LPC species on the aggregation of rabbit platelets.Platelet aggregation assays were performed as described in Materials and Methods, using synthetic 16:0-PAF and C16:0-, C18:0-, C18:1-LPC, and purified C18:2-LPC. Control platelets or platelets pre-treated for 30 min with 10 mM WEB 2086 were assayed in the absence or presence of 1 mM C16:0-PAF or the LPC species at 10 mM (C16:0-LPC, C18:0-LPC, C18:1-LPC, and C18:2-LPC) and 100 mM (C18:1-LPC). Each lipid was tested in duplicate as indicated by black and blue curves in each graph. Picture taken from Gazos-Lopes et al, 2015, *PLoS neglected tropical diseases* **8**, e3077.

2.3.4 Comparative modeling of the PAF receptor

To gain insights into the mechanism by which C18:1-LPC, but not C16:0, C18:0, C18:2, could induce platelet aggregation mediated by PAFR, we decided to build a 3D-structural model of the PAFR, since a high-quality model was not available in the literature. The structural features of our PAFR model are shown in **Figure 9A**. As a member of the class A of GPCR superfamily, the PAFR model encompasses an extracellular N-terminus, followed by seven transmembrane (TM) α-helices (TM1, TM2, TM3, TM4, TM5, TM6, and TM7) (**Fig. S6A**), connected by three extracellular loops (EL1, EL2, and EL3) (**Fig. S6B**) and three intracellular cytoplasmic loops (CL1, CL2, and CL3) (**Fig. S6C**) and, finally, a short α-helix (H8) at the intracellular C-terminus (**Fig. 9A**). Additionally, the spatial arrangement of the 7-TM bundle constitutes a hydrophilic cavity covered by EL2, which is described as a ligand-binding pocket (**Figs. 9A and S6B**) ((101), (106), (107), (108), (109), (110), (111)).

2.3.5 Structural validation of the PAFR model

The I-TASSER methodology is very accurate for the construction of protein models when the sequence identity between the target sequence and the template protein drops below 30%, where lack of a high-quality structure match may provide substantial alignment errors and, consequently, poor quality models. In addition, the I-TASSER methodology has already been used for modeling other GPCRs ((101), (111)). The structural validation of the PAFR model was performed using three programs: PROCHECK ((98)), ERRAT((99)), and PROQM ((100)). The stereochemical quality of the PAFR model was evaluated using PROCHECK program. According to an analysis of 118 known protein structures, a good quality model would be expected to have over 90% in the most favored regions. The analysis of the first Ramachandran plot revealed that 97.8% of the amino acid residues are located in the most favorable (92.0%)

and additional allowed (5.8%) regions, confirming the excellent quality of the PAFR model described here (**Fig. S7**). The analysis of the second Ramachandran plot, which considers only Φ and ψ angles for Gly residues, showed that all 11 Gly residues in the primary sequence of PAFR were in allowed regions, with favorable combinations of angles Φ and Ψ (**Fig. S8**). The properties of the main and side chains for PAFR model were also evaluated by PROCHECK program, which showed acceptable values for our model when compared to experimentally-determined protein structures (**Fig. S9 and S10**). The analysis of distortions in the geometry of the PAFR model residues was also analyzed using PROCHECK (**Fig. S11**). The parameters analyzed were the bond lengths and angles, including atoms of the main and side chains, and the results were considered acceptable for our PAFR model. In addition, we used the ERRAT program for verifying errors in non-bonded atom-atom interactions in our model. The error values are plotted as a function of the position of a sliding residue in the window ((99)). According to this analysis, structures at high resolutions, generally produce values around 95% or higher. However, for protein structures at lower resolutions (2.5 to 3 Å), the average overall quality factor can be around 91%. The ERRAT analysis gave an overall quality factor value of 87% for our PAFR model (**Fig. S12**). Although low for crystal structures, this value is acceptable for protein models ((100)). Finally, we analyzed the quality of the three-dimensional structure of our model at local and global levels, using PROQM program ((99)) (**Fig. S13**). This program uses a score function to evaluate structures of membrane proteins, including GPCRs ((100), (112), (113)). Thus, to each residue of the protein model is given a score, producing, consequently, an overall quality factor. The value of the overall quality factor generated by server PROQM ranges from 0 to 1, indicating a model of poor and excellent quality, respectively

((97)). The PROQM analysis gave a global quality score of 0.717 for our PAFR model (**Fig. S13**), which is similar to the score values for crystallographic structures of GPCR ((99)).

2.3.6 Molecular docking

To compare the binding mode of all ligands (C16:0-PAF, and C16:0-, C18:0-, C18:1-, and C18:2-LPC) to the PAFR model, we carried out ten docking simulations for each ligand (totalizing 50 poses per ligand) and, consequently, the poses with the lowest energy for each ligand was selected for analysis. The comparison between C16:0-PAF and each LPC species is represented in **Fig. 9B–E** and **Fig. S14**. The molecular docking study showed that C18:1-LPC and C16:0-PAF have similar modes of interaction with PAFR (**Fig. 9D and Fig. S14C**). On the other hand, no other LPC species was able to interact with PAFR in a similar way, which corroborates the platelet aggregation assays (**Fig. 8**). Since PAF and LPC have different structures, RMSD matrix was not calculated. Instead, distances between the heteroatoms of the functional groups (amino, phosphate, and acyl groups) of C16:0-PAF and all LPC species were measured. The nitrogen of the amino group, the phosphorous of the phosphate group, and the oxygen linking the glycerol backbone (at *sn*-1) to the carbonyl group of the acyl chain were chosen and all distances between the ligands are presented in **Table 2**. The distances between heteroatoms of C16:0-PAF and C18:1-LPC are clearly lower than the distances between C16:0-PAF and other LPC species (C16:0, C18:0, and C18:2), with the exception of the amino group of C18:2-LPC and C16:0-PAF, confirming the similarities between C16:0-PAF and C18:1-LPC binding modes. The energy of the interactions between PAFR and each ligand was also analyzed (**Table 3**). The hydrogen bonds and repulsive steric interactions were mapped using a ligand-map algorithm, generated by the MVD program ((101)). The hydrogen bonds are represented in Figure 9. C16:0-PAF and C18:1-LPC interact with the same amino acids (i.e., Asn159 and

Thr160) of the PAFR model. Other LPCs do not present the same pattern of interaction. Interestingly, C18:1-LPC is able to additionally interact with Ser157, through its hydroxyl group, in a very strong way (**Fig. 10 and Table 3**). Although C16:0-, C18:0-, and C18:2-LPC also form hydrogen bonds with amino acids, these interactions occur in a different region of the PAFR model and with lower strength. Finally, the amino group either of C16:0-PAF or any of the LPC species did not seem to interact to our PAFR model (**Fig. S15**).

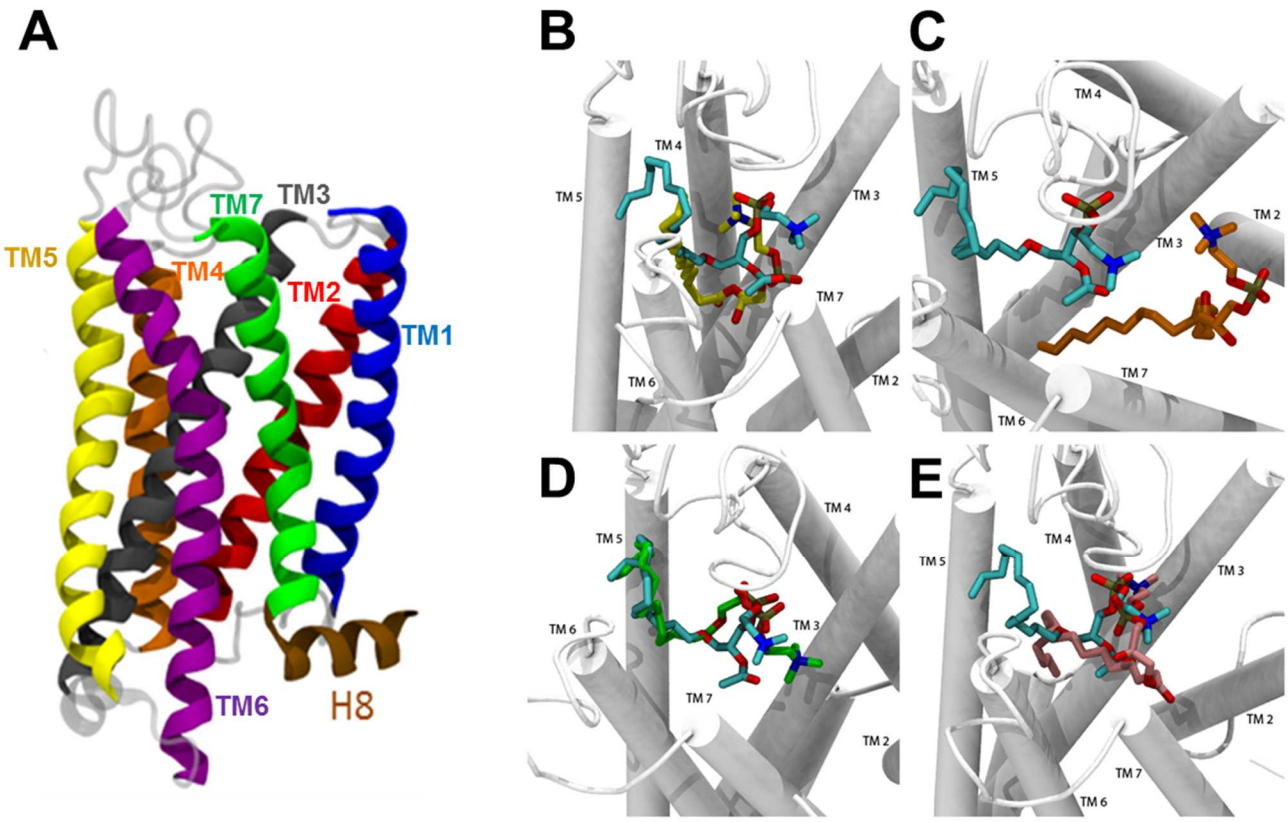

Figure 9: Structural representation of the PAFR model and its interaction with PAF and LPC species.

(A) Side view of PAFR model. Each TM (alpha-helix) is indicated in a different color: TM1, blue; TM2, red; TM3, dark gray; TM4, orange; TM5, yellow; TM6, purple; TM7, green. The helix 8 (H8) at the end of C-terminus region is indicated (brown). (B–E) Comparison of binding modes of PAF and each LPC species to PAFR. (B) C16:0-PAF (cyan) and C16:0-LPC (yellow); (C) C16:0-PAF (cyan) and C18:0-LPC (orange); (D) C16:0-PAF (cyan) and C18:1-LPC (green); and (E) C16:0-PAF (cyan) and C18:2-LPC (pink). Transmembrane (TM) regions are represented as white rods. Picture taken from Gazos-Lopes et al, 2015, *PLoS neglected tropical diseases* **8**, e3077.

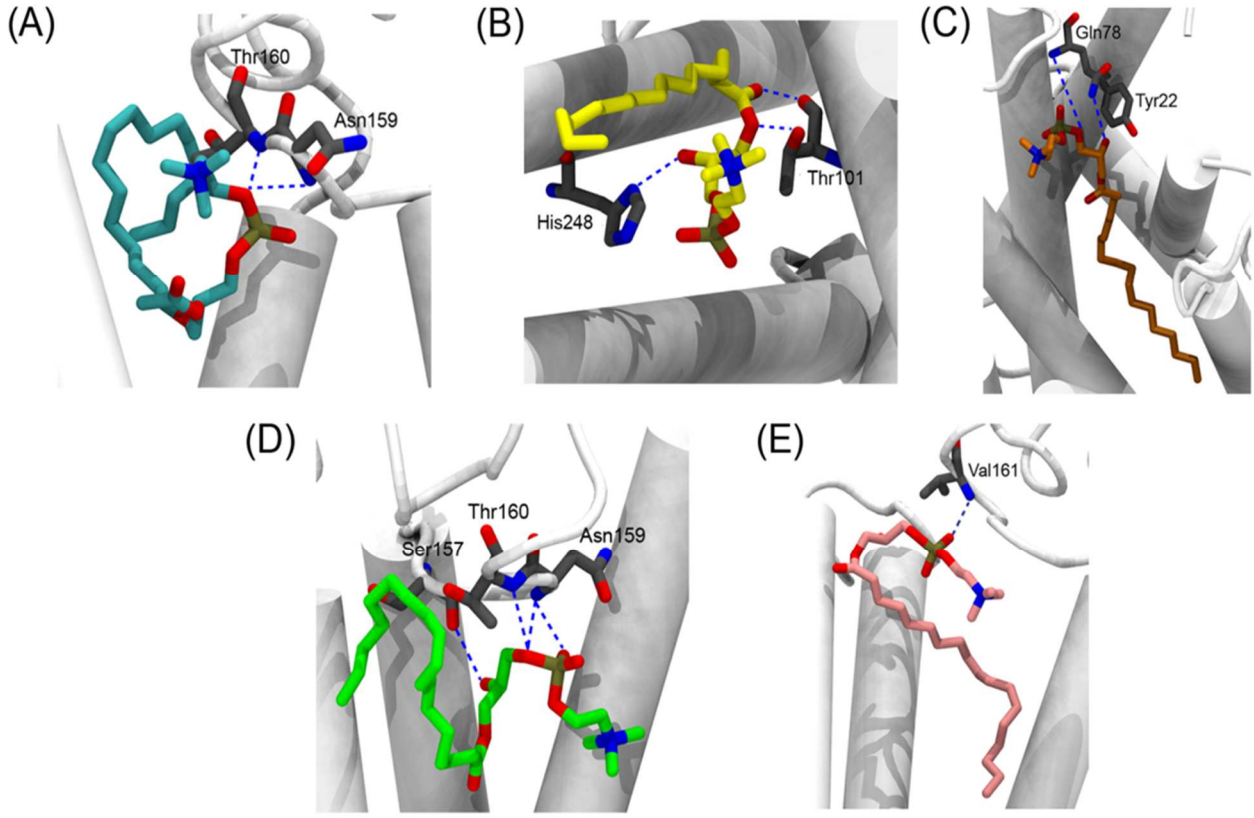

Figure 10: Hydrogen bonds between different lysophospholipid ligands and PAFR.

Hydrogen bonds are represented by blue interrupted lines. (A) C16:0-PAF; (B) C16:0-LPC; (C) C18:0-LPC; (D) C18:1-LPC; and (E) C18:2-LPC. Nitrogen atoms are shown in blue, oxygen in red, and ligand carbon chains are filled with the specific color for each ligand: C16:0-PAF, cyan; C16:0-LPC, yellow; C18:0-LPC, orange; C18:1-LPC, green; C18:2-LPC, pink. Picture taken from Gazos-Lopes et al, 2015, *PLoS neglected tropical diseases* **8**, e3077.

Table 2. Distances between the amino, phosphate, and acyl functional groups of C16:0-PAF and each LPC species.

Ligands	Atom[a]		
	Nitrogen (Å)	Phosphorous (Å)	Oxygen (Å)
PAF vs. C16:0-LPC	19.0	13.6	5.6
PAF vs. C18:0-LPC	6.1	11.1	12.0
PAF vs. C18:1-LPC	6.1	1.2	1.7
PAF vs. C18:2-LPC	5.5	3.5	9.6

[a]This refers to the nitrogen of the amino group, the phosphorous of the phosphate group, and the oxygen at *sn*-1, linking the glycerol backbone to the carbonyl group of the acyl chain.

doi:10.1371/journal.pntd.0003077.t002

Taken from Gazos-Lopes et al, 2015, *PLoS neglected tropical diseases* **8**, e3077.

Table 3. Summary of the interactions of each ligand with the PAFR model.

Ligand	H-bond energy (Kcal.mol^{-1})	Residues (H-bond interaction)	Steric interaction energy by PLP[a] (Kcal.mol-^{1})	Residues (steric interactions)	MolDock score (Kcal.mol^{-1})
C16:0-PAF	−2.84194	Asn159, Thr160	−11.453	Asn159, Thr160, Pro183, His248, Trp255, Thr256, Glu259	−167.335
C16:0-LPC	−1.33205	Thr101, His248	−18.271	Phe97, Phe98, Thr101, Tyr102, Ile187, Ile191, His248, Gln252, Trp257	−161.28
C18:0-LPC	−3.43936	Tyr22, Gln78	−0.066	Tyr22, Phe66, Ile74, Gln78, Trp83, Phe97, Val105, Phe241, Leu279, Leu282, Ser283	−161.634
C18:1-LPC	−7.24856	Ser157, Asn159, Thr160	−3.676	Phe98, Ser157, Asn159, Thr160, Ile187, Gln252, Trp255, Thr256, Glu259	−174.597
C18:2-LPC	−2.32134	Val161	−21.470	Phe98, Tyr102, Thr158, Thr160, Val161, Ile191, Trp255, Gln276, Leu279	−169.19

[a]Piecewise linear potential.

doi:10.1371/journal.pntd.0003077.t003

Taken from Gazos-Lopes et al, 2015, *PLoS neglected tropical diseases* **8**, e3077.

2.4 Discussion

Previous results from our group showed that *T. cruzi* synthesizes a PAF-like phospholipid capable of aggregating rabbit platelets ((73)). Aiming at the purification and structural characterization of this putative PAF-like molecule, we developed a fractionation protocol that proved efficient for the enrichment of PAF and other lysophospholipids such as LPAF and LPC. Tandem MS and bioactivity data obtained in the present study revealed that the *T. cruzi* PAF-like phospholipid is in fact an LPC, namely *sn*-1 C18:1(Δ^9)-LPC. However, we do not discard the possibility that very low amounts of a *bona fide* PAF species might still be synthesized by this parasite. The MS^n assignments for the C18:1-LPC we provide here are in agreement with previous reports ((87), (89)), but somewhat different from the results obtained by Smith *et al.* ((70)). Specifically, these authors analyzed a lipid species with a nearly identical fragmentation pattern as what we have identified here as C18:1-LPC, but annotated it as a novel C16:1-alkenyl-PAF. In their study, an ion species at *m/z* 265 was characterized as being derived from the neutral loss of acetyl and methyl groups from the fragment ion at *m/z* 339. In addition, a fragment ion at*m/z* 247 was proposed to be derived from the loss of water from the ion at *m/z* 265. Conversely, we show here that the non-lithiated $[R_1CO^+]^+$ and $[R_1CO^+ - H_2O]^+$ fragment ions at *m*/z 265 and 247, respectively, are in fact derived from a C18:1-acyl chain at the *sn*-1 position. This is further confirmed by the presence of lithiated ($[R_1CO_2H+Li]^+$) fragment ion from oleyl chain at *m*/z 289. Our assignments of C18:1-LPC are in complete agreement with those reported by Hsu et al.((87)). Smith et al. ((70)) also proposed the ion species at *m/z* 223 as being the protonated C16:1-alkenyl chain from the *sn*-1 position of that putative PAF species. We also observed the same fragment ion in both synthetic and *T. cruzi*-derived C18:1-LPC, but we assigned it as derived from the fragmentation of the acyl chain.

Taking all these facts into consideration, it is likely that Smith et al. ((70)) have mistakenly identified C18:1-LPC as C16:1-PAF.

Here we show that *T. cruzi* synthesizes at least five species of LPC and that only *sn*-1 C18:1(Δ^9)-LPC was able to promote rabbit platelet aggregation. These LPCs could be generated by the action of host- and/or parasite-derived phospholipase(s) A1 and/or A2 on diacyl-PCs. A PLA1 has already been well characterized in *T. cruzi* trypomastigote and amastigote forms (RA, Cvd, and K98 strains) ((114), (115)),((116)). However, since we could only identify *sn*-1 C18:0-, C18:1-, and C18:2-LPC, we believe that the parasite PLA1 is not playing a major role in the generation of these LPCs, at least under the experimental conditions used in this study. Nevertheless, we could not discard the possibility that the *T. cruzi* PLA1 might be important for the generation of LPC species using different experimental conditions and/or other parasite strains, as previously described ((114), (115)). Therefore, most likely the LPC species identified in this study were generated by the action of a PLA2 from the host and/or parasite. No PLA2 has so far been purified and fully characterized in *T. cruzi*, despite the fact that at least four putative PLA2 genes have been annotated in the parasite genome (TriTrypDB TcCLB.510743.50, TcCLB.510659.257, TCSYLVIO_005843, and Tc_MARK_4470) (104). Although a PLA2-like activity has been previously reported in epimastigotes ((117)), no further characterization of this enzymatic activity has been published. Moreover, using more rigorous enzymatic assay conditions, Belauzaran et al. ((104)) were unable to detect any PLA2 activity in *T. cruzi* epimastigote supernatants. This raises the possibility that the *T. cruzi* LPCs identified here could have been generated by the action of a host-derived PLA2 and/or by a parasite-derived enzyme that is expressed in much higher levels in the mammal-dwelling stages. Further studies are needed to address this important point.

A direct correlation between increased platelet reactivity and the incidence of acute coronary diseases has been described ((118)). Accordingly, there is an increase in platelet aggregation associated with ischemia, myonecrosis, and myocarditis in both acute and chronic stages of Chagas disease ((10), (75), (11), (119)). Noteworthy, *T. cruzi* also synthesizes TXA2, which modulates several pathophysiological aspects of Chagasic cardiomyopathy ((45)). It is not surprising that *T. cruzi* produces at least two platelet activators, given the importance of platelet aggregation in the progression of Chagas disease. Our bioactivity data with C18:1-LPC are in agreement with other results in the present study, namely the platelet aggregation assays and molecular docking predictions. We had also previously demonstrated that the putative PAF-like phospholipid was able to trigger the differentiation of *T. cruzi* epimastigotes into metacyclic trypomastigotes *in vitro* ((73)). This effect was abolished by WEB 2086, a classic competitive PAF antagonist that binds specifically to PAF receptors ((120)). The latter result along with labeling *T. cruzi* epimastigotes with polyclonal antibody raised against mouse PAFR, in immunofluorescence assays, strongly indicated that *T. cruzi* might have putative PAFR both at the cell surface and intracellularly ((73)). In fact, WEB 2086 inhibited all PAF effects upon trypanosomatids described to date ((121), (122), (123)).

LPC has messenger functions, binding to a specific receptor and not acting through physicochemical effects on the plasma membrane of the target cell. Several receptors for LPC, such as G2A, GPR4, and IP, and receptors for TXA2 (TP) and PAF (PAFR), have been described ((53) , (54), (55), (56), (57), (58), (59), (60), (61)). In the present study, we show that the platelet aggregation promoted by C18:1-LPC was abrogated by WEB 2086. This result is highly suggestive that *T. cruzi*-C18:1-LPC may be able to trigger platelet stimulation through a ligand-receptor system. Accordingly, LPC is known to induce intracellular signals ((124)) and

mediate cytokine secretion ((62)), both through PAFR. Interestingly, the *R. prolixus*-derived C16:0-LPC is able to prevent platelet aggregation triggered by PAF ((46), (48)). We may hypothesize that C16:0-LPC acts as a PAF antagonist, binding to its receptor. Indeed, here we show molecular docking calculations, which are suggestive that C16:0-, C18:0-, and C18:2-LPC could be lodged within the ligand-binding site of PAFR, preventing PAF actions. On the other hand, the predicted binding pose for C18:1-LPC evokes the possibility that this molecule and C16:0-PAF exhibit similar modes of interaction with PAFR. These results can be partially explained by the fact that, depending on the length and degree of unsaturation of the acyl-chain, each LPC species triggers different cellular activities ((59), (63), (64)). Apparently, each of these LPC species binds to different receptors, probably because of the tridimensional structure of these phospholipids. For instance, TP receptors are involved in the attenuation of vascular relaxation mediated by C18:2- and C20:4-LPC, but not C16:0- or C18:1-LPC ((59)). Additionally, similar to C16:0-PAF, C18:1-LPC exhibited the ability to elicit a rapid, receptor-mediated oxidative burst, through generation of reactive oxygen species (ROS) in neutrophils. On the other hand, C16:0- and C18:0-LPC did not share the same activity ((63)). Consistently, our docking calculations show that both C16:0-PAF and C18:1-LPC structures interact with PAFR model with Asn169 and Thr170 residues via hydrogen bonds. These amino acid residues are localized at the extracellular loop EL2, which is involved in the ligand recognition and receptor activation in the superfamily of the GPCRs ((125)). The number and the chain length of the fatty acids of lipoproteins are also substantially important for the induction of signaling through Toll-like receptor 2 (TLR2) ((126)). A cross-talk between TLR and GPCR has been described, which is essential for cellular signaling in the absence of TLR natural ligands. This cross-talk is basically a molecular organizational GPCR signaling platform that promotes the

transactivation of TLR, through potentiation of Neuraminidase 1 and matrix metalloproteinase-9 at the cell surface ((127)). Intriguingly, LPC derived from the human pathogen *Schistosoma mansoni* activates TLR-2-dependent signaling involved in eosinophil activation and recruitment, probably through cross-talk to a GPCR ((128)). More recently, we have shown that various species of LPC containing different acyl chain lengths and degrees of unsaturation may induce proinflammatory response mediated by TLR4- or TLR2/TLR1-dependent signaling pathway in HEK293A cells ((129)). Interestingly, a mixture of LPC species (mainly C16:0- and C18:0-LPC) could counteract TLR4-mediated signaling pathway triggered by *E. coli* O111:B4 lipopolysaccharide (LPS), suggesting therefore a dual role of this lysophospholipid in immunoregulation.

Over time, LPC was found not to be exclusively of mammalian origin and was described in several other organisms ((130)). Trypanosomatids tend to be rich in PC and LPC ((65), (66), (67), (68), (131)). However, in most of these cases, the presence of LPC has only been inferred indirectly and there still remains a general lack of information in the literature regarding the chemical structure and function of the LPC species in most organisms other than mammals. The results described in the present study show that *T. cruzi* is able to generate different LPC species and suggest that the levels of individual LPC species are tightly regulated in the course of this parasite cell cycle. In fact, the LPC levels are notably high in the mammal-dwelling infectious trypomastigote and intracellular amastigote stages. Taken together with the fact that there was no exogenous source (e.g., fetal bovine serum) of lipids in the TAU culture medium used for the differentiation of epimastigotes into metacyclic trypomastigotes, our data indicate that LPC species might be generated endogenously by this organism.

The saliva of *R. prolixus* is a source of LPC, which may act as an enhancing factor for Chagas disease ((46), (47)) LPC, TXA2, and PAF are lipid mediators that share a common chemical structure, biosynthetic pathways ((132)) and the ability to activate platelets ((133), (134), (135)). Previous results from our group have shown that PAF-treated *T. cruzi* is far more infective towards both mouse macrophages ((73)) and the insect vector *R. prolixus* ((136), (137)) TXA2 synthesized by *T. cruzi* controls the proliferation of the parasite and resulting inflammatory response to infection in the mouse ((45)). One may then speculate that host-vector-parasite co-evolutionary relationships may be involved in the maintenance or change in the enzymatic pathways for the synthesis and degradation of these molecules, which ultimately may dictate the success of *T. cruzi* infection.

In conclusion, here we demonstrate that *T. cruzi* synthesizes at least five LPC species, C16:0-, C18:0, C18:1-, C18:2-, and C22:6-LPC. The most abundant species are C18:2- and C18:1-LPC, being the latter the only one able to aggregate rabbit platelets, probably through a PAFR. This result was supported by molecular docking study of the interactions between LPC species and a PAFR model. These analyses showed that C18:1-LPC was able to interact with the PAFR model in a fashion similar to PAF. More studies on LPC metabolism in *T. cruzi* and relationship of the parasite with the mammalian and invertebrate hosts could, therefore, lead to the discovery of putative targets for novel therapies and control for Chagas disease.

3. CHAPTER 3: GPIOMIC ANALYSIS OF THE MAMMAL-DWELLING STAGES OF *TRYPANOSOMA CRUZI*

3.1 Introduction

3.1.1 GPI-anchor structure and function

Glycosylphosphatidylinositols (GPIs) are a class of protein post-translational modification (PTM) ubiquitously found in eukaryotes. Both GPI-anchored proteins (GPI-APs) and protein-free GPIs, known as glycoinositolphospholipids (GIPLs), are involved in diverse biological events, which include signal transduction, embryological development, immune responses, cell-cell interactions, plant development, and the survival/virulence of several pathogens (9,12,138-146).

The core structure of GPIs is highly conserved, consisting of an inositolphospholipid moiety covalently attached to a conserved carbohydrate core (Manα1-2Manα1-6Manα1-4GlcNα1-6-*myo*-inositol1-HPO_4^--lipid) (147). The lipid portion of the anchor is immersed in the outer leaflet of the plasma membrane, whereas the glycan portion projects outward, facing the extracellular environment. A single GPI can be attached to a protein via an amide linkage formed between the carboxyl group at the C-terminus of the protein and the amino group of either an ethanolamine phosphate (EtNP) or an aminoethylphosphonate (AEP) moiety present at the third mannose residue distal from the glucosamine (GlcN) residue of the conserved GPI glycan core (**Fig. 11A**) (141-145,147). Variations on the structure of the lipid moiety, as well as the addition of different side-chains to the glycan core of GPIs, greatly increase the potential diversity of

these molecules. In fact, a single cell may contain dozens of different GPI structures, with each of them potentially exhibiting different biological activities (139,142).

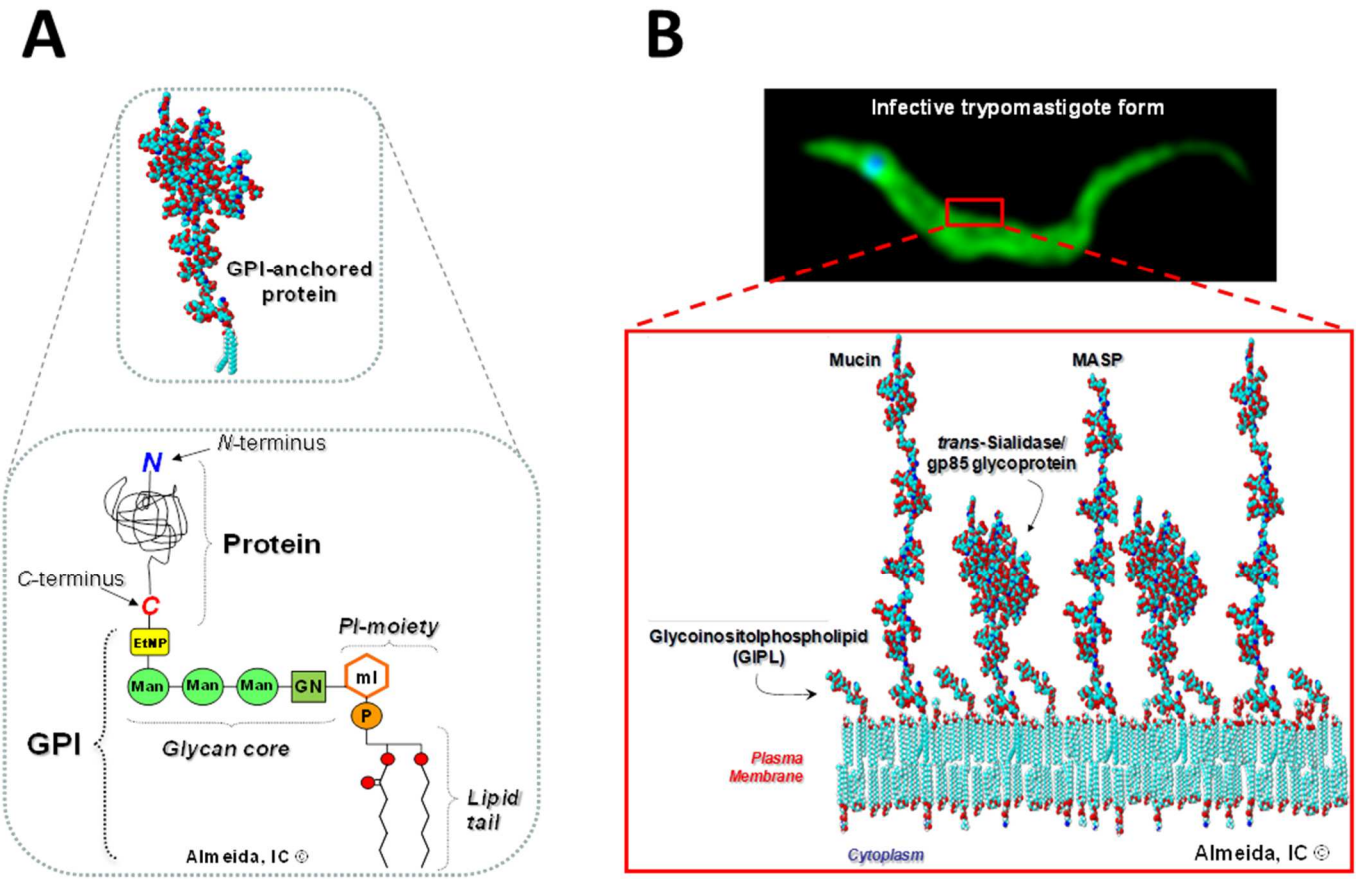

Figure 11: GPI-APs and GIPLs. (A) The core structure of GPI consists of an inositolphospholipid bound to a conserved glycan chain (Manα1-2Manα1-6Manα1-4GlcNα1-6myoinositol1-PO_4-lipid). Proteins can be covalently linked to this anchor through a peptide bound between an EtNP or AEP substituent present at the third mannose residue of the GPI distal from the glucosamine (GN) residue and the carboxyl group at the C-terminus of the protein. **(B)** The surface of *T. cruzi* is densely packed with GIPLs and GPI-APs (mostly mucins, MASPs, and *trans*-sialidases/gp85 glycoproteins) (141,143)

General interest in these molecules started with the description of the first GPI-anchor, which was discovered in *Trypanosoma brucei* (148). In this seminal work, it was shown that the main surface antigen of *T. brucei*, known as variable surface glycoprotein (VSG), was anchored to the parasite's plasma membrane by a new class of glycolipid, now known as GPI (148-151). Since then, many studies have described the effects of different trypanosomatid-derived GPI-APs and GIPLs on the immune system of vertebrates, with emphasis on mammals (143,152-154). These studies were not limited to trypanosomatid parasites, and many of them have also been performed on other important parasite models, such as *Plasmodium falciparum* (155,156) and *Toxoplasma gondii* (157).

It has been shown that GPI-APs and GIPLs cover most of the surface of *T. cruzi*, with every parasite having an estimated 2×10^6 and 2×10^7 copies of GPI-APs and GIPLs, respectively, on its surface (**Fig. 11B**). This observation is in agreement with findings that show that trypanosomatids make use of bioactive GIPLs and GPI-APs to successfully modulate the host immune system and to invade host cells. In general, parasite-derived GPI-APs and GIPLs lead to an increase in the circulating levels of proinflammatory cytokines and chemokines, the expression of nitric oxide synthase II, and the expression of macrophage adhesion molecules. It has also been shown that GPIs are required for amastigote development in host cells, without which they cannot sustain chronic infection (138,140,141,143-145,153,158,159). Various studies also indicate that these molecules activate host innate immunity, which is responsible for controlling acute Cd (140,141,154,158,160,161).

Although there still is very little information regarding the effects that parasite GIPLs and GPI-APs have on insect vectors, it is clear that a series of parasite-specific structures are associated with their ability to successfully colonize their vectors (162,163). In many cases, the

insect-dwelling parasite forms make use of certain GPI structural features, such as the presence of beta-galactofuranosyl (β-Gal*f*) residues, in order to specifically bind to lectins present on the insect vector midgut, allowing them to colonize this compartment (162-165). Parasite-derived GIPLs are also able to modulate vector immune responses, as well as their feeding efficiency, potentiating transmission to hosts (155,156,166,167). These effects are normally species and life-cycle stage specific. For this reason, different life-stages of a same parasite species will exhibit very different GPI-AP and GIPL structures, as they adapt to either colonize their insect-vector or to infect their mammalian hosts (79,167,168).

In spite of the importance of GIPLs and GPI-APs to the biology of *T. cruzi*, a better understanding of the mechanisms behind their contribution to parasite survival and virulence has been partially hampered because of the difficulties involved in the structural characterization of these molecules using more traditional approaches. This made the large-scale analysis of GIPLs and GPI-APs unfeasible. Our group has described a novel approach (i.e., GPIomics) for the large-scale analysis of GPIs and GIPLs by liquid chromatography-electron spray ionization-tandem mass spectrometry (LC-ESI-MS/MS) (138). With this approach we were able to identify 96 GPI species derived from the non-infective epimastigote stage, 79 of which were formerly unknown. Because epimastigotes are non-infective to humans, it is crucial to describe the GPIome of the mammal-dwelling stages of this parasite, so that this information can be explored in future studies regarding the effects of these molecules during infection and how to target them in the development of new therapies for Chagas disease. In fact, parasite GPIs have been validated as potential therapeutic targets in human African trypanosomiasis (169-174) and malaria (175). Here, we report the first large-scale analysis of the GPIome of the mammal-dwelling stages of *T. cruzi*.

3.1.2 GPI anchor Biosynthesis in Trypanosomatids

As mentioned on the section above, the core structure of GPIs has been conserved throughout evolution. This suggests that the GPI biosynthetic machinery of different eukaryotic clades is also relatively conserved. Most of the studies pertaining to the biosynthesis of GPIs have been conducted in mammals, yeast, and *T. brucei* (143,144,154,176,177). Because *T. brucei* is closely related to *T. cruzi*, these two species could have similar GPI biosynthetic pathways.

The first step in the GPI biosynthetic pathway of any known model is the transfer of *N*-acetylglucosamine (GlcNAc) from UDP-GlcNAc to a PI acceptor through the action of a GlcNAc-transferase complex present at the cytoplasmic side of the endoplasmic reticulum (ER) (178,179). The GlcNAc-PI is then deacetylated by a de-*N*-acetylase, giving rise to GlcN-PI (180-182). Next, the GlcN-PI is flipped to the luminal side of the ER, where it is mannosylated by a dolichol-phosphate-mannose transferase: GlcN-PI α1-4 mannosyltransferase (MT-I). This is followed by the acylation (usually with a palmitic acid) of the 2-position of the *myo*-inositol ring by an inositol acyltransferase (143).

The next step in the biosynthesis of GPIs in *T. brucei* is the transfer of a second mannose residue to the GPI precursor through the action of a dolichol-phosphate-mannose transferase: Man_1GlcN-(acyl)PIα1-6mannosyltransferase (MT-II), which has not been described in any organism. The third mannose residue of the conserved glycan core is added by a dolichol-phosphate-mannose transferase: Man_2GlcN-(acyl)PI α1-2 mannosyltransferase (MT-III) (143). An EtNP residue is then added to the position 6 of the third mannose residue through the activity of an ethanolamine phosphotransferase (183). The product of this enzyme is usually deacylated by an inositol deacylase, giving rise to the conserved "mature" core ([EtNP]Manα1-2Manα1-

6Manα1-4GlcNα1-6*myo*-inositol1-HPO_4^--lipid). After the glycan core is formed, the *T. brucei* GPI precursor is further modified by a lipid exchange process known as "GPI-lipid remodeling" (184). While most GPI intermediates in this species have *sn*-1-stearoyl (C18:0)-2-acyl-PI moieties, its mature GPIs have almost exclusively dimyristoyl (C14:0) moieties, which are generated through ordered deacylation and reacylation reactions (143,150,151,185). Several enzymes involved in the biosynthesis of GPIs in *T. brucei* have not yet been described in detail, and it is possible that many of the activities mentioned above are realized by the same enzymatic complex. After the GPI anchor is synthesized, it is attached to the C-terminus of a protein precursor by a GPI transamidase complex (GPI-TA). This enzyme recognizes and cleaves a signal sequence present at the C-terminus of a protein and replaces it with the mature GPI anchor (186,187). The GPI-AP is then transported to the Golgi complex, where the GPI anchor can be further modified through the addition of other sugar residues to the glycan core via the activity of different GPI glycosyltransferases. After processing in the Golgi complex, the GPI-AP or the protein-free GPI (or GIPL) is transported to the plasma membrane (**Fig. 12**) (188).

Although the GPI biosynthetic pathway in mammalian cells is very similar to the one described in *T. brucei,* a few crucial steps differ greatly between these two models (143,144,188). The first difference is that mammalian cells acylate the *myo*-inositol ring prior to the addition of the first mannose residue to the nascent GPI precursor (143,144). The second difference is that in mammals the lipid remodeling only occurs after the GPI-AP is transported to the Golgi complex (144,188). In some cases, this remodeling does not occur at all, as is the case of erythrocytes. The third difference, is that proper GPI-AP assembly is dependent on the sequential addition of an EtNP residue to the first and third mannose residues of the GPI precursor before the transamidase complex can attach the mature GPI to a proprotein (188,189)

(**Fig. 12**). Although the GPI-TA always attaches GPIs to proteins via the EtNP residue at the third mannose residue, it appears that in mammals the presence of an EtNP residue on the first mannose residue is necessary for efficient GPI-anchoring to occur. Mutants that do not express the enzyme responsible for the addition of this first EtNP (PIG-N) are unable to efficiently perform GPI-anchoring (189). Finally, in mammals the attachment of an EtNP residue to the second mannose residue of the mature GPI-AP is necessary for it to concentrate at the *ER-e*xit *s*ite (ERES), where they will be transported to the Golgi complex by COP II vesicles. Cells defective on the enzyme responsible for the addition of this modification tend to accumulate GPI-APs indefinitely at the ER (188,190). The addition of the EtNP residue to the second mannose residue of the GPI-AP is transient, since this modification is removed prior to transport out of the ER. It is possible that the addition of this modification acts as part of a quality control mechanism that somehow recognizes and only allows mature GPI-APs to be transported to the Golgi complex. In this sense, the addition and removal of this modification would be necessary for a GPI-AP to be considered mature and, consequently, ready to be transported out of the ER (188-191).

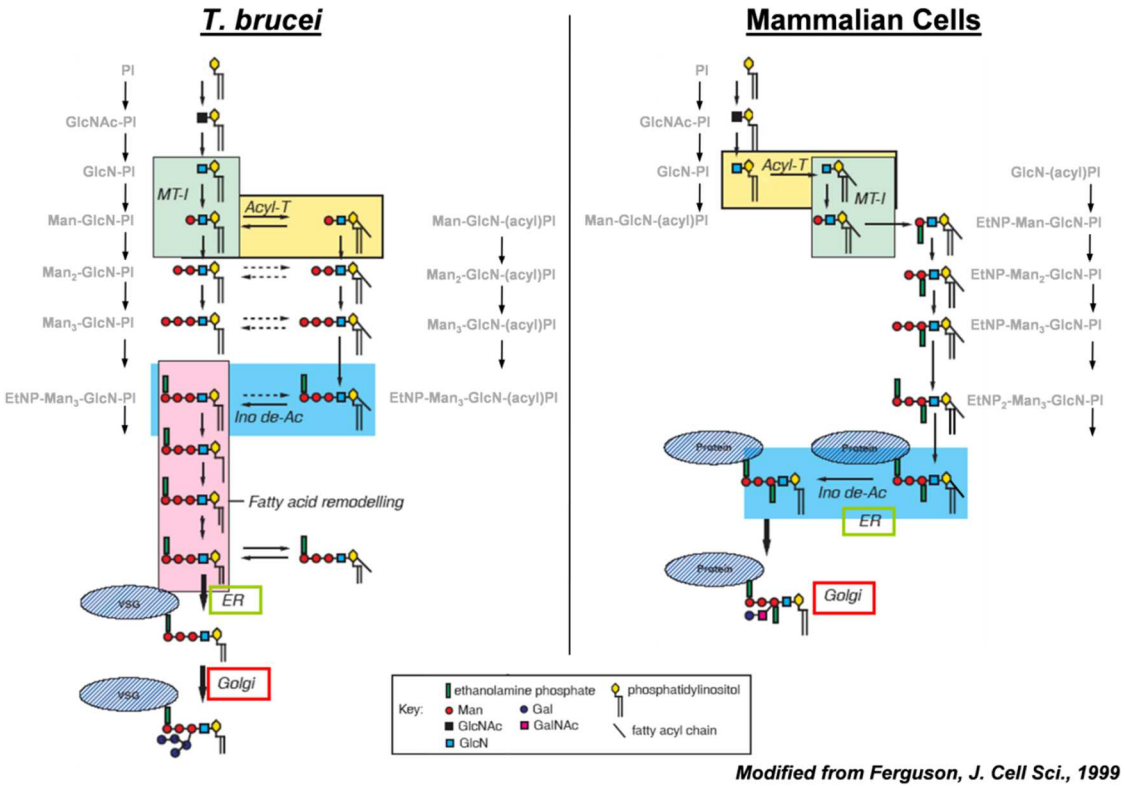

Figure 12: The GPI biosynthetic pathways in *T. brucei* (A) and in mammalian cells (B). The major steps involved in the GPI biosynthesis in both models are described in the body of the text above. Figure modified from (143)

3.1.3 AEP biosynthesis and degradation

One of the most intriguing characteristics of *T. cruzi* GIPLs and GPI-APs is the fact that they are usually modified by AEP residue(s), instead of the more common EtNP (79,138,192-194). Curiously, the only three other species known to add AEP to their GPIs, namely *Trypanosoma dionisii* (195), *Leptomonas samueli* (196), and *Herpetomonas samuelpessoai* (197), belong to the class Kinetoplastida. Interestingly, as aforementioned, other important Kinetoplastid parasites such as *Leishmania* spp. and *T. brucei* do not add AEP to their GPIs, relying on EtNP like the majority of eukaryotes.

Although EtNP and AEP are structurally very similar, AEP contains a very unusual phosphonate bond ($-H_2C–PO_3^{-2}$), instead of the common phosphate ester bond ($-H_2C–O–PO_3^{-2}$). The phosphonate bond is highly stable and is not a substrate for enzymes that recognize molecules containing phosphate ester bond bond, such as phosphotransferases. This means that molecules containing phosphonate bonds belong to a separate metabolic pool from the ones that contain phosphate ester bonds, effectively participating in very different biological processes (198).

Phosphonates are not usually synthesized in appreciable quantities by vertebrates, being more commonly found in marine invertebrates and bacteria (198). AEP is the most abundant phosphonate in living systems, being found as a conjugate of lipids (199), proteins (200), and glycans (201). The biosynthesis of this molecule usually starts with the conversion of phosphoenolpyruvate (PEP) to phosphonopyruvate (P-pyr) through the action of a phosphoenolpyruvate mutase (PEP mutase). This product is then converted to phosphonoaldehyde (P-Ald) by a P-pyr decarboxylase. This step is rate-limiting for the maintenance of phosphonate homeostasis, since PEP mutase is more efficient at converting P-pyr to PEP then at performing the opposite reaction. The final step of this pathway is the conversion of P-Ald to AEP through the activity of an AEP transaminase (AEPT). This enzyme is also responsible for converting AEP back to P-Ald, which is then broken down into inorganic phosphate and acetaldehyde by a phosphonatase in the AEP biodegradation pathway (**Fig. 13**) (198,202)**.**

The only enzyme involved in AEP metabolism to have been described in *T. cruzi* is the PEP mutase, which was shown to have a very similar sequence as to the homologous gene in the protozoan *Tetrahymena pyriformis*, and the mussel *Mytilus edulis*. This enzyme appears to be

arranged as a homotetramer, and to be localized to an as-yet unidentified organelle (203). Most studies describing AEPT structure and activity have been performed in bacteria, such as *Pseudomonas aeruginosa* (204), and in certain protozoa, such as *T. pyriformis* (205). The active site and overall fold of AEPTs appear to be relatively conserved, although the pH and temperature optima for this enzyme vary greatly across different species (202-207).

The fact that most *T. cruzi* GIPLs described to date contain an AEP residue attached to the *O*-6 position of the GlcN residue at the conserved glycan core suggests that this modification has an important function for this species (192-194). It is possible that this modification plays an analogous role to the addition of EtNP to the second mannose residue of nascent GPI-APs in mammalian models (144). In this case, the addition of AEP to the hexosamine residue could be part of a quality control mechanism that would only allow mature GPI-APs and GIPLs to exit the ER in this organism. Because of its potential relevance for GPI biosynthesis and transport in *T. cruzi*, and the fact that the AEP biosynthetic pathway is not found in humans, AEPT might be a good candidate for the development of new chemotherapeutics against this parasite. Therefore, one of our objectives is to verify whether GPI-APs and GIPLs derived from the mammal-dwelling stages of *T. cruzi* are as frequently modified with AEP as reported for the GPIome of Epis (138)

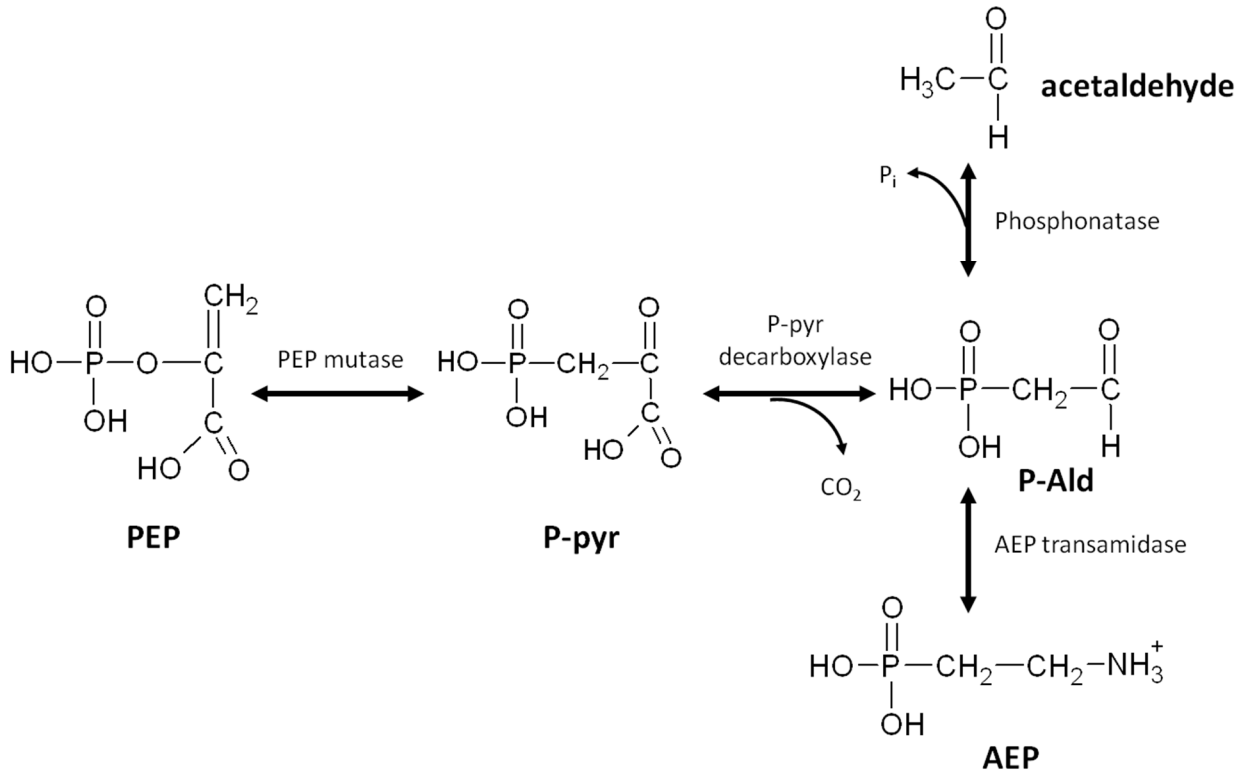

Figure 13: The conserved pathways for AEP synthesis and degradation: All major steps have been described on the text above. **AEP**, 2-aminoethylphosphonate; **PEP,** Phosphoenolpyruvate; **P-Ald**, Phosphonoaldehyde. Figure taken from (202)

3.2 Materials and Methods

3.2.1 – Chemicals

Otherwise indicated, all reagents and solvents used here were of analytical, HPLC, or mass spectrometric grade from Sigma-Aldrich (St. Louis, MO).5,h5

3.2.2 - Trypanosoma cruzi cultures

All *T. cruzi* life cycle stages or forms were obtained from the Y strain (76). Epimastigote forms (Epis) were maintained by weekly transfers using liver infusion tryptose (LIT) medium (77), supplemented with 0.002% hemin and 10% heat-inactivated fetal calf serum (FCS; Hyclone, heat-inactivated at 56°C for 30 min) at 28°C. Mammalian tissue culture-derived trypomastigotes (TCTs) were obtained from the supernatants of 5 to 6 days old *T. cruzi*-infected LLC-MK2 cells (American Type Culture Collection, Rockville, MD), maintained in RPMI-1640 medium supplemented with 2% FCS at 37°C in a 5% humidified CO_2 atmosphere (80). Intracellular amastigotes (ICAs) were obtained as described (81). Briefly, infected monolayers of LLC-MK2 cells were gently detached by scraping (BD Falcon cell scraper, BD Biosciences) and resuspended in PBS supplemented with 10% FCS. Mammalian cells were disrupted by passage through a 27-gauge needle (BD, Becton and Dickinson & Co.). ICA forms were separated from the cell debris by centrifugation (800× *g* for 5 min at 4°C). The supernatant was then harvested and passed through a DE-52 column and parasites were incubated for 2 h at 37°C in a humidified 5% CO_2 atmosphere, after which the parasites were again passed through a DE-52 column, from which they were harvested and stored. For the viability testing of all parasite forms, cells were resuspended in a Trypan Blue solution and counted in a Neubauer chamber (82). In this study, all experiments were performed using parasites that were harvested by centrifugation and washed

three times with PBS before use, unless otherwise specified. All parasite forms were counted and stored at -20 ^{o}C prior to use.

3.2.3 - Extraction of GIPLs and GPI-APs

Epi, TCT, or ICA pellets (1 x 10^9 parasites each), were suspended in 0.8-ml of ice-cold HPLC-grade water, and transferred to 8-mL PYREX^R culture tubes with PTFE-lined screw caps. HPLC-grade chloroform and methanol were added to each vial, giving rise to a final ratio of chloroform/methanol/water (C/M/W) of 1:2:0.8 (v/v/v) (3.8 mL). The samples were mixed thoroughly by vortexing for 2 min, and then centrifuged for 10 min at 1,800 x *g* at room temperature. After centrifugation, the supernatants were transferred to 8-mL PYREX^R culture tubes and the pellets dried under a constant flow of N_2 stream. The dry pellets were extracted three times with C/M (2:1, v/v) (3 mL) and another two times with C/M/W (1:2:0.8, v/v/v) (3.8 mL), according to Bligh and Dyer (84). After extraction, the dried supernatants were pooled together and subjected to Folch's partitioning (83,84), being first dissolved in C/M/W (4:2:1.5, v/v/v) (7.5 mL), then mixed vigorously for 5 min using a vortex and, finally, centrifuged for 15 min at 1,800 x *g* at room temperature. After centrifugation, the lower (organic) and upper (aqueous) phases were separated into new 8-mL PYREX^R culture tubes. The remaining delipidated pellets were extracted again with 4 ml 9% *n*-butanol, as previously described (140). The Folch aqueous phase (rich in GIPLs) and the 9% *n*-butanol phase (rich in GPI-APs) were then dried and stored at -80^{o}C until further use.

3.2.4 - Digestion of GPI-APs with proteinase K

The GPI-AP fractions (9% *n*-propanol) were digested overnight at 37 ^{0}C with proteinase K (30 units/mg protein, *Tritirachium album*, BioUltra) in 100 mM ammonium bicarbonate, pH 8.0. The digested samples (from here on referred to as GPIs) were suspended in 5% 1-propanol and purified in POROS R1 50 (Applied Biosystems) solid-phase cartridges. Each column was first conditioned with the sequential addition of methanol, 80%, 10%, and 5% 1-propanol and, after sample application, the column was sequentially washed with 5% and 10% 1-propanol. Finally, the GPIs were eluted with 80% 1-propanol. The last fraction (80% 1-propanol) was analyzed by LC-ESI-MS/MS, along with the Folch aqueous phase (containing over 90% of all GIPLs) (138).

3.2.5- LC-ESI-MS/MS of GIPL and GPI samples

The methodology used here is a modified version of the original GPIomics protocol developed by Nakayasu et al. (138). Briefly, nanocapillary columns (75-µm internal diameter by 10-cm length) were packed in-house with a suspension of 10 mg/ml POROS R1 10 resin (polystyrene-divinylbenzene beads, 10-µm particle size, Applied Biosystems) in 100% acetonitrile (ACN) at 500 psi, with the help of a high-pressure column-packing apparatus. The samples were dissolved in 20% 2-propanol/0.2% formic acid (FA), and loaded into a nanocapillary column connected to a nanoHPLC system (UltiMate® 3000 Nano LC, Dionex). The samples were eluted with a gradient of 20-80% 2-propanol containing 0.2% FA in the course of 90 min at a flow rate of 500 nL/min. Because of loading, conditioning, and washing steps, the total time for each step was 30 min (120 min total). The eluted molecules were directly analyzed in a Hybrid Quadrupole-Orbitrap mass spectrometer (Q-Exactive™, Thermo Fisher Scientific)

with a nanoelectrospray source (Nanospray Flex^{TM}, Thermo Fischer Scientific). Full MS scans were collected in positive-ion mode at the 400-1500 *m/z* range. The five most abundant ions from the survey scans (70,000 resolution) were selected for data-dependent fragmentation using higher energy collisional dissociation-type (HCD-type) fragmentation with a normalized collision energy (NCE) of 15 and a maximum injection time of 100 ms. Whenever a dynamic ion exclusion function was applied, it was set to collect each ion twice before it was excluded for 15 s, using an isolation window of 4-Th. The resolution of HCD spectra was set to 17,000. A flowchart summarizing the different steps involved in the GPIomics approach is provided bellow (**Fig. 14**).

3.2.6 - Structural assignment and relative quantification of GIPL and GPI species

All MS/MS spectra corresponding to different GIPL or GPI species were annotated manually, as described (138). Individual parent ions were plotted as extracted-ion chromatograms, and the resulting peaks were smoothed 7 times with the Gaussian method, using the Xcalibur software (Thermo Fisher Scientific). The relative quantification of different GIPL and GPI species was performed by comparing the area of the peak corresponding to each species to the sum of all areas corresponding to every species identified in each run. Results are expressed as percentage of total.

3.2.7 - GIPL and GPI monosaccharide compositional analysis

The GIPL and GPI monosaccharide compositional analysis was performed essentially as described by Ferguson (208). Briefly, one end of heat-cleaned 100-µl glass capillary tubes (Sigma-Aldrich) was flame-sealed with the aid of a small commercially available blowtorch. Each sample was pre-mixed with 1 nmol *scyllo*-inositol internal standard and dried in a vacuum centrifuge concentrator (Centrivap, Labconco). Twenty microliters of dry methanol were added to each sample and the mixture was dried again. The dehydrated samples were diluted in 50 µl 0.5 M HCl in dry methanol (Supelco, Sigma-Aldrich) and the glass tubes heat-sealed under vacuum. Then, the sealed tubes were placed in a heating block at 85°C for 4 h. The methanolysis was interrupted by breaking open one side of each tube and adding 10 µl pyridine to neutralize the HCl. Any free primary amines were *N*-acetylated through the addition of acetic anhydride. The samples were then dried on a Centrivap, diluted again in 20 µl methanol, and dried for a last time. After methanolysis, the samples were derivatized with trimethylsilanol (TMS) for 10 min through the addition of 15 µl of a mixture of hexamethyldisilazane:trimethylchlorosilane:pyridine (1.5:0.5:10 v/v/v). The gas chromatography-mass spectrometry (GC-MS) analysis was performed with a SE-54 column (30 m x 0.25 mm x 0.5 mm, Fisher Scientific) on a Trace GC (Thermo Fisher Scientific, Austin, TX) with the following running conditions: 140°C (2 min); 5°C/min gradient; 250°C (10 min) intermediate temperature; 15°C/min gradient II with a final temperature of 265°C/min (5 min). The carrier gas was helium, with a constant flow rate of 1.5 ml/min. The molecules were ionized by electron impact at 70 eV. Mass spectra acquisition was performed with a linear scanning at the 40-650 *m/z* range (Polaris Q, Thermo Fisher Scientific). Each sample was run at least three

times, and the sugar residues identified with the help of a monosaccharide standard mix, which were derivatized at the same time and under the exact conditions as the samples (209).

3.2.8 - Trypsin digestion of GPI-APs

After protein quantification, one mg of soluble proteins were precipitated with 10% trichloroacetic acid for 20 min in an ice bath, centrifuged at 16,000 xg for 20 min at 4°C, washed with ice-cold acetone, and dried in a vacuum centrifuge. Proteins were redissolved in 200 ul 0.4 M NH_4HCO_3 containing 8 M urea, and disulfide bounds were reduced with 5 mM dithiothreitol (DTT) for 15 min at 50°C. Then, cysteine residues were alkylated with 10 mM iodoacetamide (IA) for 30 min at room temperature, protected from light. Proteins were were digested with 20 µg sequencing-grade trypsin (Promega) for 24 h at 37°C. The reaction was stopped by the addition of 10 µL formic acid (FA). Peptides were then desalted in a C18-solid phase extraction cartridge (1 mL, Discovery DSC-18, Supelco, Sigma-Aldrich). The cartridge was activated with 4 mL methanol and equilibrated with 4 mL 0.05% trifluoroacetic acid (TFA). After loading and washing with 4 mL 0.05% TFA, the sample was eluted with 2 mL 80% ACN/0.05% TFA and dried in a vacuum centrifuge (Eppendorf).

3.3 Results

3.3.1 LC-ESI-MS/MS analysis of GIPLs and GIPs

Although the original GPIomics method was developed using an LTQXL ESI-linear ion trap-MS (ESI-LIT-MS) (Thermo Fisher Scientific) instrument, we conducted the current study using a Hybrid Quadrupole-Orbitrap mass spectrometer (Q-Exactive™, Thermo Fisher Scientific). This decision was based on the fact that the newer generation Hybrid Quadrupole-Orbitrap mass spectrometer outperforms the older LTQXL ESI-linear ion trap-MS because of the superior resolution and sensitivity observed for this type of instrument (210). The nano-HPLC system used was also changed from the 1D-Plus (Eksigent) to the newer UltiMate® 3000 Nano LC (Dionex) for similar reasons. We, therefore, included previously analyzed epimastigote-derived GPIs and GIPLs (eGPIs and eGIPLs, respectively) (138) to our analyses as a control.

In agreement with the original GPIomics work (138), we found that under the new experimental conditions GPIs and GIPLs also gave rise to predominantly doubly-charged ions ($[M + 2H]^{2+}$) in positive-ion mode ESI-MS in the presence of FA. With this information, we were able to filter our full MS scans using the neutral loss of -81 *m/z* (corresponding to the neutral loss of a hexose residue from a doubly-charged molecule). The neutral loss chromatograms showed that the UltiMate® 3000 Nano LC system provided for a good peak resolution, as exemplified in **Fig. 15**. Similar to what we had previously described, the POROS R1 resin led to the separation of the GIPL and GPI species based mostly on the hydrophobicity of their lipid moieties. Consequently, the species were resolved as "clusters" of peaks of similar retention times based on the length and number of unsaturations of their lipid moieties. Species containing either *lyso*-acyl- or *lyso*-alkylglycerol moieties eluted first, followed by species containing small ceramide (Cer) moieties. The next species to elute contained alkylacylglycerol

(AAG) moieties, and the last cluster of molecules to elute contained longer Cer moieties. As the molecules eluted from the column, they were immediately analyzed by full Scan-MS/MS (**Figs. 14 and 15**).

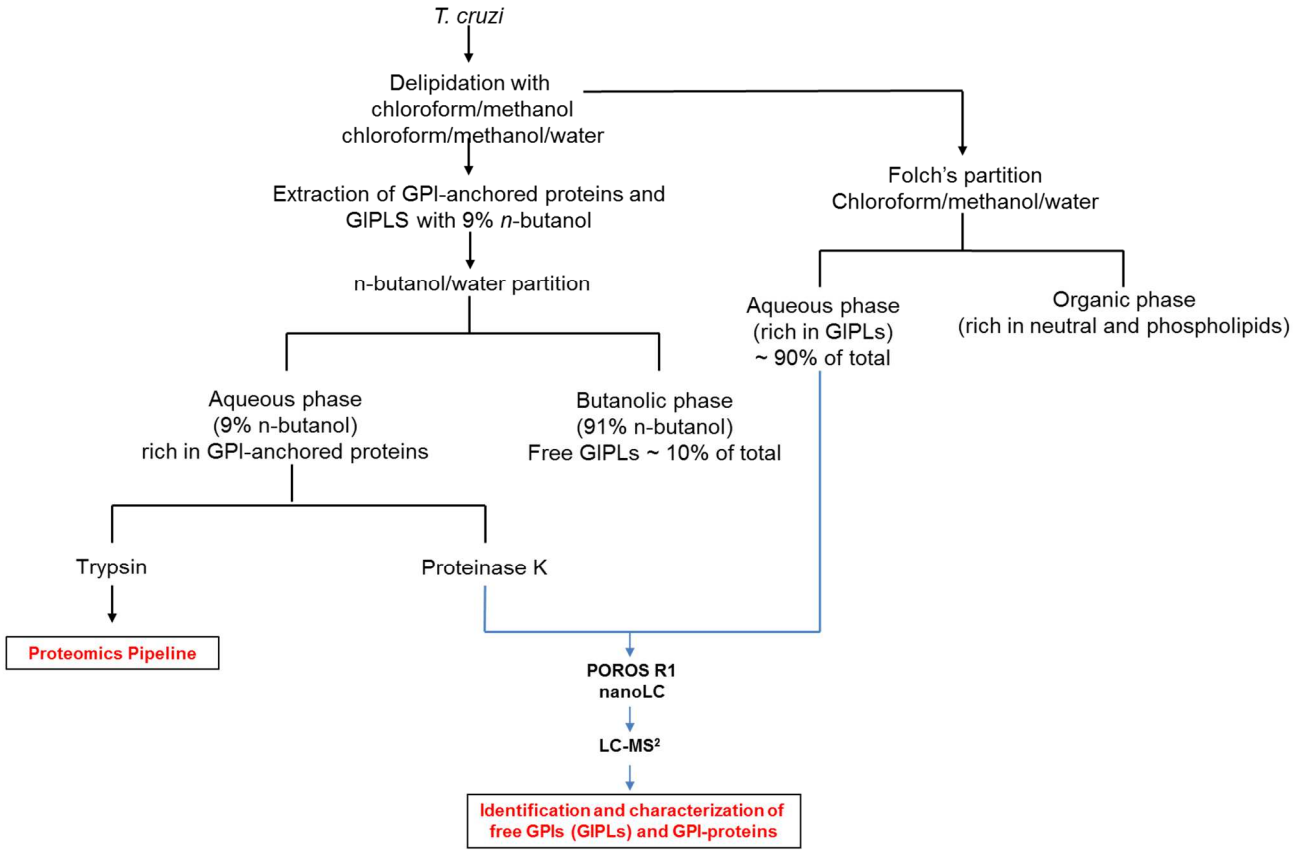

Figure 14: Schematic representation of the GPIomics methodology.

GPI-APs and GIPLs were extracted and processed as described in the Materials and Methods section. After extraction, GPI-APs digested with proteinase K and the Folch aqueous phase GIPLs were loaded into a POROS R1 column, and eluted with a 2-propanol gradient in the presence of 0.2% FA. The eluted samples were then analyzed by ESI-MS/MS in a Q-Exactive Hybrid Quadrupole-Orbitrap mass spectrometer. Acquired spectra were annotated manually. GPI-AP trypsin digests were processed and analyzed using a proteomics pipeline.

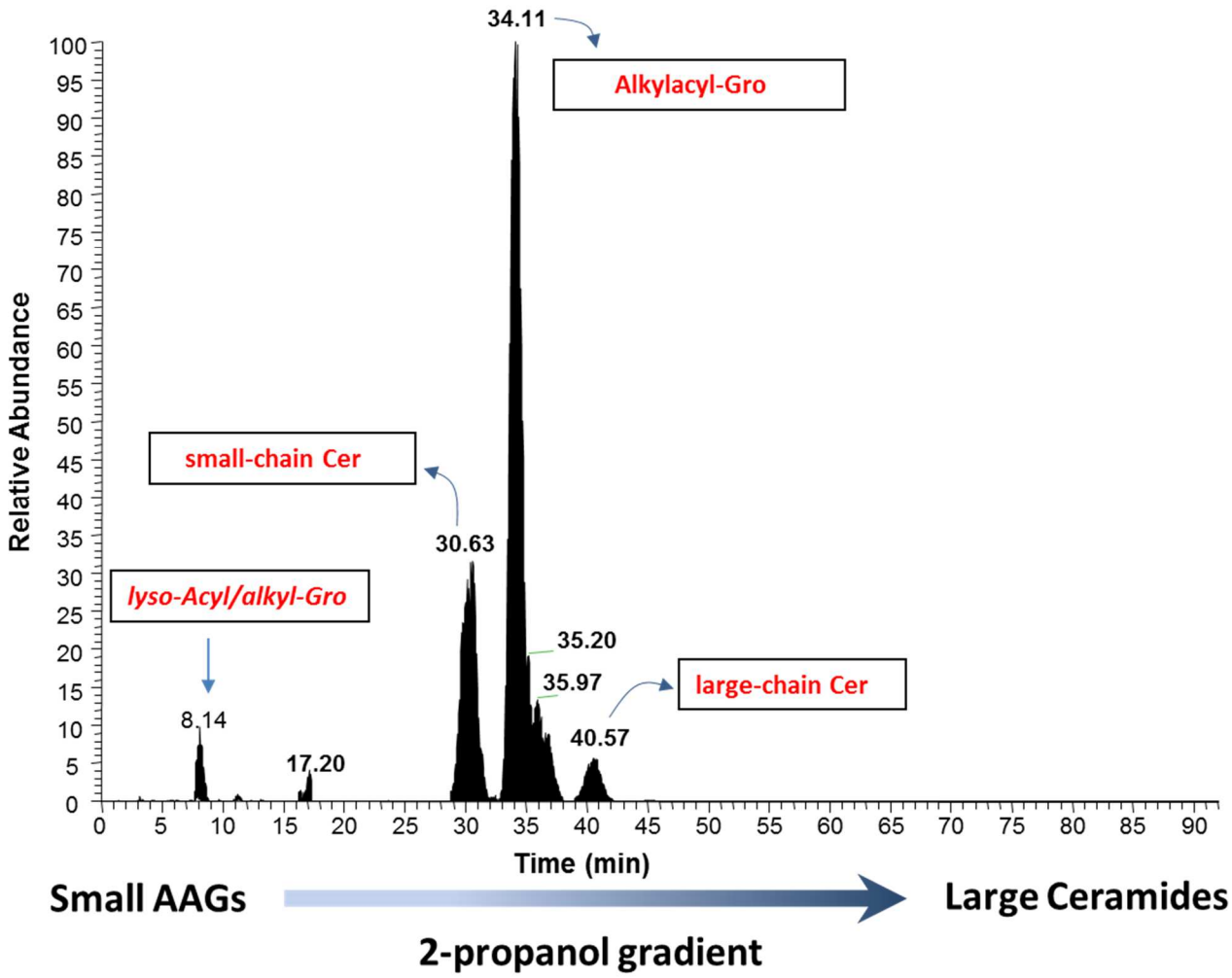

Figure 15: Representative chromatogram of ICA GIPLs.

T. cruzi ICA aqueous Folch phase GIPLs were extracted and subjected to LC-MS^n, following the steps described in the Materials and Methods section. The acquired data was plotted for the neutral loss of hexoses from a doubly-charged parent ion (neutral loss of -81 *m/z*). **Alkylacyl-Gro,** Alkylacylglycerol; **Cer,** ceramide; ***lyso*-Acyl/Alkyl-Gro,** *lyso*-Acyl- or *lyso*-alkylglycerol.

We next proceeded to carry out the manual annotation of all GIPL species found in the Folch upper phase (exemplified in **Fig. 16**) and of all GPIs found in the 9% *n*-butanol phase (exemplified in **Fig. 17**) of Epis, ICAs and TCTs. The HCD-type fragmentation of the doubly-charged ($[M + 2H]^{+2}$) GIPL parent-ions gave rise to fragments corresponding to the loss of the lipid moiety (usually either AAG or Cer), and to two series of ions corresponding to the neutral loss of multiple (usually *n*=1–6) hexose (Hex) residues. One of these series corresponds to the sequential loss of Hex residues from the doubly-charged parent ion (sequential loss of -81 *m/z* units), and the other series arises from to the sequential loss of Hex residues from the singly-charged ($[M + H]^{+}$) glycan moiety (sequential loss of -162 *m/z* units). Also of interest is the presence of a fragment at *m/z* 529.12, which corresponds to the *myo*-inositolphosphate (InsP) attached to the hexosamine (HexN) residue covalently bound to an aminoethylphosphonate (AEP) residue (AEP-HexN-InsP). Interestingly, unlike what we had described in Epis (138), most of the GIPL species derived from ICAs or TCTs had only one AEP residue (attached to HexN), instead of having either an additional AEP or an EtNP residue attached to a Hex residue (**Fig. 17**). Because of the Q-Exactive's high resolution, we were able to identify the lipid moiety with high confidence using MS^2 fragmentation alone. This identification was based on the presence of an abundant fragment-ion corresponding to a dehydrated lipid moiety, as well as to the presence of other fragments of this moiety, which can be observed in the lower ranges of the spectra (**Fig. 16**).

In general, doubly-charged GPIs gave rise to similar fragmentation patterns as to the ones described for GIPLs. The major difference between the MS^2 spectra derived from GPIs, as compared to the MS^2 spectra derived from GIPLs, comes from the fact that most GPIs have an EtNP residue attached to one of the Hex residues present on their glycan moieties. This gives rise

to a predominant fragment series corresponding to either an EtNP or AEP attached to multiple Hex residues (n=1-5). The dominant fragment in these series corresponds to either $[(EtNP)Hex_2 + H]^+$ (*m/z* 448.12) or to $[(AEP)Hex_2 + H]^+$ (*m/z* 432.12) (**Fig. 17**). These differences, however, are only observed in the mammal-dwelling ICA and TCT stages of the parasite, since we have confirmed previous observations that eGIPLs and eGPIs tend to nearly always have either an EtNP or an AEP residue linked to their glycan moieties (138).

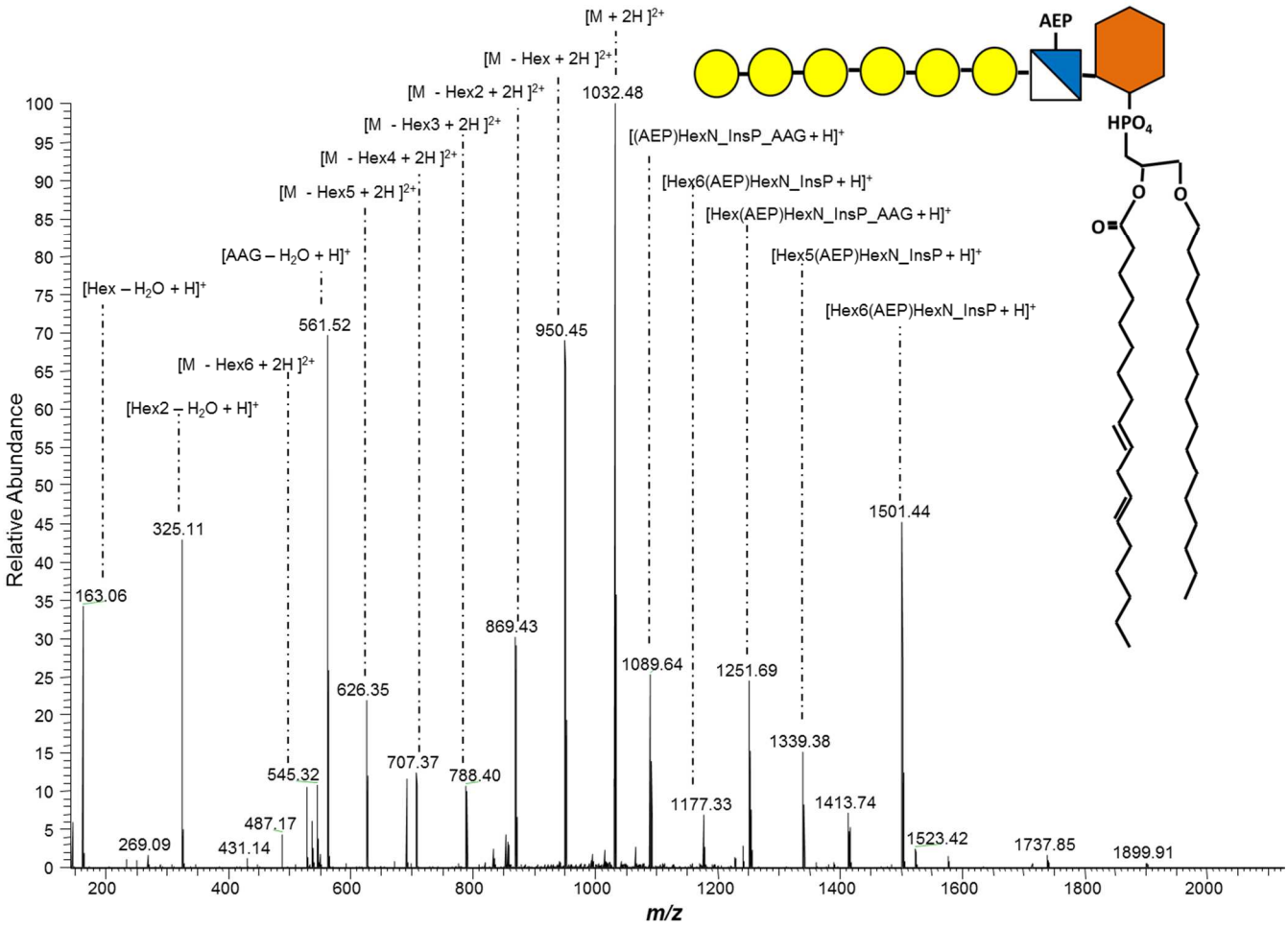

Figure 16: Representative annotated tandem MS spectrum of a *T. cruzi* trypomastigote GIPL.

T. cruzi GIPLs were mostly extracted in the Folch aqueous phase and submitted to LC-MS^n following the steps described in the Material and Methods section. Each peak corresponds to a different fragment of the same GIPL species (parent ion). The annotated spectrum corresponds to a GIPL with the following structure: Hex_6-(AEP)HexN-InsP-C16:0/C18:1-AAG (parent ion mass of 2060 a.m.u). The GIPL structure is represented on the top right corner of the figure. **AAG**, Alkylacylglycerol; **AEP**, aminoethylphosphonate**; Hex**, hexose; **HexN**, hexosamine; **InsP,** *myo*-inositolphosphate.

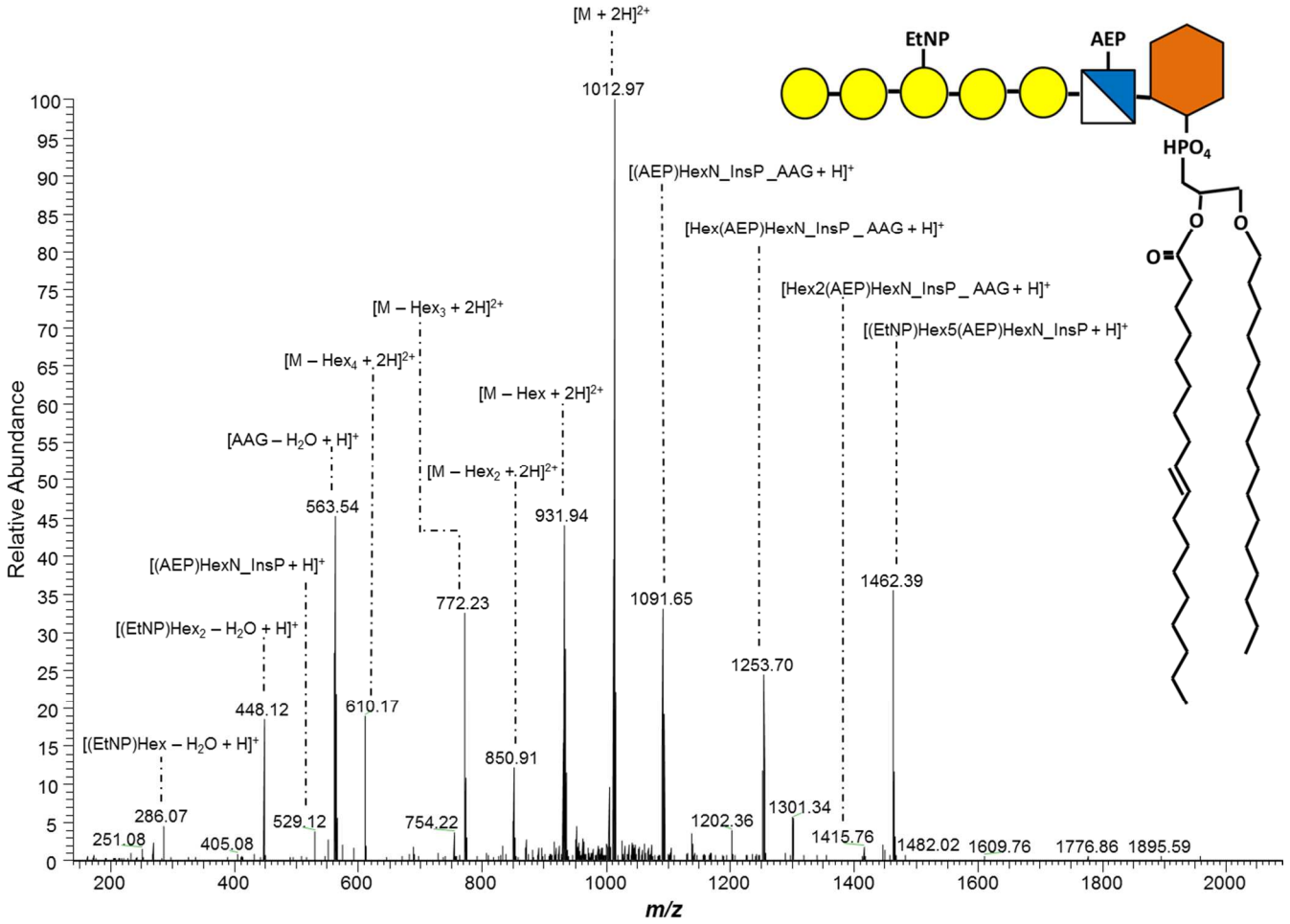

Figure 17: Representative annotated tandem MS spectrum of a *T. cruzi* trypomastigote GIPL.

T. cruzi TCT GPI-APs were extracted with 9% *n*-butanol and digested with proteinase K. Purified GPIs were then submitted to LC-MS^n following the steps described in the Material and Methods section. Each peak corresponds to a different fragment of the same GIPL species (parent ion). The annotated spectrum corresponds to a GIPL with the following structure: Hex_6-(AEP)HexN-InsP-C16:0/C18:1-AAG (parent ion mass of 2025.39 a.m.u.). The GIPL structure is represented on the top right corner of the figure. **AAG**, Alkylacylglycerol**; AEP**, aminoethylphosphonate; **EtNP**, Ethanolaminephosphate,; **Hex**, hexose; **HexN**, hexosamine; **InsP,** *myo*-inositolphosphate.

3.3.2 Trends in the structures of *T. cruzi* GIPLs and GPIs

Using this methodology, we were able to identify over 140 GIPL and GPI species from the three parasite life-cycle stages (i.e., Epi, ICA, and TCT) investigated in this study. Out of these, 44 had not been described to date. Interestingly, Epis had the largest GIPL and GPI diversity, but had the least number of species shared with any other life-cycle stages. Conversely, the mammal-dwelling (ICA and TCT) stages shared over 50% of their species in both GPI and GIPL fractions. GPI fractions were noticeably less diverse in TCTs and ICAs (tGPI and iaGPI, respectively) than in their GIPL counterparts (tGIPL and iaGIPLs, respectively), but were very diverse in Epis (**Fig. 18**).

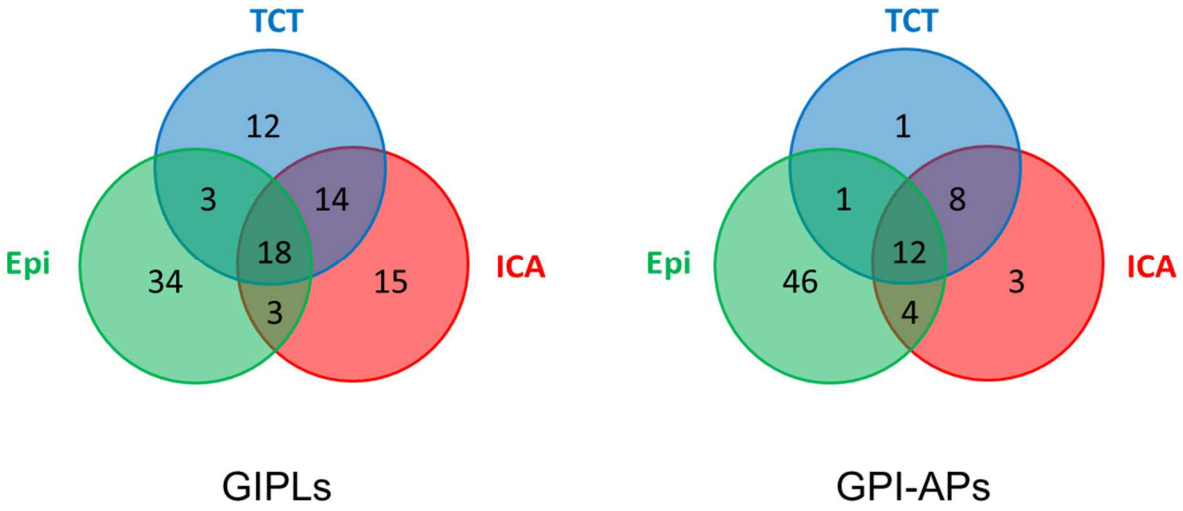

Figure 18: Distribution of the number of identified GIPLs and GPI-APs in the different *T. cruzi* life stages.

T. cruzi GIPLs obtained in the Folch aqueous phase and GPI-APs from the 9% *n*-butanol extraction submitted to LC-ESI-MS^2 following the steps described in the Materials and Methods section. The resulting MS^2 spectra were analyzed and annotated manually. All structures characterized in this work were grouped according to their distribution across the different parasite forms.

In order to better understand these trends, we performed the relative quantification of the different lipid and glycan moieties present in GIPLs and GPIs from each life-cycle stage of *T. cruzi*. To this end, the first analysis that we conducted was the determination of the relative abundance of lipid moieties composed of either Cer or AAG in GIPLs and GPIs derived from the three life-cycle stages of this parasite. We observed that GIPLs and GPIs from the mammal-dwelling (ICA and TCT) stages contain much higher levels of AAG lipid moieties than in Epis. In all cases, however, AAGs were more abundant in GPIs than in GIPLs, which is in agreement to other reports in the literature (79,138,193). As previously described (138,140,194,211,212), most eGIPL species identified here contain a Cer moiety. However, we also report appreciable levels of Cer-containing GPIs in this life-stage, which had not been observed in other studies (**Fig. 19**). We attribute this to the fact that we have used an instrument with much higher resolution than the instruments used in previous studies, which allowed us to identify the lipid moieties of these molecules with higher confidence. Also, the greater sensitivity of this instrument allowed for the identification of several low-abundance species which had not been previously described.

Next, we compared the most abundant lipid moieties of each of the three life-cycle stages aforementioned. Large structural differences were observed when the lipid moieties of the mammal-dwelling stages were compared to the moieties found in both eGIPLs and eGPIs. In general, tGIPLs and tGPIs were enriched in C16:0/C16:0-, C16:0/C18:1-, and C16:0/C18:2-AAGs. The levels of the latter two moieties were significantly larger in tGPIs than in tGIPLs. A similar trend was observed for iaGPIs and iaGIPLs, although their levels were not as expressive as the levels found in TCTs. Conversely, eGIPLs contained very low levels of AAG, with most of the species containing saturated fatty acids (primarily C16:0, C18:0, and C24:0). eGPIs had

significantly larger levels of AAG than eGIPLs, but also contained mostly saturated fatty acids. Conversely, eGIPLs contained predominantly a Cer moiety with d18:0 (sphinganine) sphingoid base and saturated fatty acid (mostly C16:0, C24:0, or C26:0), whereas eGPIs contained Cer with either d18:0- or d18:1- sphingoid base,mostly with a saturated fatty acid. Curiously, TCTs had no significant levels of Cer, but iaGIPLs contained a large amount of d18:0- and d18:1-sphingoid bases. iaGPIs also contained Cer, including high levels of C24:0/d18:1-Cer, which was significantly more abundant in this stage than in TCTs and ICAs. As a whole, the GIPLs and GPIs from the mammal-dwelling stages of this parasite tend to have significantly more lipid moieties containing unsaturated fatty acids than in Epis, which tend to have lipid moieties with predominantly saturated fatty acids (**Fig. 20**).

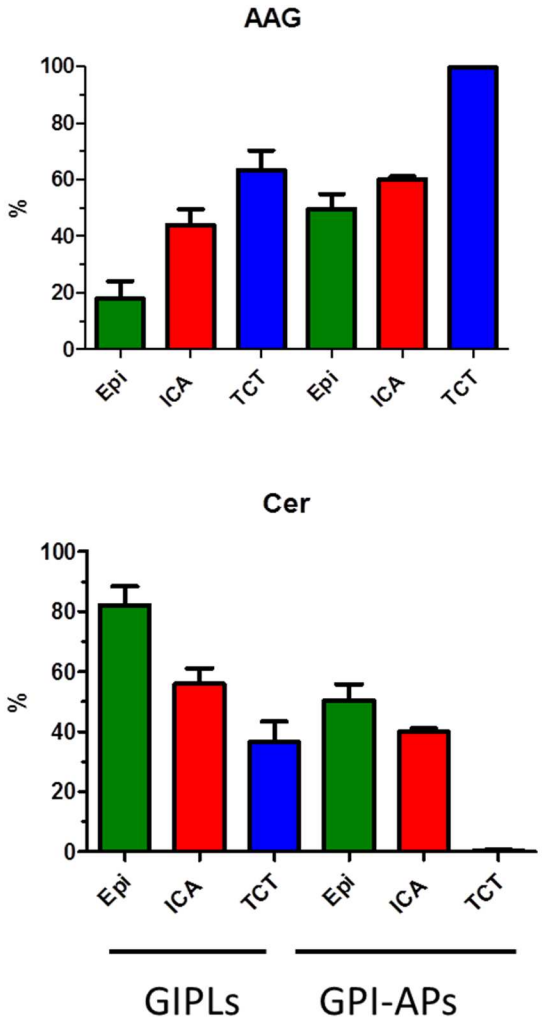

Figure 19: Ceramide and alkylacylglycerol lipid moiety distribution in different life-cycle stages of *T. cruzi*. GIPLs extracted in the Folch aqueous phase and GPI-APs obtained with 9% *n*-butanol were submitted to LC-ESI-MS^2 following the steps described in the Materials and Methods section. The relative quantification of different lipid moieties was performed by comparing the area of the peak corresponding to each GIPL or GPI species to the sum of all areas corresponding to every species identified in each nano-LC-MS run. Results are expressed as relative percentage of the total.

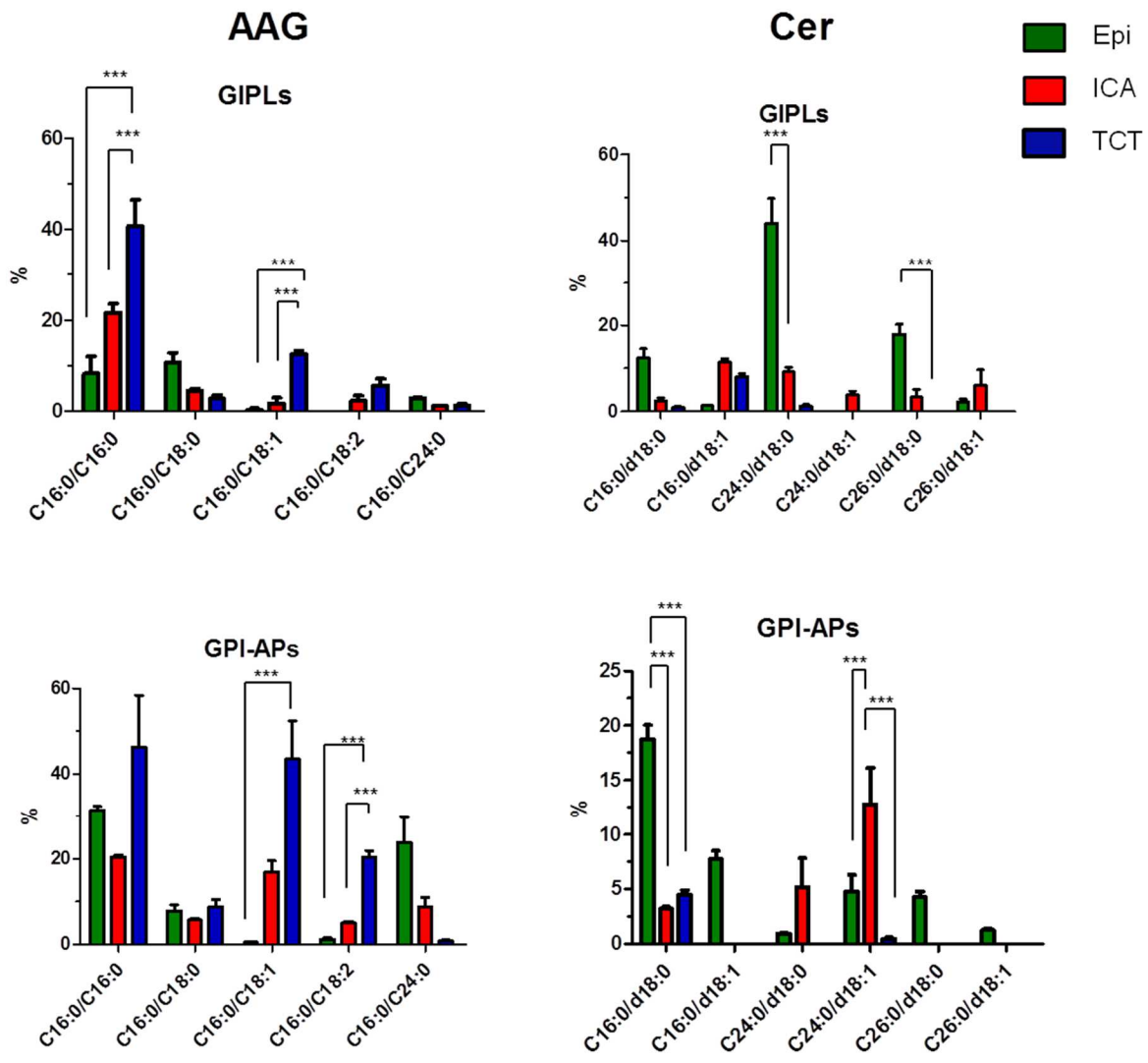

Figure 20: Distribution of the most abundant GIPL and GPI lipid moieties in different *T. cruzi* life-cycle stages. GIPLs obtained in the Folch aqueous phase and GPI-APs extracted with 9% *n*-butanol were submitted to LC-ESI-MS^2 following the steps described in the Materials and Methods section. The relative quantification of different lipid moieties was performed by comparing the area of the peak corresponding to each GIPL or GPI species to the sum of all areas corresponding to every species identified in each nano-LC-MS run. Results are expressed as relative percentage of the total**.** ***, $p<0.001$, using ANOVA statistical analysis

The analysis of the GIPL and GPI glycan moieties also showed significant differences between Epis and the mammal-dwelling ICA amd TCT stages of *T. cruzi*. As a whole, eGIPLs and eGPIs displayed almost no glycan diversity, with the vast majority of the species containing a glycan core of (EtNP)Hex_5(AEP)HexN-InsP (fragment at *m/z* 1462.39). tGIPLs and iaGIPLs have very similar glycan moiety distributions, and an overall larger diversity than eGIPLs. Also, the mammal-dwelling stages tend to have, on average, slightly larger glycan moieties than eGIPLs. As mentioned above, the vast majority of iaGIPLs and tGIPLs have no extra EtNP or AEP residue, which is present in most of the glycan moieties found in eGIPLs. In all cases, most GPIs derived from all life-cycle stages have a glycan core comprising (EtNP)Hex_5(AEP)HexN-InsP . However, the mammal-dwelling stages also have a high proportion of (EtNP)Hex_4(AEP)HexN-InsP) glycan core, which is significantly less abundant in eGPIs (**Fig. 21**). Curiously, we have also identified a few GIPLs containing 1-2 pentose residues, which had not been previously described. Monosaccharide compositional analysis by GC-MS revealed the presence of xylose (Xyl), but no other pentose, on GIPL and GPI fractions of the two mammal-dwelling stages of this parasite (**Fig. 22**).

These analyses allowed us to identify several GIPL and GPI structural features not shared between *T. cruzi* and their mammalian hosts (including humans) (summarized on **Table 4**). Of interest, we observed that AEP substituents bound to HexN (AEP-HexN) was present in nearly all GPI and GIPL species from the three life-cycle stages of this parasite. Other interesting features include the presence of Xyl on a few GIPL species, the high abundance of AAGs containing unsaturated fatty acid (C18:1 or C18:2), and the presence of α-Gal residues in GPIs and GIPLs derived from TCTs and ICAs.

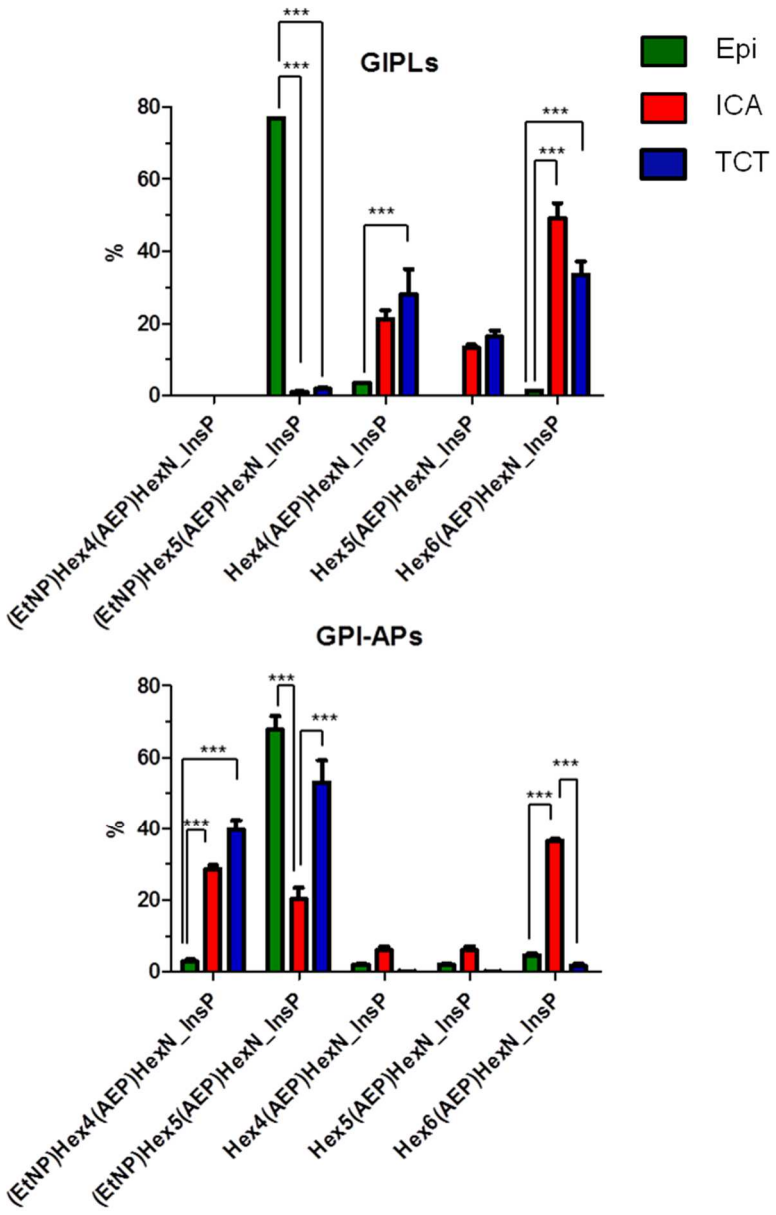

Figure 21: Distribution of the most abundant GIPL and GPI glycan moieties in different *T. cruzi* life-cycle stages.

Aqueous Folch phase GIPLs and 9% *n*-butanol GPI-APs were extracted, processed, and submitted to LC-ESI-MS^2 following the steps described in the Materials and Methods section. The relative quantification of different glycan moieties was performed by comparing the area of the peak corresponding to each GIPL or GPI species to the sum of all areas corresponding to every species identified in each nano-LC-MS run. Results are expressed as relative percentage of the total**.** ***, $p<0.001$, using ANOVA statistical analysis.

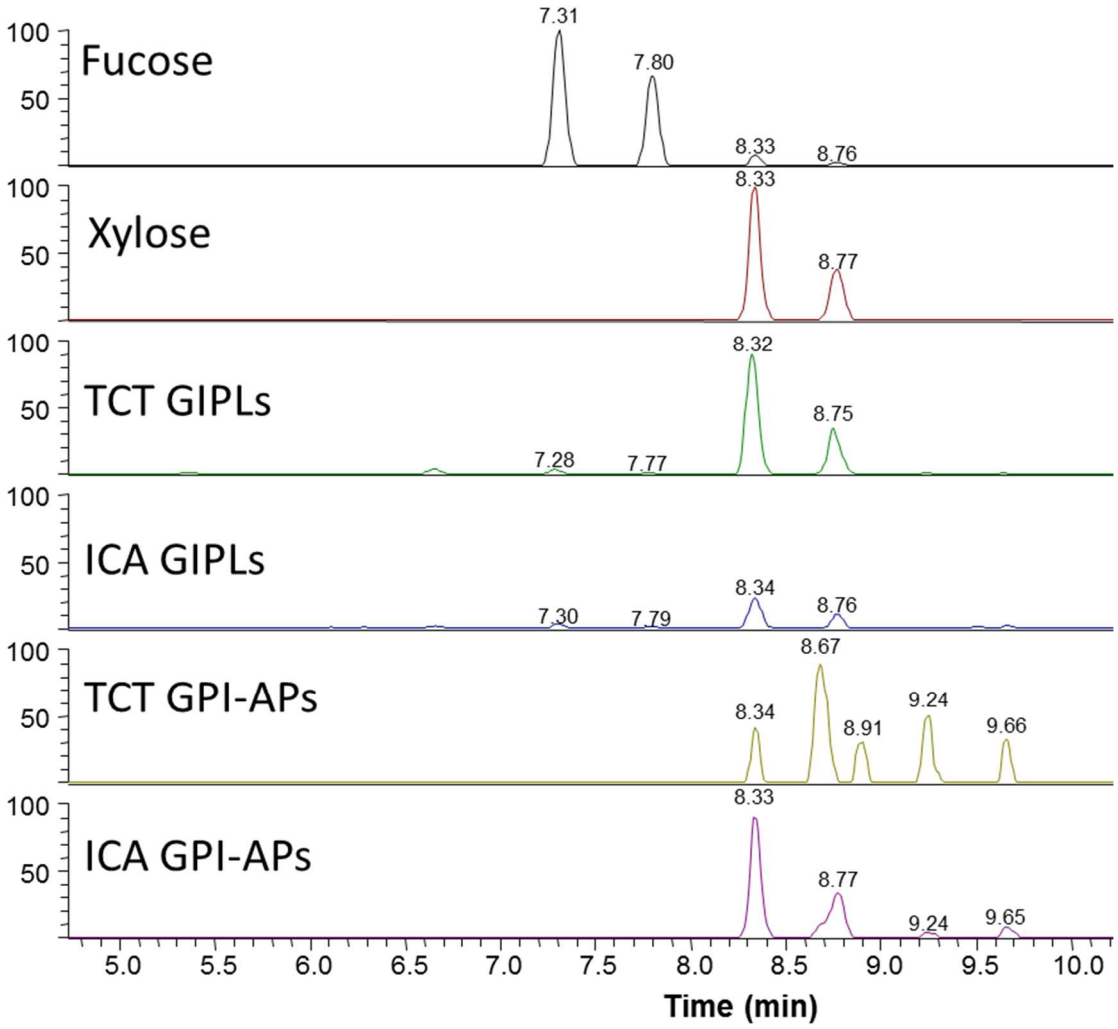

Figure 22: GPI and GIPL monosaccharide compositional analysis. GIPLs from the Folch aqueous phase and GPI-APs extracted with 9% *n*-butanol were processed according to the steps described in the Material and Methods section. The derivatized samples were analyzed by GC-MS, and peaks were identified according to their retention times and fragmentation pattern, as compared to an internal standard mix.

Table 4: Major structural differences between mammalian and *T. cruzi* GPIs.

Structural Feature	Mammalian Cell	*T. cruzi* (TCT and ICA)
Major Lipid Moieties	• AAG and DAG (usually containing saturated fatty acids)	• Cer and AAG (containing unsaturated fatty acids)
Glycan Chain	• βGalNAc • 3-4 Man residues	• α-Gal • Xylose • 5-6 residues
Major Substitutions	• *myo*-Inositol Acylation • EtNP (on Man 1-3)	• **AEP (HexN)**

T. cruzi GIPL structures were characterized using the GPIomic approach. Information about the structural features from mammalian GPIs was collected from available literature (65,139,142,143,177). The structural features unique to each group are indicated. **AAG**, alkylacylglycerol; **Cer,** ceramide; **DAG,** diacylglycerol; **EtNP**, ethanolaminephosphate; **AEP**, aminoethylphosphonate; **Man,** Mannose; **α-Gal**, α-Galactose; **β-GalNAc**, β-*N*-acetylgalactosamine.

Given the differences described above, we proceeded to compare the protein profile of the GPI-AP enriched fractions (9% *n*-butanol) from the three life-cycle stages of *T. cruzi* using a proteomics pipeline. To this end, we focused only on the proteins that had a high probability of being GPI-anchored according to the FragAnchor algorithm (University of Hawaii at Manoa) http://navet.ics.hawaii.edu/~fraganchor/NNHMM/NNHMM.html. In total, we identified 54 GPI-

APs, the majority of which were unique to the TCT stage. As was the trend for the GPIs and GIPLs, the mammal-dwelling stages shared the most number of proteins, and Epis shared the least number of proteins with any other life-stage. In fact, Epis had a very low abundance of GPI-APs (n=13) when compared to the other two stages (n= 49) (**Fig. 23**).

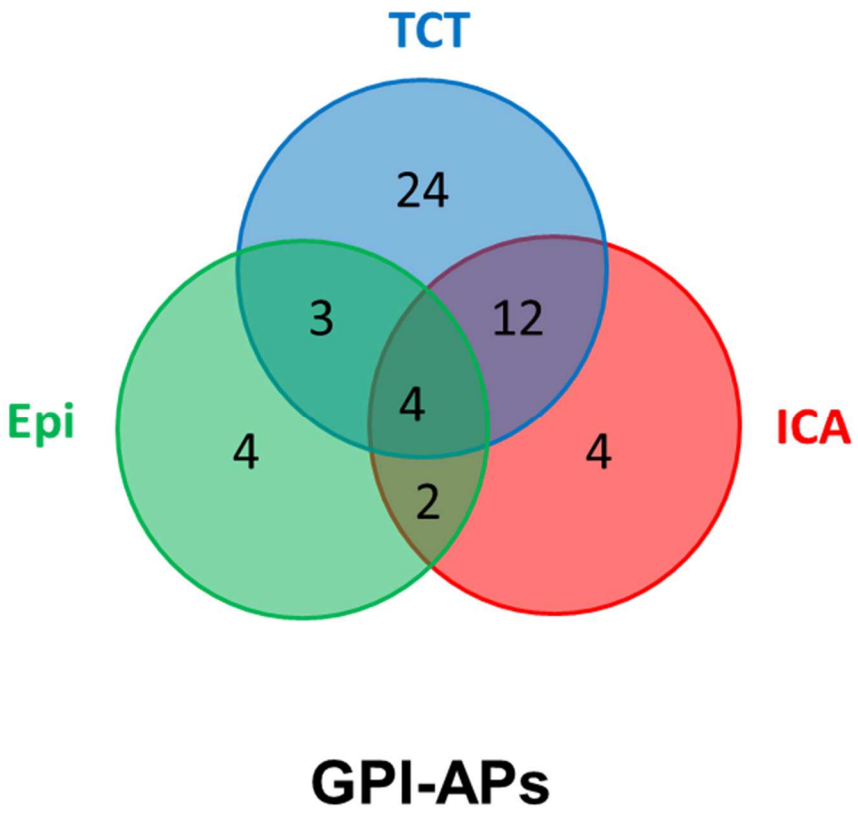

Figure 23: Distribution of the number of identified GPI-APs in the different life-cycle stages of *T. cruzi*.

T. cruzi GPI-APs were extracted with 9%*n*-butanol, digested with trypsin, and submitted to LC-ESI-MS/MS following the steps described in the Materials and Methods section. The resulting MS^2 spectra were analyzed using the Proteome Discoverer™ software (Thermo Scientific), followed by a second analysis using the Scaffold™ software (Proteome Software, Inc). *Bona fide* GPI-APs were identified using the FragAnchor software (University of Hawaii at Manoa, Information and Computer Sciences).

A more detailed analysis of these results showed that the majority of GPI-APs identified in TCTs belonged to the *trans*-sialidase (TS) multigene family. Other abundant GPI-APs in this stage included TolT3 and GP63. These results are in agreement with those by Nakayasu et al. (213). In spite of not having the same GPI-AP diversity as TCTs, ICAs had higher levels of MASPs and two uncharacterized proteins unique to this stage. These results are summarized on **Table 5**.

Table 5: *T. cruzi* GPI-APs identified by proteomic analysis of the 9% *n*-butanol fraction from Epi, ICA, and TCT stages.

		Total number of spectra counts[b]		
Identified Protein	**Accession Number[a]**	**Epi**	**ICA**	**TCT**
Trans-sialidase (TS) family				
Trans-sialidase, putative	Q4CSI1_TRYCC	0	0	236
Trans-sialidase, putative	Q4DVJ1_TRYCC	0	0	184
Trans-sialidase, putative	Q4CRR3_TRYCC	0	1	91
Trans-sialidase, putative	Q4CXS5_TRYCC	0	0	71
Trans-sialidase, putative	Q4CUU4_TRYCC	0	0	57
Trans-sialidase, putative	Q4CUS9_TRYCC	1	0	54
Trans-sialidase, putative	Q4D9H3_TRYCC	0	0	41
Trans-sialidase, putative	Q4CXW0_TRYCC	0	0	39
Trans-sialidase, putative	Q4CPW8_TRYCC	0	0	38
Trans-sialidase, putative	Q4CN26_TRYCC	0	0	35
Trans-sialidase, putative	Q4CTA6_TRYCC	0	0	35
Trans-sialidase, putative	Q4CSS2_TRYCC	0	9	33
Trans-sialidase, putative	Q4DLR5_TRYCC	0	0	30

Trans-sialidase, putative	Q4DQA2_TRYCC	0	1	29
Trans-sialidase, putative	Q4E1H2_TRYCC	0	0	28
Trans-sialidase, putative	Q4DCG7_TRYCC	0	1	27
Trans-sialidase, putative	Q4D2F9_TRYCC	0	0	22
Trans-sialidase, putative	Q4CRY2_TRYCC	0	1	13
Trans-sialidase, putative	Q4CQV3_TRYCC	0	0	9
Trans-sialidase, putative	Q4DVE4_TRYCC	1	3	0
TolT family				
Surface protein TolT, putative	Q4CNL2_TRYCC	0	10	81
Surface protein TolT, putative	Q4CM39_TRYCC	0	10	72
Surface protein TolT, putative	Q4CM38_TRYCC	0	0	51
TolT3	O96649_TRYCR	0	12	48
GP63 family				
Surface protease GP63, putative	Q4DVY4_TRYCC	0	0	34
Surface protease GP63, putative	Q4CQ32_TRYCC	0	0	12
Surface protease GP63, putative	Q4E479_TRYCC	0	0	5
MASP family				
Mucin-associated surface protein (MASP), putative	Q4CS13_TRYCC	0	6	6
Mucin-associated surface protein (MASP), putative	Q4DYV1_TRYCC	0	1	4
Mucin-associated surface protein (MASP), putative	Q4DM97_TRYCC	0	7	0
Mucin-associated surface protein (MASP), putative	Q4DKW6_TRYCC	0	3	0
Mucin family				
Mucin TcMUCII, putative	Q4E483_TRYCC	0	5	2
Mucin TcMUCII, putative	Q4E284_TRYCC	0	4	1
TASV family				
Surface antigen TASV, putative,mucin-like glycoprotein, putative	K2NK03_TRYCR	3	4	0

Vesicle-associated membrane protein, putative	K4DKF0_TRYCR	4	3	13
Uncharacterized proteins				
Uncharacterized protein	Q4E1W3_TRYCC	0	0	12
Uncharacterized protein	Q4E1V5_TRYCC	0	0	5
Uncharacterized protein	K2MMA3_TRYCR	0	1	3
Uncharacterized protein	K4DXF9_TRYCR	0	31	0
Uncharacterized protein	Q4DXT4_TRYCC	0	7	0
Uncharacterized protein	K4DKF3_TRYCR	0	5	0
Uncharacterized protein	Q4DIA5_TRYCC	2	3	0
Uncharacterized protein	V5BPJ5_TRYCR	3	0	0

[a] UniProt database

[b] The total number of spectral counts gives a semi-quantitative idea about the abundance of the identified protein.

3.4 Discussion

Here, we have successfully implemented the modified GPIomic approach to characterize for the first time the GPIome of the mammal-dwelling stages of *T. cruzi*, including the first descriptions of ICA- and TCT-derived GPIs. As mentioned above, we have described 140 GPI/GIPL species, many of which are novel to the literature. It is clear from this study that GIPLs and GPI-APs from TCTs and ICAs share many structural features not found in appreciable levels in GIPLs/GPIs derived from Epis. These features include the enrichment in AAG lipid moieties containing unsaturated fatty acid (C18:1 or C18:2). This is especially noticeable in GPI-AP fractions, as previously described (140,141). eGIPLs and eGPIs, on the other hand, tend to either have ceramide moieties or AAG moieties with saturated fatty acid substituents (mostly C16:0 or C18:0) (79,138,214). The presence of mature GPIs with AAG moieties containing unsaturated fatty acids is in stark contrast to what has been described in *T. brucei*, *P. falciparum, Leishmania spp.*, yeast, *T. gondii* and in mammals. In most cases, the lipid moieties of GPIs are either composed of diacylglycerol (DAG) (mammals, *T. brucei, Plasmodium falciparum and T. gondii*) or AAG containing a saturated fatty acid substituent, as observed in*T. cruzi* epimastigotes, *Leishmania ssp.* and mammals (143,144,154,176,177). Unlike TCTs, ICAs also express high levels of Cer-containing GPIs. TheseCer moieties, however, tended to have much longer fatty acid substituents than in Epis. GPIs containing Cer moieties are rarely found, having only been described in *T. cruzi* (79,138,214,215), *Saccharomyces cerevisae* (216), and *Dictyostelium discoideum* (217).

The large structural differences between the mature GPIs and GIPLs derived from Epis, ICAs, and TCTs suggest that *T. cruzi* is able to regulate several of the steps involved in the GPI and GIPL biosynthetic pathway, so theparasite can adapt to the specific needs of each of its life-cycle stages. To date, very little is known about the GPI and GIPL biosynthetic pathway in *T. cruzi*. Recently, a study was conducted to characterize genes encoding for key components of the GPI/GIPL biosynthetic pathway in this species, based on their sequence similarity to orthologous genes found in yeast, mammals, *T. brucei,* and *P. falciparum*. Using yeast complementation and cellular localization studies, the authors were able to identify 18 components of this pathway (218). Interestingly, in spite of the structural differences between the mature GPIs and GIPLs derived from the three parasite life-stages, all 18 genes described in that study were constitutively expressed in all life-stages of *T. cruzi*. This suggests that the structural differences found in the GIPLs and GPIs from the different stages of this parasite are not generated through a mechanism dependent on the regulation of the levels of distinct protein components of the GPI and GIPL biosynthetic pathway. We suggest that these differences might be achieved through changes in substrate availability and in post-translational modifications affecting the activity of different components of the GIPL and GPI biosynthetic machinery. These changes in substrate availability can be partially explained from the fact that Epis and the mammal-dwelling stages of this parasite inhabit very different environments. It has been shown, for instance, that the metabolism of ICAs and of their host cells are interconnected (219). On that study, it was shown that parasite survival is dependent on cofactors and metabolites incorporated from the host cells. Considering the striking differences in the extracellular environment of the insect-dwelling and mammalian-dwelling stages of this parasite, is would be reasonable to assume that each stage of this parasite would have access to very different precursors for GPI and GIPL synthesis. Similar

results were recently found by Kleohn et al. in *Leishmania mexicana* (220). These authors showed that intracellular amastigote stages were able to incorporate $^{2}H_2O$-labeled pentose sugars, fatty acids, and amino acids from macrophages in the murine footpad lesion. Interestingly, lesion-derived parasite showed a considerably lower growth rate, strongly suggesting a refined adaptive strategy to survive within the host for longer periods without activating immune defense mechanisms.

As aforementioned, one of the most remarkable differences between the GIPLs and GPIs derived from the different life-stages of *T. cruzi* lies on their lipid moieties. In general, it has been described that GPI precursors in mammals and in yeast tend to have AAG moieties with an unsaturated fatty acid at the *sn*-2 position (usually, arachidonic acid, C20:4), which is substituted by a saturated fatty acid (usually, C18:0) during the lipid remodeling stage that takes place after the covalent attachment of the GPI to the mature protein C-terminus. This also happens to yeast, despite the fact that several GPIs suffer a more drastic AAG to Cer substitution (185,221,222). *T. brucei* GPIs are also remodeled, with the mature structure having mostly a dimyristoyl- (C14:0/C14:0) DAG moiety (143). Recent studies show that this fatty acid remodeling takes place during trafficking of GPI-APs from the Golgi network to the plasma membrane, and that a disruption in this remodeling leads to intracellular GPI-AP accumulation (143,144,185,222). Many authors suggest that the presence of the straight saturated lipid chains of these mature GPIs is required for their lipid-raft association, which is hypothesized to be an important determinant of their biological function (144,223). This theory would agree well with the data we have described for *T. cruzi* Epis (138), and with what has been described for metacyclic trypomastigotes (79), but not with what we describe in ICAs and TCTs. The prevalence of AAG moieties containing unsaturated fatty acids would suggest that either *T. cruzi* makes use of a

different sorting mechanism, or that the association of GPI-APs to lipid rafts is not a dominant feature of these parasites. We have in the past, however, shown that the presence of these unsaturated fatty acids is relevant for the production of proinflammatory cytokines by host immune cells, through the activation of Toll-like receptor 2 (TLR2) (140,141,160). It is possible that the relevance of unsaturated fatty acid substituents during infection outweighs any potential benefits involved in the association of *T. cruzi*-derived GPI-APs to lipid rafts, or that having GIPLs and GPI-APs uniformely distributed across the membrane is in itself beneficial to these parasites.

The enzymatic machinery involved in the GPI lipid remodeling pathway has not yet been fully described in any organism. It is, however, known that the first steps in the lipid remodeling pathway in mammalian CHO cells requires a PLA_2 activity to remove the unsaturated fatty acid from the GPI precursor, and of an acyltransferase activity to generate a mature GPI containing a saturated fatty acid at the *sn*-2 position of its glycerol backbone. In these organisms it is known that either the *p*ost-*G*PI *a*ttachment to *p*roteins *2* (PGAP2) by itself or a complex containing this protein is involved in both of these steps (224). The same observation has also been made for the yeast PGAP2 homolog, GUp1p, which is important for both AAG remodeling and for the enzymatic steps that will lead to ceramide remodel (225). Both of these proteins belong to the membrane-bound-*O*-acyltransferase (MBOAT) family, which are speculated to have an affinity for saturated fatty acids (223,225,226). Although only a few studies have been conducted to describe the structure of GPI precursors in *T. cruzi*, it is known from classic experiments that these precursors have AAG moieties that closely resemble the AAG moieties from *T. brucei* GPI precursors (227). In this case, the lipid remodeling in Epis could take place through similar steps as those described for *T. brucei*, yeast, and in mammals. It is possible that *T. cruzi* has a PGAP2

ortholog, which would be involved in the deacylation of the fatty acid at the *sn*-2 position of the AAG moiety of the GPI precursors from Epis, and of reacylating it with a saturated fatty acid (C16:0 or C18:0). We have so far formulated two hypotheses that would explain the presence of unsaturated fatty acids in mature GPIs/GIPLs from the mammal-dwelling stages of *T. cruzi*. The first hypothesis is that the putative *T. cruzi* PGAP2 homolog, or another protein in the complex, is either not expressed or inactive in TCTs and ICAs. In this case, the deacylation step of the remodeling pathway would not take place, and the mature GPIs/GIPLs would retain their unsaturated fatty acid moiety. The other alternative is that the GPI/GIPL precursors in the mammal-dwelling stages of this parasite retain the *myo*-inositol-ring acylation for a longer time than in Epis. The presence of this modification would hinder the PLA_2 from the remodeling machinery, also leading to the expression of mature GPI/GIPLs retaining the unsaturated fatty acid at the *sn*-2 position of the AAG moiety. This would be in agreement with observations that some mature GPI-APs (i.e., Tc-85 surface glycoproteins) in *T. cruzi* trypomastigotes retain a fatty acid substitution at the C-2 position of their *myo*-inositol (228). Both hypotheses have the benefit of being parsimonious, since we are proposing that the differences between the structure of GPIs/GIPLs from Epis and the mammalian-dwelling stages of *T. cruzi* can be explained by the absence of one enzymatic activity. This would make it more difficult, however, for the GPI/GIPL lipid remodeling in the mammal-dwelling stages of *T. cruzi* to be explored for the development of new therapies for Cd.

The presence of Cer moieties on GIPLs and GPIs from *T. cruzi* have also been proposed as potential targets for the development of novel drugs for Cd. This idea comes from studies that show that GPIs derived from Metas are enriched in Cer moieties, and that the incorporation of said moieties to nascent GPIs require the *de novo* synthesis of sphingoid bases (79,229,230).

Also, it has been shown that several steps in the biosynthesis of sphingolipids in *T. cruzi* are not shared with mammals (230). Although we agree that this might be a sound strategy to prevent vector-borne transmission of *T. cruzi* to humans, we do not believe that this would be a good approach to the treatment of chronic Cd. The reasons for this are that our results show that neither TCTs nor ICAs have high levels of Cer-containing GIPLs and GPIs, and that there is no evidence that these two life-cycle stages would rely as heavily on the *de novo* Cer synthesis as is the case for the insect-dwelling stages. We suggest that a better target for the development of novel therapies for Cd should at the same time be relevant for parasite infectivity and survival in the human host, be conserved and ubiquitous in the mammal-dwelling stages of the parasite, and not be shared with the mammalian host.

The GPIome of the mammal-dwelling stages of this parasite confirmed the observations made in Epis, where over 99% of GIPL and GPI species in *T. cruzi* contain an AEP substitution bound to the GlcN residue of their conserved glycan core (138,192-194). The fact that this modification is highly conserved suggests that it might play an important function in either parasite survival and/or during infection. As mentioned above, we also hypothesize that this modification could play an analogous role as that of the addition of EtNP to the second mannose residue of nascent GPI-APs in mammalian cells (144), where it is believed to serve as part of a quality control mechanism. We believe that further research in conserved structural features of lipids and glycolipids not shared between *T. cruzi* and humans could lead to the development of new therapies for Cd. Here, we suggest that one of these potential targets would be the AEP biosynthetic pathway (not present in mammals) responsible for the generation of the AEP residue that is covalently attached to the GlcN residue of great majority of *T. cruzi* GIPLs and GPIs

4. REFERENCES

1. Rassi, A., Jr., Rassi, A., and Marin-Neto, J. A. (2010) Chagas disease. *Lancet* **375**, 1388-1402
2. Coura, J. R., and Borges-Pereira, J. (2010) Chagas disease: 100 years after its discovery. A systemic review. *Acta tropica* **115**, 5-13
3. Bellini, M. F., Silistino-Souza, R., Varella-Garcia, M., de Azeredo-Oliveira, M. T., and Silva, A. E. (2012) Biologic and genetics aspects of chagas disease at endemic areas. *Journal of tropical medicine* **2012**, 357948
4. Perez-Molina, J. A., Norman, F., and Lopez-Velez, R. (2012) Chagas disease in non-endemic countries: epidemiology, clinical presentation and treatment. *Current infectious disease reports* **14**, 263-274
5. Custer, B., Agapova, M., Bruhn, R., Cusick, R., Kamel, H., Tomasulo, P., Biswas, H., Tobler, L., Lee, T. H., Caglioti, S., and Busch, M. (2012) Epidemiologic and laboratory findings from 3 years of testing United States blood donors for Trypanosoma cruzi. *Transfusion* **52**, 1901-1911
6. Schmunis, G. A. (2007) Epidemiology of Chagas disease in non-endemic countries: the role of international migration. *Memorias do Instituto Oswaldo Cruz* **102 Suppl 1**, 75-85
7. Castro, J. A., de Mecca, M. M., and Bartel, L. C. (2006) Toxic side effects of drugs used to treat Chagas' disease (American trypanosomiasis). *Human & experimental toxicology* **25**, 471-479
8. Tanowitz, H. B., Machado, F. S., Jelicks, L. A., Shirani, J., de Carvalho, A. C., Spray, D. C., Factor, S. M., Kirchhoff, L. V., and Weiss, L. M. (2009) Perspectives on Trypanosoma cruzi-induced heart disease (Chagas disease). *Progress in cardiovascular diseases* **51**, 524-539
9. Combs, T. P., Nagajyothi, Mukherjee, S., de Almeida, C. J., Jelicks, L. A., Schubert, W., Lin, Y., Jayabalan, D. S., Zhao, D., Braunstein, V. L., Landskroner-Eiger, S., Cordero, A., Factor, S. M., Weiss, L. M., Lisanti, M. P., Tanowitz, H. B., and Scherer, P. E. (2005) The adipocyte as an

important target cell for Trypanosoma cruzi infection. *The Journal of biological chemistry* **280**, 24085-24094

10. Mukherjee, S., Machado, F. S., Huang, H., Oz, H. S., Jelicks, L. A., Prado, C. M., Koba, W., Fine, E. J., Zhao, D., Factor, S. M., Collado, J. E., Weiss, L. M., Tanowitz, H. B., and Ashton, A. W. (2011) Aspirin treatment of mice infected with *Trypanosoma cruzi* and implications for the pathogenesis of Chagas disease. *PloS one* **6**, e16959
11. Carod-Artal, F. J., Vargas, A. P., Horan, T. A., and Nunes, L. G. (2005) Chagasic cardiomyopathy is independently associated with ischemic stroke in Chagas disease. *Stroke* **36**, 965-970
12. Gourbiere, S., Dorn, P., Tripet, F., and Dumonteil, E. (2012) Genetics and evolution of triatomines: from phylogeny to vector control. *Heredity* **108**, 190-202
13. Yeagle, P. L. (1989) Regulation of membrane function through composition, structure, and dynamics. *Annals of the New York Academy of Sciences* **568**, 29-34
14. Yeagle, P. L. (1989) Lipid regulation of cell membrane structure and function. *FASEB journal : official publication of the Federation of American Societies for Experimental Biology* **3**, 1833-1842
15. Wenk, M. R. (2005) The emerging field of lipidomics. *Nature reviews. Drug discovery* **4**, 594-610
16. Watson, A. D. (2006) Thematic review series: systems biology approaches to metabolic and cardiovascular disorders. Lipidomics: a global approach to lipid analysis in biological systems. *Journal of lipid research* **47**, 2101-2111
17. Boullier, A., Friedman, P., Harkewicz, R., Hartvigsen, K., Green, S. R., Almazan, F., Dennis, E. A., Steinberg, D., Witztum, J. L., and Quehenberger, O. (2005) Phosphocholine as a pattern recognition ligand for CD36. *Journal of lipid research* **46**, 969-976

18. Hu, C., van der Heijden, R., Wang, M., van der Greef, J., Hankemeier, T., and Xu, G. (2009) Analytical strategies in lipidomics and applications in disease biomarker discovery. *Journal of chromatography. B, Analytical technologies in the biomedical and life sciences* **877**, 2836-2846

19. Muro, E., Atilla-Gokcumen, G. E., and Eggert, U. S. (2014) Lipids in cell biology: how can we understand them better? *Molecular biology of the cell* **25**, 1819-1823

20. Fahy, E., Subramaniam, S., Brown, H. A., Glass, C. K., Merrill, A. H., Jr., Murphy, R. C., Raetz, C. R., Russell, D. W., Seyama, Y., Shaw, W., Shimizu, T., Spener, F., van Meer, G., VanNieuwenhze, M. S., White, S. H., Witztum, J. L., and Dennis, E. A. (2005) A comprehensive classification system for lipids. *Journal of lipid research* **46**, 839-861

21. Fahy, E., Subramaniam, S., Murphy, R. C., Nishijima, M., Raetz, C. R., Shimizu, T., Spener, F., van Meer, G., Wakelam, M. J., and Dennis, E. A. (2009) Update of the LIPID MAPS comprehensive classification system for lipids. *Journal of lipid research* **50 Suppl**, S9-14

22. Ruiz-Rodriguez, A., Reglero, G., and Ibanez, E. (2010) Recent trends in the advanced analysis of bioactive fatty acids. *Journal of pharmaceutical and biomedical analysis* **51**, 305-326

23. Funk, C. D. (2001) Prostaglandins and leukotrienes: advances in eicosanoid biology. *Science* **294**, 1871-1875

24. Calder, P. C. (2008) Polyunsaturated fatty acids, inflammatory processes and inflammatory bowel diseases. *Molecular nutrition & food research* **52**, 885-897

25. Lands, W. E. (2000) Stories about acyl chains. *Biochimica et biophysica acta* **1483**, 1-14

26. Kuzuyama, T., and Seto, H. (2003) Diversity of the biosynthesis of the isoprene units. *Natural product reports* **20**, 171-183

27. Demmig-Adams, B., and Adams, W. W., 3rd. (2002) Antioxidants in photosynthesis and human nutrition. *Science* **298**, 2149-2153

28. Ricciarelli, R., Zingg, J. M., and Azzi, A. (2001) Vitamin E: protective role of a Janus molecule. *FASEB journal : official publication of the Federation of American Societies for Experimental Biology* **15**, 2314-2325

29. Meganathan, R. (2001) Biosynthesis of menaquinone (vitamin K2) and ubiquinone (coenzyme Q): a perspective on enzymatic mechanisms. *Vitamins and hormones* **61**, 173-218

30. Meganathan, R. (2001) Ubiquinone biosynthesis in microorganisms. *FEMS microbiology letters* **203**, 131-139

31. Helenius, A., and Aebi, M. (2001) Intracellular functions of N-linked glycans. *Science* **291**, 2364-2369

32. Schenk, B., Fernandez, F., and Waechter, C. J. (2001) The ins(ide) and out(side) of dolichyl phosphate biosynthesis and recycling in the endoplasmic reticulum. *Glycobiology* **11**, 61R-70R

33. Lazar, K., and Walker, S. (2002) Substrate analogues to study cell-wall biosynthesis and its inhibition. *Current opinion in chemical biology* **6**, 786-793

34. Wollam, J., and Antebi, A. (2011) Sterol regulation of metabolism, homeostasis, and development. *Annual review of biochemistry* **80**, 885-916

35. Bach, D., and Wachtel, E. (2003) Phospholipid/cholesterol model membranes: formation of cholesterol crystallites. *Biochimica et biophysica acta* **1610**, 187-197

36. Tsai, M. J., and O'Malley, B. W. (1994) Molecular mechanisms of action of steroid/thyroid receptor superfamily members. *Annual review of biochemistry* **63**, 451-486

37. Carreira, A. C., Ventura, A. E., Varela, A. R., and Silva, L. C. (2015) Tackling the biophysical properties of sphingolipids to decipher their biological roles. *Biological chemistry*

38. Stam, H., Schoonderwoerd, K., and Hulsmann, W. C. (1987) Synthesis, storage and degradation of myocardial triglycerides. *Basic research in cardiology* **82 Suppl 1**, 19-28

39. Goldberg, I. (1996) Lipid metabolism. *Current opinion in lipidology* **7**, U184-192

40. Stanley, W. C., Lopaschuk, G. D., and McCormack, J. G. (1997) Regulation of energy substrate metabolism in the diabetic heart. *Cardiovascular research* **34**, 25-33

41. Fernandis, A. Z., and Wenk, M. R. (2007) Membrane lipids as signaling molecules. *Current opinion in lipidology* **18**, 121-128

42. Hishikawa, D., Hashidate, T., Shimizu, T., and Shindou, H. (2014) Diversity and function of membrane glycerophospholipids generated by the remodeling pathway in mammalian cells. *Journal of lipid research* **55**, 799-807

43. Hermansson, M., Hokynar, K., and Somerharju, P. (2011) Mechanisms of glycerophospholipid homeostasis in mammalian cells. *Progress in lipid research* **50**, 240-257

44. Aliberti, J. C., Machado, F. S., Gazzinelli, R. T., Teixeira, M. M., and Silva, J. S. (1999) Platelet-activating factor induces nitric oxide synthesis in *Trypanosoma cruzi*-infected macrophages and mediates resistance to parasite infection in mice. *Infection and immunity* **67**, 2810-2814

45. Ashton, A. W., Mukherjee, S., Nagajyothi, F. N., Huang, H., Braunstein, V. L., Desruisseaux, M. S., Factor, S. M., Lopez, L., Berman, J. W., Wittner, M., Scherer, P. E., Capra, V., Coffman, T. M., Serhan, C. N., Gotlinger, K., Wu, K. K., Weiss, L. M., and Tanowitz, H. B. (2007) Thromboxane A2 is a key regulator of pathogenesis during *Trypanosoma cruzi* infection. *The Journal of experimental medicine* **204**, 929-940

46. Mesquita, R. D., Carneiro, A. B., Bafica, A., Gazos-Lopes, F., Takiya, C. M., Souto-Padron, T., Vieira, D. P., Ferreira-Pereira, A., Almeida, I. C., Figueiredo, R. T., Porto, B. N., Bozza, M. T., Graca-Souza, A. V., Lopes, A. H., Atella, G. C., and Silva-Neto, M. A. (2008) *Trypanosoma cruzi* infection is enhanced by vector saliva through immunosuppressant mechanisms mediated by lysophosphatidylcholine. *Infection and immunity* **76**, 5543-5552

47. Silva-Neto, M. A., Carneiro, A. B., Silva-Cardoso, L., and Atella, G. C. (2012) Lysophosphatidylcholine: a novel modulator of *Trypanosoma cruzi t*ransmission. *Journal of parasitology research* **2012**, 625838

48. Golodne, D. M., Monteiro, R. Q., Graca-Souza, A. V., Silva-Neto, M. A., and Atella, G. C. (2003) Lysophosphatidylcholine acts as an anti-hemostatic molecule in the saliva of the blood-sucking bug *Rhodnius prolixus*. *The Journal of biological chemistry* **278**, 27766-27771

49. Bassa, B. V., Noh, J. W., Ganji, S. H., Shin, M. K., Roh, D. D., and Kamanna, V. S. (2007) Lysophosphatidylcholine stimulates EGF receptor activation and mesangial cell proliferation: regulatory role of Src and PKC. *Biochimica et biophysica acta* **1771**, 1364-1371

50. Kabarowski, J. H. (2009) G2A and LPC: regulatory functions in immunity. *Prostaglandins & other lipid mediators* **89**, 73-81

51. Oestvang, J., Anthonsen, M. W., and Johansen, B. (2011) LysoPC and PAF trigger arachidonic acid release by divergent signaling mechanisms in monocytes. *Journal of lipids* **2011**, 532145

52. Legradi, A., Chitu, V., Szukacsov, V., Fajka-Boja, R., Szekely Szucs, K., and Monostori, E. (2004) Lysophosphatidylcholine is a regulator of tyrosine kinase activity and intracellular Ca(2+) level in Jurkat T cell line. *Immunology letters* **91**, 17-21

53. Meyer zu Heringdorf, D., and Jakobs, K. H. (2007) Lysophospholipid receptors: signalling, pharmacology and regulation by lysophospholipid metabolism. *Biochimica et biophysica acta* **1768**, 923-940

54. Honda, Z., Nakamura, M., Miki, I., Minami, M., Watanabe, T., Seyama, Y., Okado, H., Toh, H., Ito, K., Miyamoto, T., and et al. (1991) Cloning by functional expression of platelet-activating factor receptor from guinea-pig lung. *Nature* **349**, 342-346

55. Lin, P., and Ye, R. D. (2003) The lysophospholipid receptor G2A activates a specific combination of G proteins and promotes apoptosis. *The Journal of biological chemistry* **278**, 14379-14386

56. Lum, H., Qiao, J., Walter, R. J., Huang, F., Subbaiah, P. V., Kim, K. S., and Holian, O. (2003) Inflammatory stress increases receptor for lysophosphatidylcholine in human microvascular endothelial cells. *American journal of physiology. Heart and circulatory physiology* **285**, H1786-1789

57. Murugesan, G., Sandhya Rani, M. R., Gerber, C. E., Mukhopadhyay, C., Ransohoff, R. M., Chisolm, G. M., and Kottke-Marchant, K. (2003) Lysophosphatidylcholine regulates human

microvascular endothelial cell expression of chemokines. *Journal of molecular and cellular cardiology* **35**, 1375-1384

58. Pexa, A., and Deussen, A. (2005) Modulation of ecto-5'-nucleotidase by phospholipids in human umbilical vein endothelial cells (HUVEC). *Naunyn-Schmiedeberg's archives of pharmacology* **372**, 131-138

59. Rao, S. P., Riederer, M., Lechleitner, M., Hermansson, M., Desoye, G., Hallstrom, S., Graier, W. F., and Frank, S. (2013) Acyl chain-dependent effect of lysophosphatidylcholine on endothelium-dependent vasorelaxation. *PloS one* **8**, e65155

60. Tsuda, M., Tozaki-Saitoh, H., and Inoue, K. (2011) Platelet-activating factor and pain. *Biological & pharmaceutical bulletin* **34**, 1159-1162

61. Zhu, K., Baudhuin, L. M., Hong, G., Williams, F. S., Cristina, K. L., Kabarowski, J. H., Witte, O. N., and Xu, Y. (2001) Sphingosylphosphorylcholine and lysophosphatidylcholine are ligands for the G protein-coupled receptor GPR4. *The Journal of biological chemistry* **276**, 41325-41335

62. Huang, Y. H., Schafer-Elinder, L., Wu, R., Claesson, H. E., and Frostegard, J. (1999) Lysophosphatidylcholine (LPC) induces proinflammatory cytokines by a platelet-activating factor (PAF) receptor-dependent mechanism. *Clinical and experimental immunology* **116**, 326-331

63. Ojala, P. J., Hirvonen, T. E., Hermansson, M., Somerharju, P., and Parkkinen, J. (2007) Acyl chain-dependent effect of lysophosphatidylcholine on human neutrophils. *Journal of leukocyte biology* **82**, 1501-1509

64. Riederer, M., Ojala, P. J., Hrzenjak, A., Graier, W. F., Malli, R., Tritscher, M., Hermansson, M., Watzer, B., Schweer, H., Desoye, G., Heinemann, A., and Frank, S. (2010) Acyl chain-dependent effect of lysophosphatidylcholine on endothelial prostacyclin production. *Journal of lipid research* **51**, 2957-2966

65. Agusti, R., Couto, A. S., Alves, M. J., Colli, W., and Lederkremer, R. M. (2000) Lipids shed into the culture medium by trypomastigotes of Trypanosoma cruzi. *Memorias do Instituto Oswaldo Cruz* **95**, 97-102

66. Ramos, R. G., Libong, D., Rakotomanga, M., Gaudin, K., Loiseau, P. M., and Chaminade, P. (2008) Comparison between charged aerosol detection and light scattering detection for the analysis of *Leishmania* membrane phospholipids. *Journal of chromatography. A* **1209**, 88-94

67. Zheng, L., T'Kind, R., Decuypere, S., von Freyend, S. J., Coombs, G. H., and Watson, D. G. (2010) Profiling of lipids in *Leishmania donovani* using hydrophilic interaction chromatography in combination with Fourier transform mass spectrometry. *Rapid communications in mass spectrometry : RCM* **24**, 2074-2082

68. Werbovetz, K. A., and Englund, P. T. (1996) Lipid metabolism in *Trypanosoma brucei*: utilization of myristate and myristoyllysophosphatidylcholine for myristoylation of glycosyl phosphatidylinositols. *The Biochemical journal* **318 (Pt 2)**, 575-581

69. Asahi, H. (2009) *Plasmodium falciparum*: Chemically defined medium for continuous intraerythrocytic growth using lipids and recombinant albumin. *Experimental parasitology* **121**, 22-28

70. Smith, J. C., Hou, W., Whitehead, S. N., Ethier, M., Bennett, S. A., and Figeys, D. (2008) Identification of lysophosphatidylcholine (LPC) and platelet activating factor (PAF) from PC12 cells and mouse cortex using liquid chromatography/multi-stage mass spectrometry (LC/MS3). *Rapid communications in mass spectrometry : RCM* **22**, 3579-3587

71. Honda, Z., Ishii, S., and Shimizu, T. (2002) Platelet-activating factor receptor. *Journal of biochemistry* **131**, 773-779

72. Kasperska-Zajac, A., Brzoza, Z., and Rogala, B. (2008) Platelet-activating factor (PAF): a review of its role in asthma and clinical efficacy of PAF antagonists in the disease therapy. *Recent patents on inflammation & allergy drug discovery* **2**, 72-76

73. Gomes, M. T., Monteiro, R. Q., Grillo, L. A., Leite-Lopes, F., Stroeder, H., Ferreira-Pereira, A., Alviano, C. S., Barreto-Bergter, E., Neto, H. C., Cunha, E. S. N. L., Almeida, I. C., Soares, R. M., and Lopes, A. H. (2006) Platelet-activating factor-like activity isolated from *Trypanosoma cruzi*. *Int J Parasitol* **36**, 165-173

74. Machado, F. S., Dutra, W. O., Esper, L., Gollob, K. J., Teixeira, M. M., Factor, S. M., Weiss, L. M., Nagajyothi, F., Tanowitz, H. B., and Garg, N. J. (2012) Current understanding of immunity to *Trypanosoma cruzi* infection and pathogenesis of Chagas disease. *Semin Immunopathol* **34**, 753-770

75. Tanowitz, H. B., Burns, E. R., Sinha, A. K., Kahn, N. N., Morris, S. A., Factor, S. M., Hatcher, V. B., Bilezikian, J. P., Baum, S. G., and Wittner, M. (1990) Enhanced platelet adherence and aggregation in Chagas' disease: a potential pathogenic mechanism for cardiomyopathy. *The American journal of tropical medicine and hygiene* **43**, 274-281

76. Silva, L. H. P., and Nussenzweig, V. (1953) Sobre uma cepa de *Trypanosoma cruzi* altamente virulenta para o camundongo branco. *Folia Clinica et Biologica (S. Paulo)* **20**, 191-207

77. Camargo, E. P. (1964) Growth and differentiation In *Trypanosoma cruzi*. I. Origin of metacyclic trypanosomes in liquid media. *Rev Inst Med Trop Sao Paulo* **12**, 93-100

78. de Sousa, M. A. (1983) A simple method to purify biologically and antigenically preserved bloodstream trypomastigotes of *Trypanosoma cruzi* using DEAE-cellulose columns. *Memorias do Instituto Oswaldo Cruz* **78**, 317-333

79. Serrano, A. A., Schenkman, S., Yoshida, N., Mehlert, A., Richardson, J. M., and Ferguson, M. A. (1995) The lipid structure of the glycosylphosphatidylinositol-anchored mucin-like sialic acid acceptors of Trypanosoma cruzi changes during parasite differentiation from epimastigotes to infective metacyclic trypomastigote forms. *The Journal of biological chemistry* **270**, 27244-27253

80. Andrews, N. W., and Colli, W. (1982) Adhesion and interiorization of Trypanosoma cruzi in mammalian cells. *The Journal of protozoology* **29**, 264-269

81. Marques, A. F., Nakayasu, E. S., and Almeida, I. C. (2011) Purification of extracellular and intracellular amastigotes of *Trypanosoma cruzi* from mammalian host-infected cells. in *Protocol Exchange*, http://www.nature.com/protocolexchange/protocols/2240

82. Black, L., and Berenbaum, M. C. (1964) Factors affecting the dye exclusion test for cell viability. *Experimental cell research* **35**, 9-13

83. Folch, J., Lees, M., and Sloane Stanley, G. H. (1957) A simple method for the isolation and purification of total lipides from animal tissues. *The Journal of biological chemistry* **226**, 497-509

84. Bligh, E. G., and Dyer, W. J. (1959) A rapid method of total lipid extraction and purification. *Canadian journal of biochemistry and physiology* **37**, 911-917

85. Pernet, F., Pelletier, C. J., and Milley, J. (2006) Comparison of three solid-phase extraction methods for fatty acid analysis of lipid fractions in tissues of marine bivalves. *Journal of chromatography. A* **1137**, 127-137

86. Whitney, D., McCoy, M., Gordon, N., and Afeyan, N. (1998) Characterization of large-pore polymeric supports for use in perfusion biochromatography. *Journal of chromatography. A* **807**, 165-184

87. Hsu, F. F., Turk, J., Thukkani, A. K., Messner, M. C., Wildsmith, K. R., and Ford, D. A. (2003) Characterization of alkylacyl, alk-1-enylacyl and lyso subclasses of glycerophosphocholine by tandem quadrupole mass spectrometry with electrospray ionization. *Journal of mass spectrometry : JMS* **38**, 752-763

88. Silva-Cardoso, L., Caccin, P., Magnabosco, A., Patron, M., Targino, M., Fuly, A., Oliveira, G. A., Pereira, M. H., do Carmo, M., Souza, A. S., Silva-Neto, M. A., Montecucco, C., and Atella, G. C. (2010) Paralytic activity of lysophosphatidylcholine from saliva of the waterbug *Belostoma anurum*. *The Journal of experimental biology* **213**, 3305-3310

89. Hsu, F. F., Turk, J., Williams, T. D., and Welti, R. (2007) Electrospray ionization multiple stage quadrupole ion-trap and tandem quadrupole mass spectrometric studies on phosphatidylglycerol from *Arabidopsis* leaves. *Journal of the American Society for Mass Spectrometry* **18**, 783-790

90. Bayer-Santos, E., Aguilar-Bonavides, C., Rodrigues, S. P., Cordero, E. M., Marques, A. F., Varela-Ramirez, A., Choi, H., Yoshida, N., da Silveira, J. F., and Almeida, I. C. (2013) Proteomic

analysis of *Trypanosoma cruzi* secretome: characterization of two populations of extracellular vesicles and soluble proteins. *Journal of proteome research* **12**, 883-897

91. Monteiro, R. Q., Carlini, C. R., Guimaraes, J. A., Bon, C., and Zingali, R. B. (1997) Distinct bothrojaracin isoforms produced by individual jararaca (*Bothrops jararaca*) snakes. *Toxicon : official journal of the International Society on Toxinology* **35**, 649-657

92. Gasteiger, E., Gattiker, A., Hoogland, C., Ivanyi, I., Appel, R. D., and Bairoch, A. (2003) ExPASy: The proteomics server for in-depth protein knowledge and analysis. *Nucleic acids research* **31**, 3784-3788

93. Roy, A., Kucukural, A., and Zhang, Y. (2010) I-TASSER: a unified platform for automated protein structure and function prediction. *Nature protocols* **5**, 725-738

94. Zhang, Y. (2009) I-TASSER: fully automated protein structure prediction in CASP8. *Proteins* **77 Suppl 9**, 100-113

95. Zhang, Y. (2007) Template-based modeling and free modeling by I-TASSER in CASP7. *Proteins* **69 Suppl 8**, 108-117

96. Marti-Renom, M. A., Stuart, A. C., Fiser, A., Sanchez, R., Melo, F., and Sali, A. (2000) Comparative protein structure modeling of genes and genomes. *Annual review of biophysics and biomolecular structure* **29**, 291-325

97. Eswar, N., Webb, B., Marti-Renom, M. A., Madhusudhan, M. S., Eramian, D., Shen, M. Y., Pieper, U., and Sali, A. (2007) Comparative protein structure modeling using MODELLER. *Current protocols in protein science / editorial board, John E. Coligan ... [et al.]* **Chapter 2**, Unit 2.9

98. Laskowski, R., Macarthur, M., Moss, D., and Thornton, J. (1993) PROCHECK: a program to check the stereochemical quality of protein structures. *J. Applied Crystallography* **26**, 283-291

99. Colovos, C., and Yeates, T. O. (1993) Verification of protein structures: patterns of nonbonded atomic interactions. *Protein science : a publication of the Protein Society* **2**, 1511-1519

100. Ray, A., Lindahl, E., and Wallner, B. (2010) Model quality assessment for membrane proteins. *Bioinformatics* **26**, 3067-3074

101. Thomsen, R., and Christensen, M. H. (2006) MolDock: a new technique for high-accuracy molecular docking. *Journal of medicinal chemistry* **49**, 3315-3321

102. Gazos-Lopes, F., Oliveira, M. M., Hoelz, L. V., Vieira, D. P., Marques, A. F., Nakayasu, E. S., Gomes, M. T., Salloum, N. G., Pascutti, P. G., Souto-Padron, T., Monteiro, R. Q., Lopes, A. H., and Almeida, I. C. (2014) Structural and functional analysis of a platelet-activating lysophosphatidylcholine of Trypanosoma cruzi. *PLoS neglected tropical diseases* **8**, e3077

103. Hsu, F. F., and Turk, J. (2010) Electrospray ionization multiple-stage linear ion-trap mass spectrometry for structural elucidation of triacylglycerols: assignment of fatty acyl groups on the glycerol backbone and location of double bonds. *Journal of the American Society for Mass Spectrometry* **21**, 657-669

104. Belaunzaran, M. L., Lammel, E. M., and de Isola, E. L. (2011) Phospholipases A in trypanosomatids. *Enzyme research* **2011**, 392082

105. Huang, Y. H., Schäfer-Elinder, L., Wu, R., Claesson, H. E., and Frostegard, J. (1999) Lysophosphatidylcholine (LPC) induces proinflammatory cytokines by a platelet-activating factor (PAF) receptor-dependent mechanism. *Clinical and experimental immunology* **116**, 326-331

106. Gao, Q., and Wang, Z. (2006) Classification of G-protein coupled receptors at four levels. *Prot Engin Des Selec* **19**, 511-516

107. Kobilka, B. K. (2007) G protein coupled receptor structure and activation. *Biochimica et biophysica acta* **1768**, 794-807

108. Hoelz, L. V. B., Bernardi, R. C., Horta, B. A. C., Araujo, J. Q., Albuquerque, M. G., da Silva, J. F. M., Pascutti, P. G., and de Alencastro, R. B. (2011) Dynamical behaviour of the human beta(1)-adrenoceptor under agonist binding. *Mol Simul* **37**, 907-913

109. Hoelz, L. V. B., Ribeiro, A. A. S. T., Bernardi, R. C., Horta, B. A. C., Albuquerque, M. G., da Silva, J. F. M., Pascutti, P. G., and de Alencastro, R. B. (2012) The role of helices 5 and 6 on the human beta(1)-adrenoceptor activation mechanism. *Mol Simul* **38**, 236-240

110. Ishii, I., Izumi, T., Tsukamoto, H., Umeyama, H., Ui, M., and Shimizu, T. (1997) Alanine exchanges of polar amino acids in the transmembrane domains of a platelet-activating factor receptor generate both constitutively active and inactive mutants. *The Journal of biological chemistry* **272**, 7846-7854

111. Fredriksson, R., Lagerstrom, M. C., Lundin, L. G., and Schioth, H. B. (2003) The G-protein-coupled receptors in the human genome form five main families. Phylogenetic analysis, paralogon groups, and fingerprints. *Molecular pharmacology* **63**, 1256-1272

112. Heim, A. J., and Li, Z. (2012) Developing a high-quality scoring function for membrane protein structures based on specific inter-residue interactions. *J Comput Aided Mol Des* **26**, 301-309

113. Gutierrez-de-Teran, H., Bello, X., and Rodriguez, D. (2013) Characterization of the dynamic events of GPCRs by automated computational simulations. *Biochemical Society transactions* **41**, 205-212

114. Belaunzaran, M. L., Wainszelbaum, M. J., Lammel, E. M., Gimenez, G., Aloise, M. M., Florin-Christensen, J., and Isola, E. L. (2007) Phospholipase A1 from *Trypanosoma cruzi* infective stages generates lipid messengers that activate host cell protein kinase c. *Parasitology* **134**, 491-502

115. Belaunzaran, M. L., Wilkowsky, S. E., Lammel, E. M., Gimenez, G., Bott, E., Barbieri, M. A., and de Isola, E. L. (2013) Phospholipase A1: a novel virulence factor in *Trypanosoma cruzi*. *Molecular and biochemical parasitology* **187**, 77-86

116. Richmond, G. S., and Smith, T. K. (2007) A novel phospholipase from *Trypanosoma brucei*. *Molecular microbiology* **63**, 1078-1095

117. Lujan, H. D., and Bronia, D. H. (1994) Intermembrane lipid transfer during *Trypanosoma cruzi*-induced erythrocyte membrane destabilization. *Parasitology* **108 (Pt 3)**, 323-334

118. Kabbani, S. S., Watkins, M. W., Ashikaga, T., Terrien, E. F., Holoch, P. A., Sobel, B. E., and Schneider, D. J. (2001) Platelet reactivity characterized prospectively: a determinant of outcome 90 days after percutaneous coronary intervention. *Circulation* **104**, 181-186

119. Tanowitz, H. B., Kirchhoff, L. V., Simon, D., Morris, S. A., Weiss, L. M., and Wittner, M. (1992) Chagas' disease. *Clinical microbiology reviews* **5**, 400-419

120. Chao, W., and Olson, M. S. (1993) Platelet-activating factor: receptors and signal transduction. *The Biochemical journal* **292**, 617-629

121. Eswar, N., Webb, B., Marti-Renom, M. A., Madhusudhan, M. S., Eramian, D., Shen, M. Y., Pieper, U., and Sali, A. (2006) Comparative protein structure modeling using Modeller. *Current protocols in bioinformatics / editoral board, Andreas D. Baxevanis ... [et al.]* **Chapter 5**, Unit 5.6

122. Lopes, A. H., Gomes, M. T., Dutra, F. L., Vermelho, A. B., Meyer-Fernandes, J. R., Silva-Neto, M. A., Souto-Padrón, T., and Vieira, D. P. (2010) Intracellular signaling pathways involved in cell differentiation in trypanosomatids. *Open Parasitol J* **4**, 102-110

123. Silva-Neto, M. A., Carneiro, A. B., Vieira, D. P., Mesquita, R. D., and Lopes, A. H. (2002) Platelet-activating factor (PAF) activates casein kinase 2 in the protozoan parasite *Herpetomonas muscarum muscarum*. *Biochem Biophys Res Commun* **293**, 1358-1363

124. Ogita, T., Tanaka, Y., Nakaoka, T., Matsuoka, R., Kira, Y., Nakamura, M., Shimizu, T., and Fujita, T. (1997) Lysophosphatidylcholine transduces Ca2+ signaling via the platelet-activating factor receptor in macrophages. *Am J Physiol* **272**, H17-24

125. Seibt, B. F., Schiedel, A. C., Thimm, D., Hinz, S., Sherbiny, F. F., and Müller, C. E. (2013) The second extracellular loop of GPCRs determines subtype-selectivity and controls efficacy as evidenced by loop exchange study at A2 adenosine receptors. *Biochem Pharmacol* **85**, 1317-1329

126. Buwitt-Beckmann, U., Heine, H., Wiesmüller, K., Jung, G., Brock, R., and Ulmer, A. J. (2005) Lipopeptide structure determines TLR2 dependent cell activation level. *FEBS J* **272**, 6354-6364

127. Abdulkhalek, S., Guo, M., Amith, S. R., Jayanth, P., and Szewczuk, M. R. (2012) G-protein coupled receptor agonists mediate Neu1 sialidase and matrix metalloproteinase-9 cross-talk to induce transactivation of Toll-like receptors and cellular signaling. *Cell Signal* **24** 2035-2042

128. Magalhães, K., Almeida, P. E., Atella, G., Maya-Monteiro, C. M., Castro-Faria-Neto, H. C., Pelajo-Machado, M., Lenzi, H. L., Bozza, M. T., and Bozza, P. T. (2010) Schistosomal-derived lysophosphatidylcholine are involved in eosinophil activation and recruitment through Toll-like receptor-2-dependent mechanisms. *J Infect Dis* **202** 1369-1379

129. Carneiro, A. B., Iaciura, B. M. F., Nohara, L. L., Lopes, C. D., Cordero Veas, E. M., Mariano, V. S., Bozza, P. T., Lopes, U. G., Atella, G. C., Almeida, I. C., and Silva-Neto, M. A. C. (2013) Lysophosphatidylcholine triggers TLR2- and TLR4-mediated signaling pathways but counteracts LPS-induced NO synthesis in peritoneal macrophages by inhibiting NF-κB translocation and MAPK/ERK phosphorylation. *PloS one* **8**, e76233

130. Testet, E., Laroche-Traineau, J., Noubhani, A., Coulon, D., Bunoust, O., Camougrand, N., Manon, S., Lessire, R., and Bessoule, J. J. (2005) Ypr140wp, 'the yeast tafazzin', displays a mitochondrial lysophosphatidylcholine (lyso-PC) acyltransferase activity related to triacylglycerol and mitochondrial lipid synthesis. *The Biochemical journal* **387**, 617-626

131. Richmond, G. S., Gibellini, F., Young, S. A., Major, L., Denton, H., Lilley, A., and Smith, T. K. (2010) Lipidomic analysis of bloodstream and procyclic form *Trypanosoma brucei*. *Parasitology* **137**, 1357-1392

132. Eyster, K. M. (2007) The membrane and lipids as integral participants in signal transduction: lipid signal transduction for the non-lipid biochemist. *Adv Physiol Educ* **31**, 5-16

133. Murohara, T., Ikeda, H., Katoh, A., Takajo, Y., Otsuka, Y., Haramaki, N., and Imaizumi, T. (2002) Vitamin E inhibits lysophosphatidylcholine-induced endothelial dysfunction and platelet activation. *Antioxid Redox Signal* **4**, 791-798

134. Ogletree, M. L. (1987) Overview of physiological and pathophysiological effects of thromboxane A2. *FASEB journal : official publication of the Federation of American Societies for Experimental Biology* **46**, 133-138

135. Prescott, S. M., Zimmerman, G. A., Stafforini, D. M., and McIntyre, T. M. (2000) Platelet-activating factor and related lipid mediators. *Annual review of biochemistry* **69**, 419-445

136. Zimmermann, L. T., Folly, E., Gomes, M. T., Alviano, D. S., Alviano, C. S., Silva-Filho, F. C., Atella, G. C., and Lopes, A. H. (2011) Effects of platelet-activating factor on the interaction of *Trypanosoma cruzi* with *Rhodnius prolixus*. *Parasitol Res* **108**, 1473-1478

137. Pereira-Chioccola, V. L., Acosta-Serrano, A., Correia de Almeida, I., Ferguson, M. A., Souto-Padron, T., Rodrigues, M. M., Travassos, L. R., and Schenkman, S. (2000) Mucin-like molecules form a negatively charged coat that protects *Trypanosoma cruzi* trypomastigotes from killing by human anti-alpha-galactosyl antibodies. *Journal of cell science* **113 (Pt 7)**, 1299-1307

138. Nakayasu, E. S., Yashunsky, D. V., Nohara, L. L., Torrecilhas, A. C., Nikolaev, A. V., and Almeida, I. C. (2009) GPIomics: global analysis of glycosylphosphatidylinositol-anchored molecules of Trypanosoma cruzi. *Molecular systems biology* **5**, 261

139. Paulick, M. G., and Bertozzi, C. R. (2008) The glycosylphosphatidylinositol anchor: a complex membrane-anchoring structure for proteins. *Biochemistry* **47**, 6991-7000

140. Almeida, I. C., Camargo, M. M., Procopio, D. O., Silva, L. S., Mehlert, A., Travassos, L. R., Gazzinelli, R. T., and Ferguson, M. A. (2000) Highly purified glycosylphosphatidylinositols from Trypanosoma cruzi are potent proinflammatory agents. *The EMBO journal* **19**, 1476-1485

141. Almeida, I. C., and Gazzinelli, R. T. (2001) Proinflammatory activity of glycosylphosphatidylinositol anchors derived from Trypanosoma cruzi: structural and functional analyses. *Journal of leukocyte biology* **70**, 467-477

142. Low, M. G. (1989) Glycosyl-phosphatidylinositol: a versatile anchor for cell surface proteins. *FASEB journal : official publication of the Federation of American Societies for Experimental Biology* **3**, 1600-1608

143. Ferguson, M. A., Brimacombe, J. S., Brown, J. R., Crossman, A., Dix, A., Field, R. A., Guther, M. L., Milne, K. G., Sharma, D. K., and Smith, T. K. (1999) The GPI biosynthetic pathway as a therapeutic target for African sleeping sickness. *Biochimica et biophysica acta* **1455**, 327-340

144. Maeda, Y., and Kinoshita, T. (2011) Structural remodeling, trafficking and functions of glycosylphosphatidylinositol-anchored proteins. *Progress in lipid research* **50**, 411-424

145. Anderson, R. G. (1994) Functional specialization of the glycosylphosphatidylinositol membrane anchor. *Seminars in immunology* **6**, 89-95

146. Gillmor, C. S., Lukowitz, W., Brininstool, G., Sedbrook, J. C., Hamann, T., Poindexter, P., and Somerville, C. (2005) Glycosylphosphatidylinositol-anchored proteins are required for cell wall synthesis and morphogenesis in Arabidopsis. *The Plant cell* **17**, 1128-1140

147. McConville, M. J., and Ferguson, M. A. (1993) The structure, biosynthesis and function of glycosylated phosphatidylinositols in the parasitic protozoa and higher eukaryotes. *The Biochemical journal* **294 (Pt 2)**, 305-324

148. Ferguson, M. A., Homans, S. W., Dwek, R. A., and Rademacher, T. W. (1988) Glycosyl-phosphatidylinositol moiety that anchors Trypanosoma brucei variant surface glycoprotein to the membrane. *Science* **239**, 753-759

149. Cross, G. A. (1975) Identification, purification and properties of clone-specific glycoprotein antigens constituting the surface coat of Trypanosoma brucei. *Parasitology* **71**, 393-417

150. Ferguson, M. A., Haldar, K., and Cross, G. A. (1985) Trypanosoma brucei variant surface glycoprotein has a sn-1,2-dimyristyl glycerol membrane anchor at its COOH terminus. *The Journal of biological chemistry* **260**, 4963-4968

151. Ferguson, M. A., Low, M. G., and Cross, G. A. (1985) Glycosyl-sn-1,2-dimyristylphosphatidylinositol is covalently linked to Trypanosoma brucei variant surface glycoprotein. *The Journal of biological chemistry* **260**, 14547-14555

152. Tachado, S. D., Gerold, P., Schwarz, R., Novakovic, S., McConville, M., and Schofield, L. (1997) Signal transduction in macrophages by glycosylphosphatidylinositols of Plasmodium,

Trypanosoma, and Leishmania: activation of protein tyrosine kinases and protein kinase C by inositolglycan and diacylglycerol moieties. *Proceedings of the National Academy of Sciences of the United States of America* **94**, 4022-4027

153. Medeiros, M. M., Peixoto, J. R., Oliveira, A. C., Cardilo-Reis, L., Koatz, V. L., Van Kaer, L., Previato, J. O., Mendonca-Previato, L., Nobrega, A., and Bellio, M. (2007) Toll-like receptor 4 (TLR4)-dependent proinflammatory and immunomodulatory properties of the glycoinositolphospholipid (GIPL) from Trypanosoma cruzi. *Journal of leukocyte biology* **82**, 488-496

154. Previato, J. O., Wait, R., Jones, C., DosReis, G. A., Todeschini, A. R., Heise, N., and Previato, L. M. (2004) Glycoinositolphospholipid from Trypanosoma cruzi: structure, biosynthesis and immunobiology. *Advances in parasitology* **56**, 1-41

155. Arrighi, R. B., and Faye, I. (2010) Plasmodium falciparum GPI toxin: a common foe for man and mosquito. *Acta tropica* **114**, 162-165

156. Zhu, J., Krishnegowda, G., Li, G., and Gowda, D. C. (2011) Proinflammatory responses by glycosylphosphatidylinositols (GPIs) of Plasmodium falciparum are mainly mediated through the recognition of TLR2/TLR1. *Experimental parasitology* **128**, 205-211

157. Debierre-Grockiego, F., Azzouz, N., Schmidt, J., Dubremetz, J. F., Geyer, H., Geyer, R., Weingart, R., Schmidt, R. R., and Schwarz, R. T. (2003) Roles of glycosylphosphatidylinositols of Toxoplasma gondii. Induction of tumor necrosis factor-alpha production in macrophages. *The Journal of biological chemistry* **278**, 32987-32993

158. Ropert, C., Ferreira, L. R., Campos, M. A., Procopio, D. O., Travassos, L. R., Ferguson, M. A., Reis, L. F., Teixeira, M. M., Almeida, I. C., and Gazzinelli, R. T. (2002) Macrophage signaling by glycosylphosphatidylinositol-anchored mucin-like glycoproteins derived from Trypanosoma cruzi trypomastigotes. *Microbes and infection / Institut Pasteur* **4**, 1015-1025

159. Garg, N., Postan, M., Mensa-Wilmot, K., and Tarleton, R. L. (1997) Glycosylphosphatidylinositols are required for the development of Trypanosoma cruzi amastigotes. *Infection and immunity* **65**, 4055-4060

160. Campos, M. A., Almeida, I. C., Takeuchi, O., Akira, S., Valente, E. P., Procopio, D. O., Travassos, L. R., Smith, J. A., Golenbock, D. T., and Gazzinelli, R. T. (2001) Activation of Toll-like receptor-2 by glycosylphosphatidylinositol anchors from a protozoan parasite. *J Immunol* **167**, 416-423

161. Ropert, C., Almeida, I. C., Closel, M., Travassos, L. R., Ferguson, M. A., Cohen, P., and Gazzinelli, R. T. (2001) Requirement of mitogen-activated protein kinases and I kappa B phosphorylation for induction of proinflammatory cytokines synthesis by macrophages indicates functional similarity of receptors triggered by glycosylphosphatidylinositol anchors from parasitic protozoa and bacterial lipopolysaccharide. *J Immunol* **166**, 3423-3431

162. Pimenta, P. F., Turco, S. J., McConville, M. J., Lawyer, P. G., Perkins, P. V., and Sacks, D. L. (1992) Stage-specific adhesion of Leishmania promastigotes to the sandfly midgut. *Science* **256**, 1812-1815

163. Pimenta, P. F., Saraiva, E. M., Rowton, E., Modi, G. B., Garraway, L. A., Beverley, S. M., Turco, S. J., and Sacks, D. L. (1994) Evidence that the vectorial competence of phlebotomine sand flies for different species of Leishmania is controlled by structural polymorphisms in the surface lipophosphoglycan. *Proceedings of the National Academy of Sciences of the United States of America* **91**, 9155-9159

164. Nogueira, N. F., Gonzalez, M. S., Gomes, J. E., de Souza, W., Garcia, E. S., Azambuja, P., Nohara, L. L., Almeida, I. C., Zingales, B., and Colli, W. (2007) Trypanosoma cruzi: involvement of glycoinositolphospholipids in the attachment to the luminal midgut surface of Rhodnius prolixus. *Experimental parasitology* **116**, 120-128

165. Dinglasan, R. R., and Jacobs-Lorena, M. (2005) Insight into a conserved lifestyle: protein-carbohydrate adhesion strategies of vector-borne pathogens. *Infection and immunity* **73**, 7797-7807

166. Lim, J., Gowda, D. C., Krishnegowda, G., and Luckhart, S. (2005) Induction of nitric oxide synthase in Anopheles stephensi by Plasmodium falciparum: mechanism of signaling and the role of parasite glycosylphosphatidylinositols. *Infection and immunity* **73**, 2778-2789

167. Gazos-Lopes, F., Mesquita, R. D., Silva-Cardoso, L., Senna, R., Silveira, A. B., Jablonka, W., Cudischevitch, C. O., Carneiro, A. B., Machado, E. A., Lima, L. G., Monteiro, R. Q., Nussenzveig, R. H., Folly, E., Romeiro, A., Vanbeselaere, J., Mendonca-Previato, L., Previato, J. O., Valenzuela, J. G., Ribeiro, J. M., Atella, G. C., and Silva-Neto, M. A. (2012) Glycoinositolphospholipids from Trypanosomatids subvert nitric oxide production in Rhodnius prolixus salivary glands. *PloS one* **7**, e47285

168. Savage, A. F., Cerqueira, G. C., Regmi, S., Wu, Y., El Sayed, N. M., and Aksoy, S. (2012) Transcript expression analysis of putative Trypanosoma brucei GPI-anchored surface proteins during development in the tsetse and mammalian hosts. *PLoS neglected tropical diseases* **6**, e1708

169. Urbaniak, M. D., Capes, A. S., Crossman, A., O'Neill, S., Thompson, S., Gilbert, I. H., and Ferguson, M. A. (2014) Fragment screening reveals salicylic hydroxamic acid as an inhibitor of Trypanosoma brucei GPI GlcNAc-PI de-N-acetylase. *Carbohydr Res* **387**, 54-58

170. Capes, A. S., Crossman, A., Urbaniak, M. D., Gilbert, S. H., Ferguson, M. A., and Gilbert, I. H. (2014) Probing the substrate specificity of Trypanosoma brucei GlcNAc-PI de-N-acetylase with synthetic substrate analogues. *Organic & biomolecular chemistry* **12**, 1919-1934

171. Abdelwahab, N. Z., Urbaniak, M. D., Ferguson, M. A., and Crossman, A. T. (2011) Synthesis of potential metal-binding group compounds to examine the zinc dependency of the GPI de-N-acetylase metalloenzyme in Trypanosoma brucei. *Carbohydr Res* **346**, 708-714

172. Urbaniak, M. D., Yashunsky, D. V., Crossman, A., Nikolaev, A. V., and Ferguson, M. A. (2008) Probing enzymes late in the trypanosomal glycosylphosphatidylinositol biosynthetic pathway with synthetic glycosylphosphatidylinositol analogues. *ACS Chem Biol* **3**, 625-634

173. Smith, T. K., Crossman, A., Brimacombe, J. S., and Ferguson, M. A. (2004) Chemical validation of GPI biosynthesis as a drug target against African sleeping sickness. *EMBO J* **23**, 4701-4708

174. Smith, T. K., Crossman, A., Borissow, C. N., Paterson, M. J., Dix, A., Brimacombe, J. S., and Ferguson, M. A. (2001) Specificity of GlcNAc-PI de-N-acetylase of GPI biosynthesis and synthesis of parasite-specific suicide substrate inhibitors. *EMBO J* **20**, 3322-3332

175. Schofield, L., Hewitt, M. C., Evans, K., Siomos, M. A., and Seeberger, P. H. (2002) Synthetic GPI as a candidate anti-toxic vaccine in a model of malaria. *Nature* **418**, 785-789

176. Hong, Y., and Kinoshita, T. (2009) Trypanosome glycosylphosphatidylinositol biosynthesis. *The Korean journal of parasitology* **47**, 197-204

177. Yeh, E. T., Kamitani, T., and Chang, H. M. (1994) Biosynthesis and processing of the glycosylphosphatidylinositol anchor in mammalian cells. *Seminars in immunology* **6**, 73-80

178. Vidugiriene, J., and Menon, A. K. (1993) Early lipid intermediates in glycosyl-phosphatidylinositol anchor assembly are synthesized in the ER and located in the cytoplasmic leaflet of the ER membrane bilayer. *The Journal of cell biology* **121**, 987-996

179. Vidugiriene, J., and Menon, A. K. (1994) The GPI anchor of cell-surface proteins is synthesized on the cytoplasmic face of the endoplasmic reticulum. *The Journal of cell biology* **127**, 333-341

180. Doering, T. L., Masterson, W. J., Englund, P. T., and Hart, G. W. (1989) Biosynthesis of the glycosyl phosphatidylinositol membrane anchor of the trypanosome variant surface glycoprotein. Origin of the non-acetylated glucosamine. *The Journal of biological chemistry* **264**, 11168-11173

181. Sharma, D. K., Smith, T. K., Crossman, A., Brimacombe, J. S., and Ferguson, M. A. (1997) Substrate specificity of the N-acetylglucosaminyl-phosphatidylinositol de-N-acetylase of glycosylphosphatidylinositol membrane anchor biosynthesis in African trypanosomes and human cells. *The Biochemical journal* **328 (Pt 1)**, 171-177

182. Smith, T. K., Sharma, D. K., Crossman, A., Dix, A., Brimacombe, J. S., and Ferguson, M. A. (1997) Parasite and mammalian GPI biosynthetic pathways can be distinguished using synthetic substrate analogues. *The EMBO journal* **16**, 6667-6675

183. Menon, A. K., and Stevens, V. L. (1992) Phosphatidylethanolamine is the donor of the ethanolamine residue linking a glycosylphosphatidylinositol anchor to protein. *The Journal of biological chemistry* **267**, 15277-15280

184. Masterson, W. J., Raper, J., Doering, T. L., Hart, G. W., and Englund, P. T. (1990) Fatty acid remodeling: a novel reaction sequence in the biosynthesis of trypanosome glycosyl phosphatidylinositol membrane anchors. *Cell* **62**, 73-80

185. Fujita, M., and Jigami, Y. (2008) Lipid remodeling of GPI-anchored proteins and its function. *Biochimica et biophysica acta* **1780**, 410-420

186. Kodukula, K., Maxwell, S. E., and Udenfriend, S. (1995) Processing of nascent proteins to glycosylphosphatidylinositol-anchored forms in cell-free systems. *Methods in enzymology* **250**, 536-547

187. Chen, R., Knez, J. J., Merrick, W. C., and Medof, M. E. (2001) Comparative efficiencies of C-terminal signals of native glycophosphatidylinositol (GPI)-anchored proproteins in conferring GPI-anchoring. *Journal of cellular biochemistry* **84**, 68-83

188. Kinoshita, T., Fujita, M., and Maeda, Y. (2008) Biosynthesis, remodelling and functions of mammalian GPI-anchored proteins: recent progress. *Journal of biochemistry* **144**, 287-294

189. Vainauskas, S., and Menon, A. K. (2006) Ethanolamine phosphate linked to the first mannose residue of glycosylphosphatidylinositol (GPI) lipids is a major feature of the GPI structure that is recognized by human GPI transamidase. *The Journal of biological chemistry* **281**, 38358-38364

190. Fujita, M., Maeda, Y., Ra, M., Yamaguchi, Y., Taguchi, R., and Kinoshita, T. (2009) GPI glycan remodeling by PGAP5 regulates transport of GPI-anchored proteins from the ER to the Golgi. *Cell* **139**, 352-365

191. Castillon, G. A., Aguilera-Romero, A., Manzano-Lopez, J., Epstein, S., Kajiwara, K., Funato, K., Watanabe, R., Riezman, H., and Muniz, M. (2011) The yeast p24 complex regulates GPI-anchored protein transport and quality control by monitoring anchor remodeling. *Molecular biology of the cell* **22**, 2924-2936

192. Ferguson, M. A., Allen, A. K., and Snary, D. (1982) The detection of phosphonolipids in the protozoan Trypanosoma cruzi. *The Biochemical journal* **207**, 171-174

193. Previato, J. O., Jones, C., Xavier, M. T., Wait, R., Travassos, L. R., Parodi, A. J., and Mendonca-Previato, L. (1995) Structural characterization of the major glycosylphosphatidylinositol membrane-anchored glycoprotein from epimastigote forms of Trypanosoma cruzi Y-strain. *The Journal of biological chemistry* **270**, 7241-7250

194. Carreira, J. C., Jones, C., Wait, R., Previato, J. O., and Mendonca-Previato, L. (1996) Structural variation in the glycoinositolphospholipids of different strains of Trypanosoma cruzi. *Glycoconjugate journal* **13**, 955-966

195. Branquinha, M. H., Vermelho, A. B., Almeida, I. C., Mehlert, A., and Ferguson, M. A. (1999) Structural studies on the polar glycoinositol phospholipids of Trypanosoma (Schizotrypanum) dionisii from bats. *Molecular and biochemical parasitology* **102**, 179-189

196. Previato, J. O., Mendonca-Previato, L., Jones, C., Wait, R., and Fournet, B. (1992) Structural characterization of a novel class of glycophosphosphingolipids from the protozoan Leptomonas samueli. *The Journal of biological chemistry* **267**, 24279-24286

197. Routier, F. H., da Silveira, E. X., Wait, R., Jones, C., Previato, J. O., and Mendonca-Previato, L. (1995) Chemical characterisation of glycosylinositolphospholipids of Herpetomonas samuelpessoai. *Molecular and biochemical parasitology* **69**, 81-92

198. Villarreal-Chiu, J. F., Quinn, J. P., and McGrath, J. W. (2012) The genes and enzymes of phosphonate metabolism by bacteria, and their distribution in the marine environment. *Frontiers in microbiology* **3**, 19

199. Kariotoglou, D. M., and Mastronicolis, S. K. (2001) Sphingophosphonolipids, phospholipids, and fatty acids from Aegean jellyfish Aurelia aurita. *Lipids* **36**, 1255-1264

200. Hard, K., Van Doorn, J. M., Thomas-Oates, J. E., Kamerling, J. P., and Van der Horst, D. J. (1993) Structure of the asn-linked oligosaccharides of apolipophorin III from the insect Locusta migratoria. Carbohydrate-linked 2-aminoethylphosphonate as a constituent of a glycoprotein. *Biochemistry* **32**, 766-775

201. Baumann, H., Tzianabos, A. O., Brisson, J. R., Kasper, D. L., and Jennings, H. J. (1992) Structural elucidation of two capsular polysaccharides from one strain of Bacteroides fragilis using high-resolution NMR spectroscopy. *Biochemistry* **31**, 4081-4089

202. Kim, A. D., Baker, A. S., Dunaway-Mariano, D., Metcalf, W. W., Wanner, B. L., and Martin, B. M. (2002) The 2-aminoethylphosphonate-specific transaminase of the 2-aminoethylphosphonate degradation pathway. *Journal of bacteriology* **184**, 4134-4140

203. Sarkar, M., Hamilton, C. J., and Fairlamb, A. H. (2003) Properties of phosphoenolpyruvate mutase, the first enzyme in the aminoethylphosphonate biosynthetic pathway in Trypanosoma cruzi. *The Journal of biological chemistry* **278**, 22703-22708

204. Lacoste, A. M., Dumora, C., and Cassaigne, A. (1984) 2-Aminoethylphosphonate: pyruvate aminotransferase from Pseudomonas aeruginosa. *Progress in clinical and biological research* **144B**, 321-327

205. Jiang, W., Metcalf, W. W., Lee, K. S., and Wanner, B. L. (1995) Molecular cloning, mapping, and regulation of Pho regulon genes for phosphonate breakdown by the phosphonatase pathway of Salmonella typhimurium LT2. *Journal of bacteriology* **177**, 6411-6421

206. Barry, R. J., Bowman, E., McQueney, M., and Dunaway-Mariano, D. (1988) Elucidation of the 2-aminoethylphosphonate biosynthetic pathway in Tetrahymena pyriformis. *Biochem Biophys Res Commun* **153**, 177-182

207. Chen, C. C., Zhang, H., Kim, A. D., Howard, A., Sheldrick, G. M., Mariano-Dunaway, D., and Herzberg, O. (2002) Degradation pathway of the phosphonate ciliatine: crystal structure of 2-aminoethylphosphonate transaminase. *Biochemistry* **41**, 13162-13169

208. Ferguson, M. A. J. (1993) GPI-membrane anchors: isolation and analysis. in *Glycobiology: a practical approach* (Fukuda, M., and Kobata, A. eds.), Oxford University Press, New York, NY. pp 349-383

209. Ruiz-Matute, A. I., Hernandez-Hernandez, O., Rodriguez-Sanchez, S., Sanz, M. L., and Martinez-Castro, I. (2011) Derivatization of carbohydrates for GC and GC-MS analyses. *Journal of chromatography. B, Analytical technologies in the biomedical and life sciences* **879**, 1226-1240

210. Almeida, R., Pauling, J. K., Sokol, E., Hannibal-Bach, H. K., and Ejsing, C. S. (2015) Comprehensive lipidome analysis by shotgun lipidomics on a hybrid quadrupole-orbitrap-linear ion trap mass spectrometer. *Journal of the American Society for Mass Spectrometry* **26**, 133-148

211. de Lederkremer, R. M., Lima, C., Ramirez, M. I., Ferguson, M. A., Homans, S. W., and Thomas-Oates, J. (1991) Complete structure of the glycan of lipopeptidophosphoglycan from Trypanosoma cruzi Epimastigotes. *The Journal of biological chemistry* **266**, 23670-23675

212. Previato, J. O., Gorin, P. A., Mazurek, M., Xavier, M. T., Fournet, B., Wieruszesk, J. M., and Mendonca-Previato, L. (1990) Primary structure of the oligosaccharide chain of lipopeptidophosphoglycan of epimastigote forms of Trypanosoma cruzi. *The Journal of biological chemistry* **265**, 2518-2526

213. Nakayasu, E. S., Sobreira, T. J., Torres, R., Jr., Ganiko, L., Oliveira, P. S., Marques, A. F., and Almeida, I. C. (2012) Improved proteomic approach for the discovery of potential vaccine targets in Trypanosoma cruzi. *Journal of proteome research* **11**, 237-246

214. de Lederkremer, R. M., Lima, C. E., Ramirez, M. I., Goncalvez, M. F., and Colli, W. (1993) Hexadecylpalmitoylglycerol or ceramide is linked to similar glycophosphoinositol anchor-like structures in Trypanosoma cruzi. *European journal of biochemistry / FEBS* **218**, 929-936

215. Agusti, R., Couto, A. S., Campetella, O. E., Frasch, A. C., and de Lederkremer, R. M. (1997) The trans-sialidase of Trypanosoma cruzi is anchored by two different lipids. *Glycobiology* **7**, 731-735

216. Fankhauser, C., Homans, S. W., Thomas-Oates, J. E., McConville, M. J., Desponds, C., Conzelmann, A., and Ferguson, M. A. (1993) Structures of glycosylphosphatidylinositol membrane anchors from Saccharomyces cerevisiae. *The Journal of biological chemistry* **268**, 26365-26374

217. Haynes, P. A., Gooley, A. A., Ferguson, M. A., Redmond, J. W., and Williams, K. L. (1993) Post-translational modifications of the Dictyostelium discoideum glycoprotein PsA. Glycosylphosphatidylinositol membrane anchor and composition of O-linked oligosaccharides. *European journal of biochemistry / FEBS* **216**, 729-737

218. Cardoso, M. S., Junqueira, C., Trigueiro, R. C., Shams-Eldin, H., Macedo, C. S., Araujo, P. R., Gomes, D. A., Martinelli, P. M., Kimmel, J., Stahl, P., Niehus, S., Schwarz, R. T., Previato, J. O., Mendonca-Previato, L., Gazzinelli, R. T., and Teixeira, S. M. (2013) Identification and functional analysis of Trypanosoma cruzi genes that encode proteins of the glycosylphosphatidylinositol biosynthetic pathway. *PLoS neglected tropical diseases* **7**, e2369

219. Caradonna, K. L., Engel, J. C., Jacobi, D., Lee, C. H., and Burleigh, B. A. (2013) Host metabolism regulates intracellular growth of Trypanosoma cruzi. *Cell host & microbe* **13**, 108-117

220. Kloehn, J., Saunders, E. C., O'Callaghan, S., Dagley, M. J., and McConville, M. J. (2015) Characterization of metabolically quiescent leishmania parasites in murine lesions using heavy water labeling. *PLoS pathogens* **11**, e1004683

221. Fujita, M., and Kinoshita, T. (2010) Structural remodeling of GPI anchors during biosynthesis and after attachment to proteins. *FEBS letters* **584**, 1670-1677

222. Reggiori, F., Canivenc-Gansel, E., and Conzelmann, A. (1997) Lipid remodeling leads to the introduction and exchange of defined ceramides on GPI proteins in the ER and Golgi of Saccharomyces cerevisiae. *The EMBO journal* **16**, 3506-3518

223. Maeda, Y., Tashima, Y., Houjou, T., Fujita, M., Yoko-o, T., Jigami, Y., Taguchi, R., and Kinoshita, T. (2007) Fatty acid remodeling of GPI-anchored proteins is required for their raft association. *Molecular biology of the cell* **18**, 1497-1506

224. Tashima, Y., Taguchi, R., Murata, C., Ashida, H., Kinoshita, T., and Maeda, Y. (2006) PGAP2 is essential for correct processing and stable expression of GPI-anchored proteins. *Molecular biology of the cell* **17**, 1410-1420

225. Bosson, R., Jaquenoud, M., and Conzelmann, A. (2006) GUP1 of Saccharomyces cerevisiae encodes an O-acyltransferase involved in remodeling of the GPI anchor. *Molecular biology of the cell* **17**, 2636-2645

226. Pittet, M., and Conzelmann, A. (2007) Biosynthesis and function of GPI proteins in the yeast Saccharomyces cerevisiae. *Biochimica et biophysica acta* **1771**, 405-420

227. Heise, N., Raper, J., Buxbaum, L. U., Peranovich, T. M., and de Almeida, M. L. (1996) Identification of complete precursors for the glycosylphosphatidylinositol protein anchors of Trypanosoma cruzi. *The Journal of biological chemistry* **271**, 16877-16887

228. Abuin, G., Couto, A. S., de Lederkremer, R. M., Casal, O. L., Galli, C., Colli, W., and Alves, M. J. (1996) Trypanosoma cruzi: the Tc-85 surface glycoprotein shed by trypomastigotes bears a modified glycosylphosphatidylinositol anchor. *Exp Parasitol* **82**, 290-297

229. Bertello, L. E., Alves, M. J., Colli, W., and de Lederkremer, R. M. (2004) Inositolphosphoceramide is not a substrate for the first steps in the biosynthesis of glycoinositolphospholipids in Trypanosoma cruzi. *Molecular and biochemical parasitology* **133**, 71-80

230. Koeller, C. M., and Heise, N. (2011) The Sphingolipid Biosynthetic Pathway Is a Potential Target for Chemotherapy against Chagas Disease. *Enzyme research* **2011**, 648159

APPENDIX

SUPPLEMENTARY FIGURES

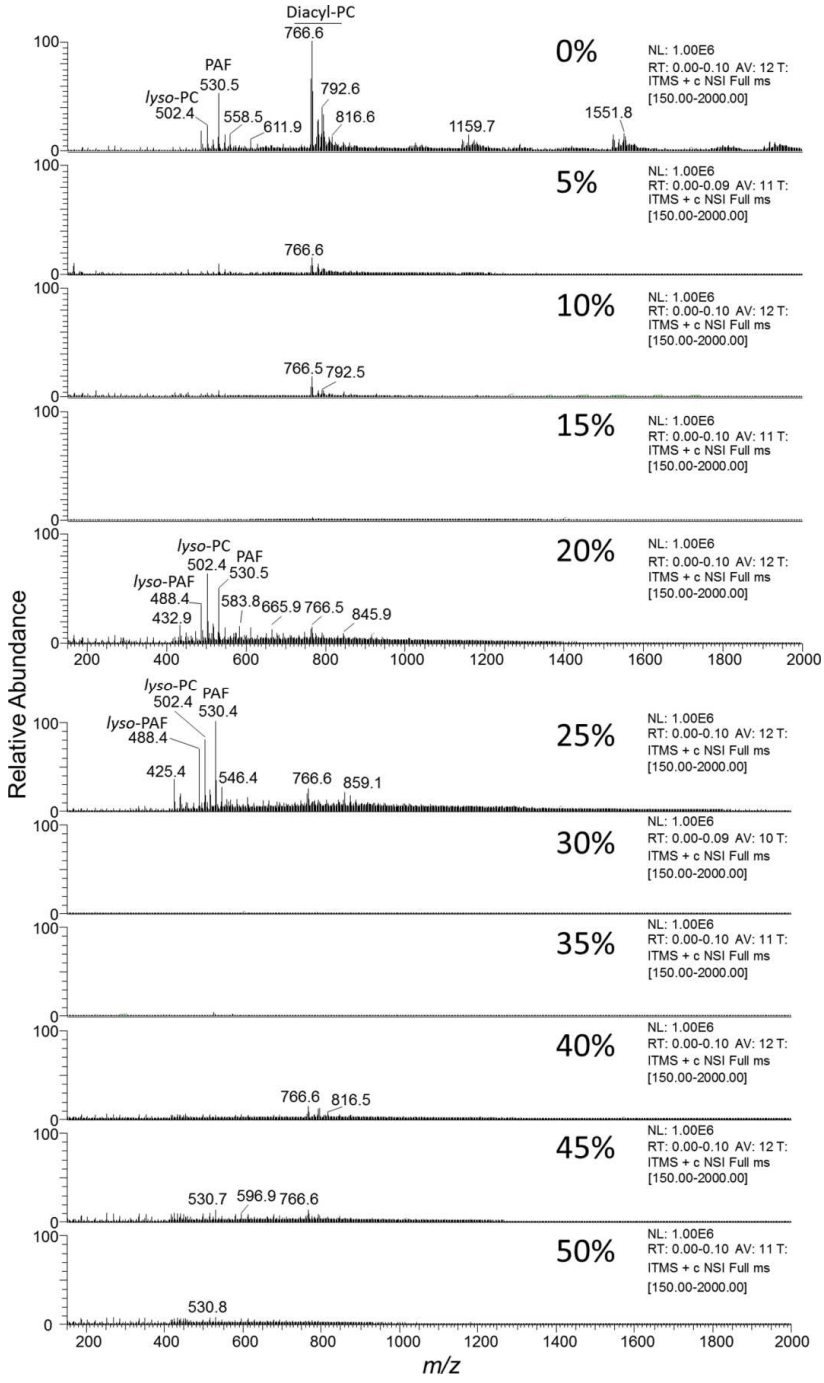

Figure S1. Fractionation of phospholipid standards using POROS R1 perfusion chromatography. A mixture of phospholipid standards, containing synthetic C16:0-*lyso*-PAF (LPAF) (*m/z* 488.4), C16:0-*lyso*-LPC (LPC) (*m/z* 502.4), C16:0-PAF (PAF) (*m/z* 530.5), and purified diacyl-PCs (700–900 *m/z* range), was suspended in HPLC-grade water and applied onto the POROS R1 mini-column, which was eluted with a 0%–50% *n*-propanol gradient. All fractions were diluted in methanol containing 5 mM LiOH and analyzed by direct infusion in an LTQXL ESI-LIT-MS, in positive-ion mode.

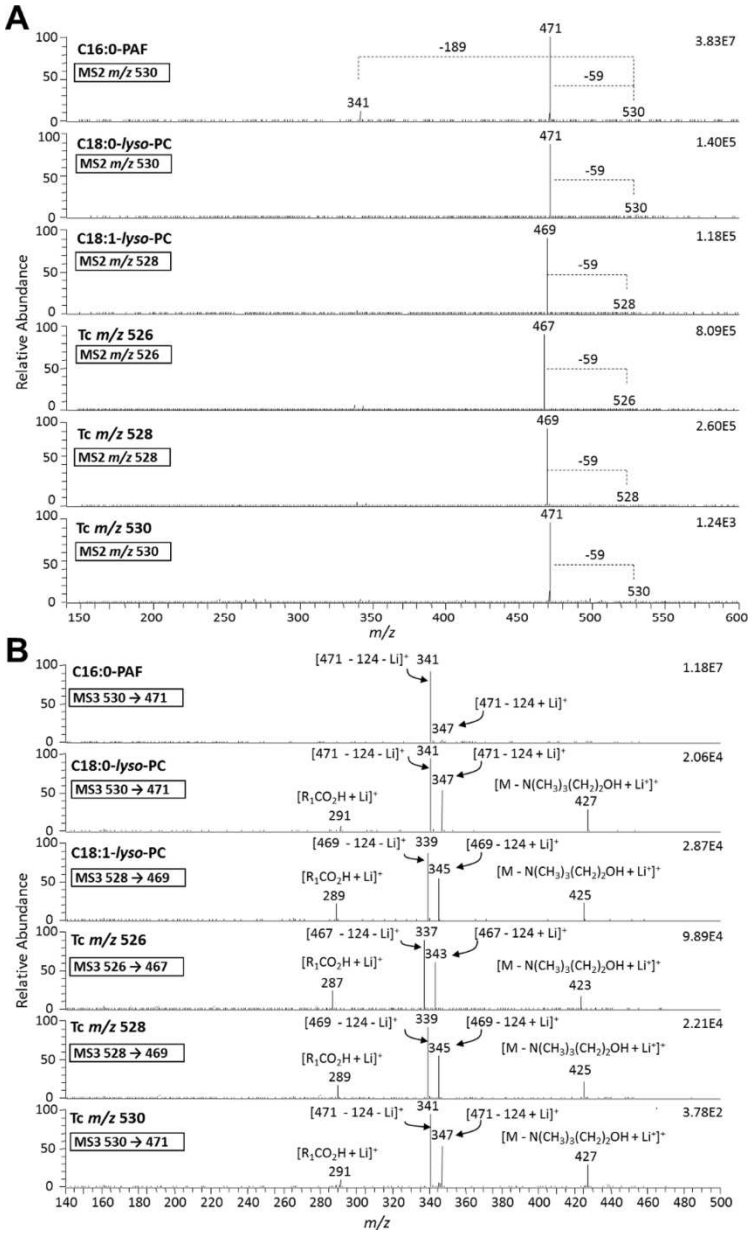

Figure S2. ESI-LIT-MS^n analysis of major *T. cruzi* ion species enriched by POROS R1 fractionation. (**A**) ESI-LIT-MS^2 spectra. Phospholipid standards (C16:0-PAF, C18:0-LPC, and C18:1-LPC) or purified *T. cruzi* phospholipids from the POROS R1 25% *n*-propanol fractions were diluted in methanol containing 5 mM LiOH and then infused directly into the LTQXL MS using an Advion Triversa NanoMate nanoelectrospray system. Major parent-ion species observed in the MS spectra (Fig. 2) were subjected to MS^2 fragmentation. (**B**) ESI-LIT-MS^3 spectra of selected ion species found in (**A**). Ion species corresponding to a neutral loss of 59 *m/z* (trimethylamine) from the parent ion were selected for MS^3 fragmentation.

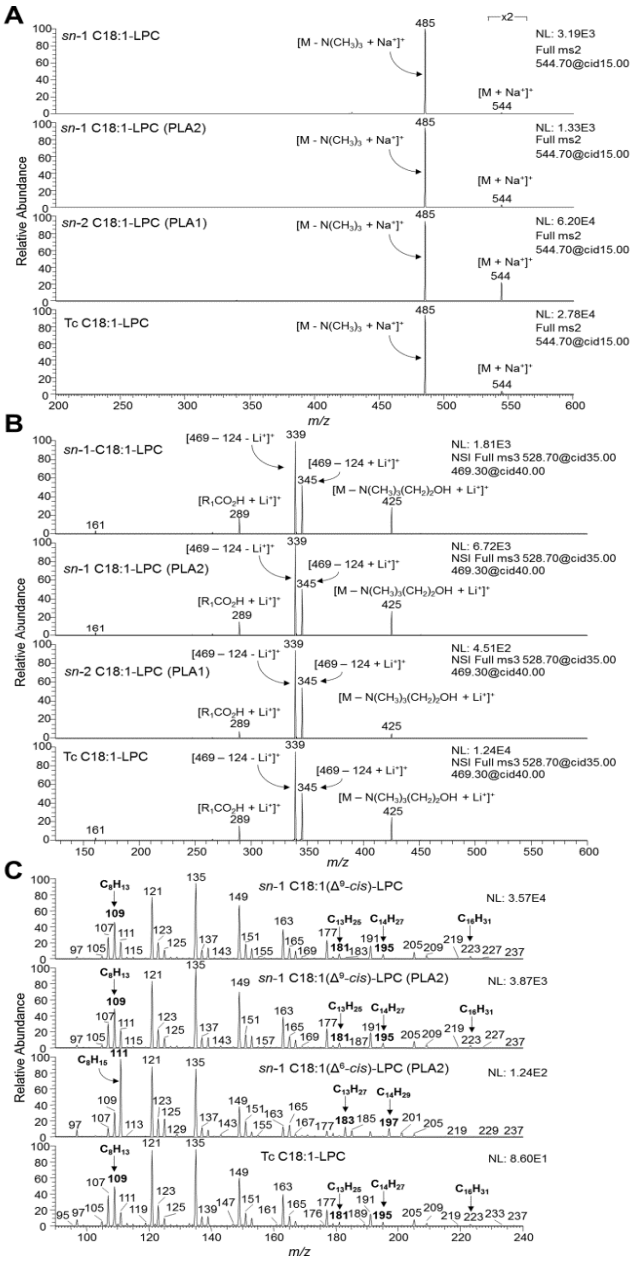

Figure S3. Determination of the acyl chain and double bond positions on *T. cruzi* C18:1-LPC. (**A–B**) Acyl chain position analysis. The *sn*-1 C18:1-LPC and *sn*-2 C18:1-LPC regioisomer standards were generated by treatment of 18:1(Δ^9-*cis*)-diacyl-PC with PLA2 and PLA1, respectively, as described in Materials and Methods. (**A**) MS^2 analysis. All LPCs were diluted in methanol containing 2.5 mM NaCl and analyzed by direct infusion using an Advion Triversa NanoMate nanoelectrospray system coupled to an LTQXL MS. MS^2 spectra were acquired in positive-ion mode. (**B**) MS^3 analysis. All LPCs were diluted in methanol containing 2.5 mM LiOH and analyzed by MS^3 (MS^2 528.7→MS^3 469.3), under the same MS experimental conditions. (**C**) Double-bond position analysis. The *sn*-1 C18:1(Δ^6-*cis*)-LPC and *sn*-1 C18:1(Δ^9-*cis*)-LPC standards were generated by treatment of 18:1(Δ^6-*cis*)-diacyl-PC and 18:1(Δ^9-*Cis*)-diacyl-PC with PLA2, respectively, as described in Materials and Methods. The position of the unsaturation on the acyl moiety of *T. cruzi* C18:1-LPC was determined by comparing the MS^4 fragmentation pattern of this ion (MS^2 528.7→MS^3 469.3→MS^4 339.3) to the fragmentation pattern of *sn*-1 C18:1(Δ^6-*cis*)-LPC and *sn*-1 C18:1(Δ^9-*cis*)-LPC under identical conditions to (**B**). Diagnostic ions (bold) are indicated.

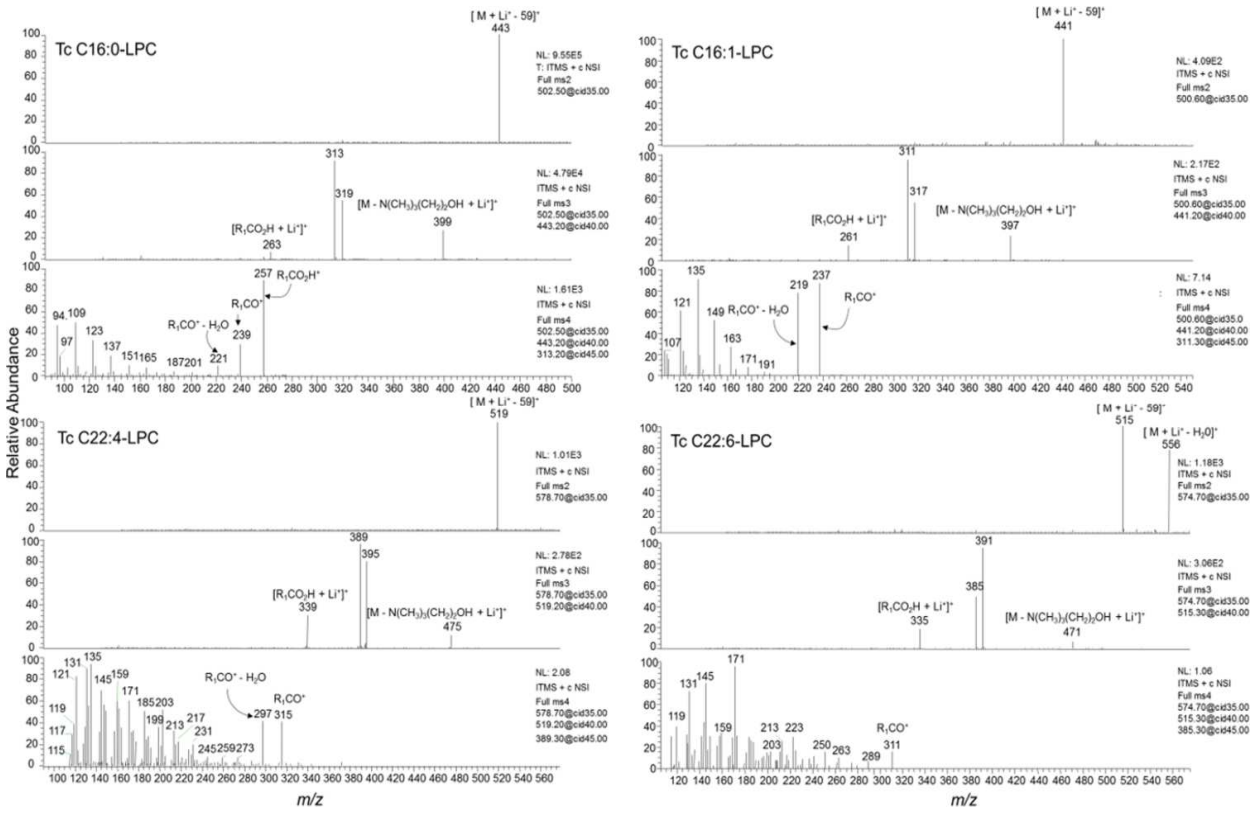

Figure S4. Tandem ESI-LIT-MS spectra of the low-abundance *T. cruzi* LPC-species enriched by POROS R1 fractionation. *T. cruzi* phospholipids from the 25% *n*-propanol fractions were diluted in methanol containing 5 mM LiOH and then infused directly into an LTQXL ESI-LIT-MS. Selected peaks were sequentially fragmented (MS^2-MS^4) by CID, as follows: C16:0-LPC (MS^2 502→MS^3 443→MS^4 313); C16:1-LPC (MS^2 500→MS^3 441→MS^4 311); C22:4-LPC (MS^2 578→MS^3 519→MS^4 389); and C22:6-LPC (MS^2 574→MS^3 515→MS^4 385).

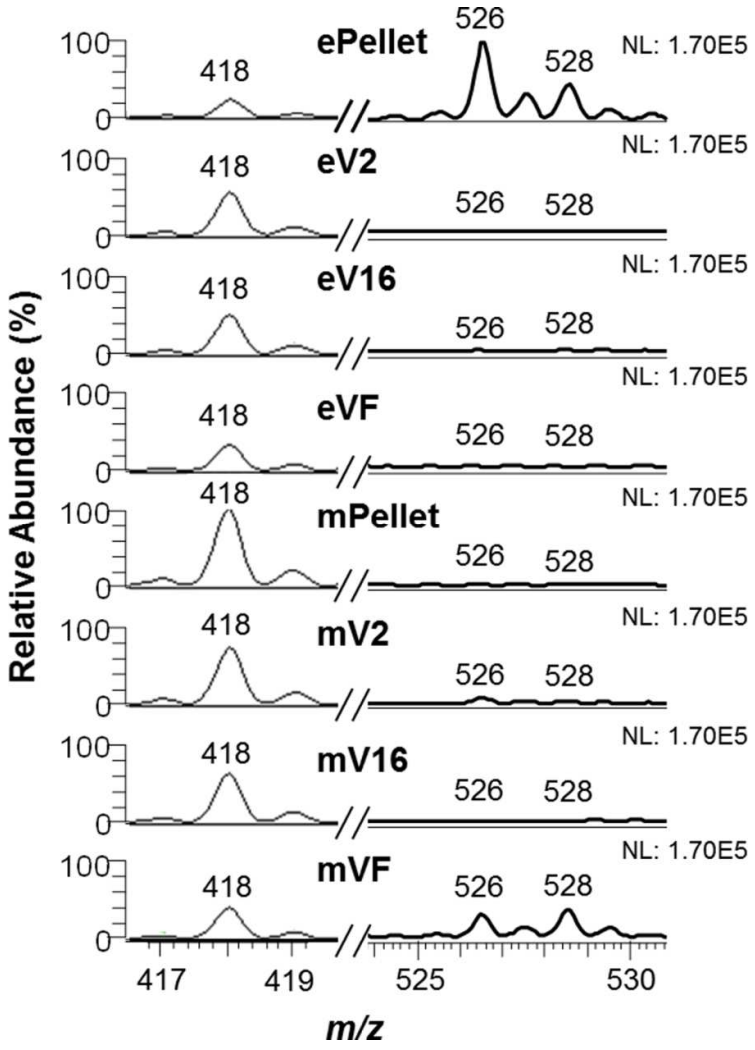

Figure S5. Quantification of LPC species in extracellular vesicles (EV) and EV-free supernatant of *T. cruzi*. C10:0-LPC (*m/z* 418) was used as an internal standard for quantification of the most abundant *T. cruzi* LPC species. C10:0-LPC was added to fresh pellets or EV preparations from Epis and Metas, prior to lipid extraction with C:M (2:1, v/v) and C:M:W (1:2:0.8, v/v/v), followed by Folch's partition. The Folch lower phase was analyzed by ESI-LIT-MS. C18:1- and C18:2-LPC are indicated at *m/z* 528 and 526, respectively. ePellet, Epi total pellet; eV2, Epi-derived ectosomes; eV16, Epi-derived exosomes; eVF, Epi-derived EV-free supernatant (or conditioned medium); mPellet, Meta total pellet; mV2, Meta-derived ectosomes; mV16, Meta-derived exosomes; mVF, Meta-derived EV-free supernatant.

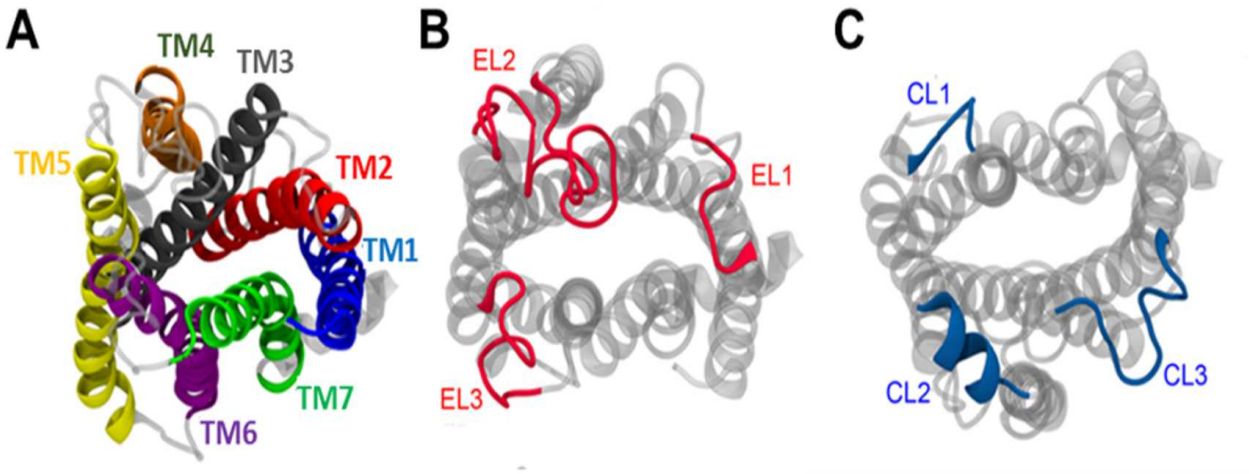

Figure S6 Structural representation of the PAFR model. (A) Arrangement of the 7 transmembrane (TM) helices forming a cavity. (**B**) The extracellular loops (EL1-EL3). (**C**) The intracellular loops (CL1-CL3). Each TM (alpha-helix) is indicated in a different color. TM1, blue; TM2, red; TM3, dark gray; TM4, orange; TM5, yellow; TM6, purple; TM7, green.

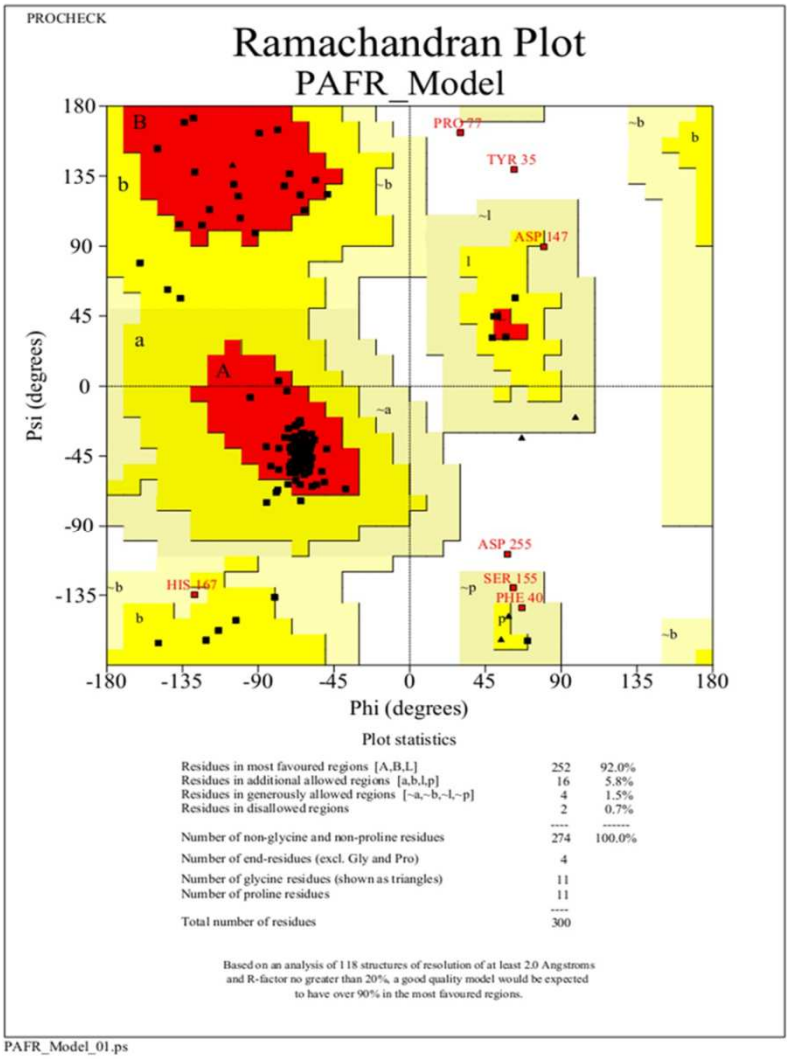

Figure S7. Main Ramachandran plot of the PAFR model. The main Ramachandran plot represents all amino acid residues by squares, whereas the glycine (Gly) residues are separately identified by black triangles, because these are not restricted to the regions in the generic Ramachandran plot. Red (A, B, and L) and dark yellow (a, b, l, and p) colors correspond to combinations of phi (Φ) and psi (Ψ) torsion angles of amino acid residues in the most favorable and additional allowed regions, respectively. In addition, pale yellow (~a, ~b, ~l, and ~p) and white colors represent less favorable and disallowed regions, respectively. The amino acid residues lying in those regions are highlighted in red.

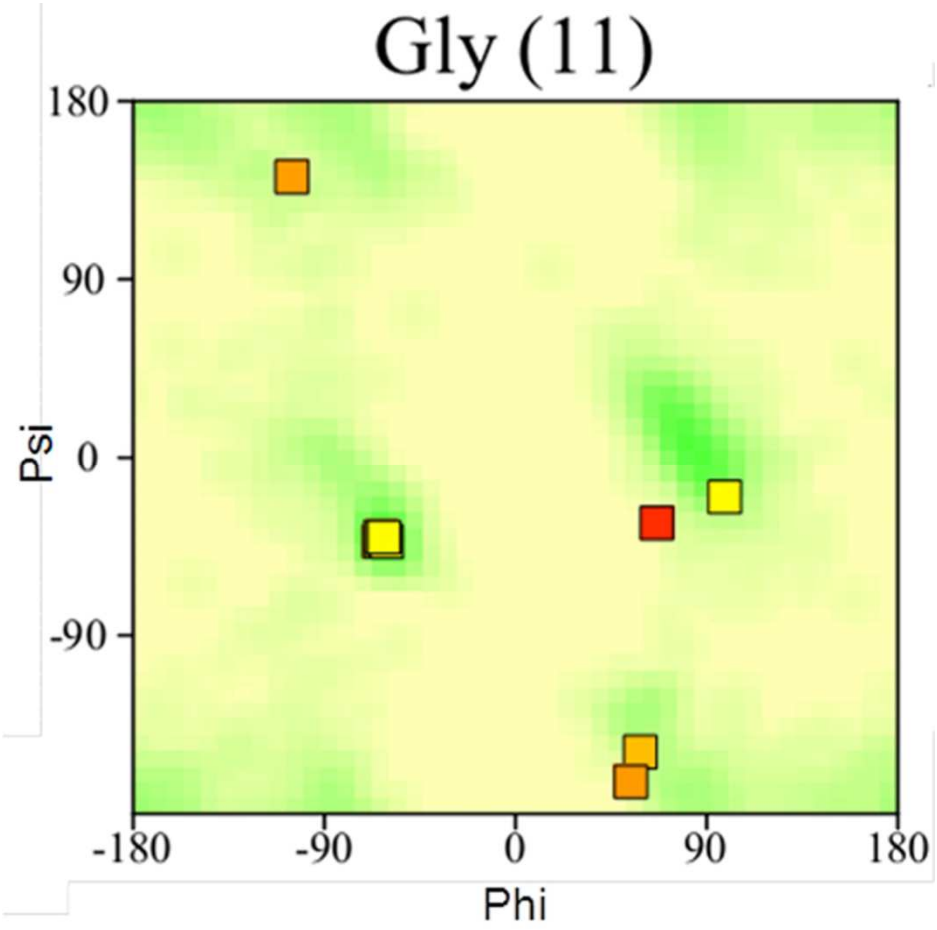

Figure S8. Ramachandran plot for Gly residues of the PAFR model. The second Ramachandran plot considers only Φ and ψ angles for Gly residues, where the number in parenthesis indicates the total number of these residues in the primary sequence of PAFR. The favorable combinations of these angles are represented by green areas and the values of standard deviations greater than 2.5 Å are labeled in red in the graph, describing combinations of disallowed angles. All Gly residues are in allowed regions, with favorable combinations of angles Φ and Ψ.

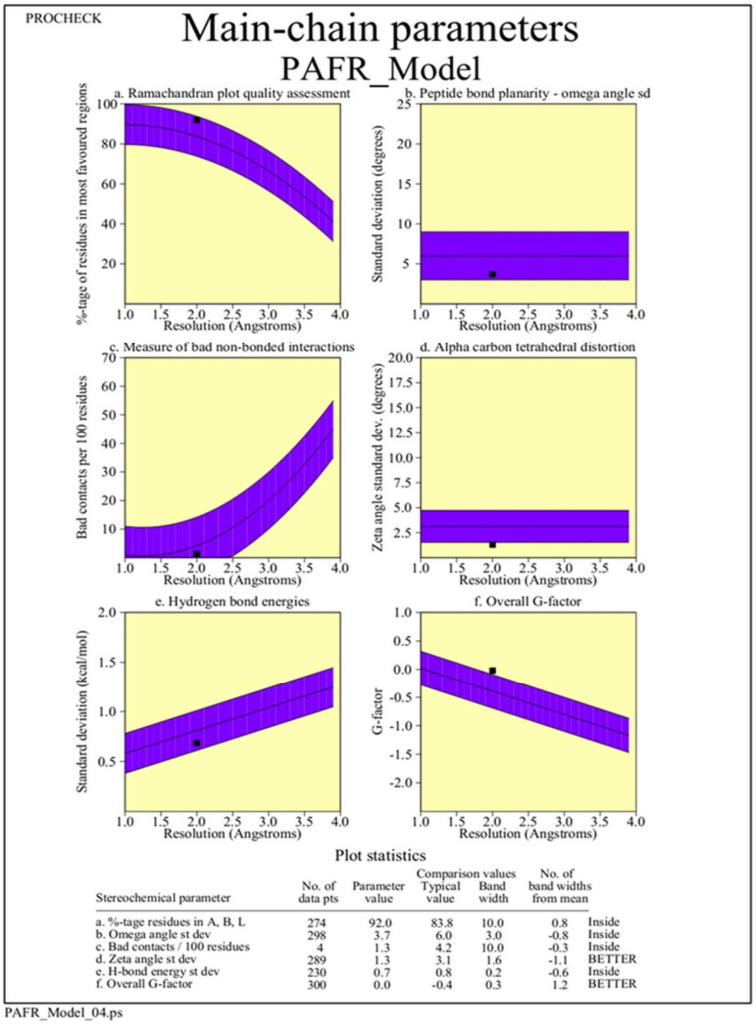

Figure S9. Analysis of the main-chain parameters of the PAFR model. The six graphs on the main chain parameters plot show how the PAFR model (represented by the black square) compares with a database of well-refined protein structures. The blue band in each graph represents the results from the well-refined protein structures; the central line is the least squares fitting to the mean trend as a function of resolution, whereas the width of the band on either side of it corresponds to a variation of one standard deviation from the mean. The six properties plotted are: (a) Ramachandran plot quality assessment; (b) peptide bond planarity; (c) number of bad contacts per 100 residues; (d) α-carbon tetrahedral distortion (this property is measured by calculating the standard deviation of the zeta torsion angle); (e) main chain hydrogen bond energy; and (f) overall G-factor (the overall value is obtained from an average of all the different G-factors for each residue in the protein structure). The G-factor provides a measure of how "normal", or alternatively how "unusual", a given stereochemical property is and, in PROCHECK, it is computed for the following properties: Φ-Ψ combination, chi1-chi2 (X_1-X_2; side chain torsion angles) combination, X_1 torsion for those residues that do not have a X_2, combined X_3 and X_4 torsion angles, omega torsion angles, main chain bond lengths, and main chain bond angles.

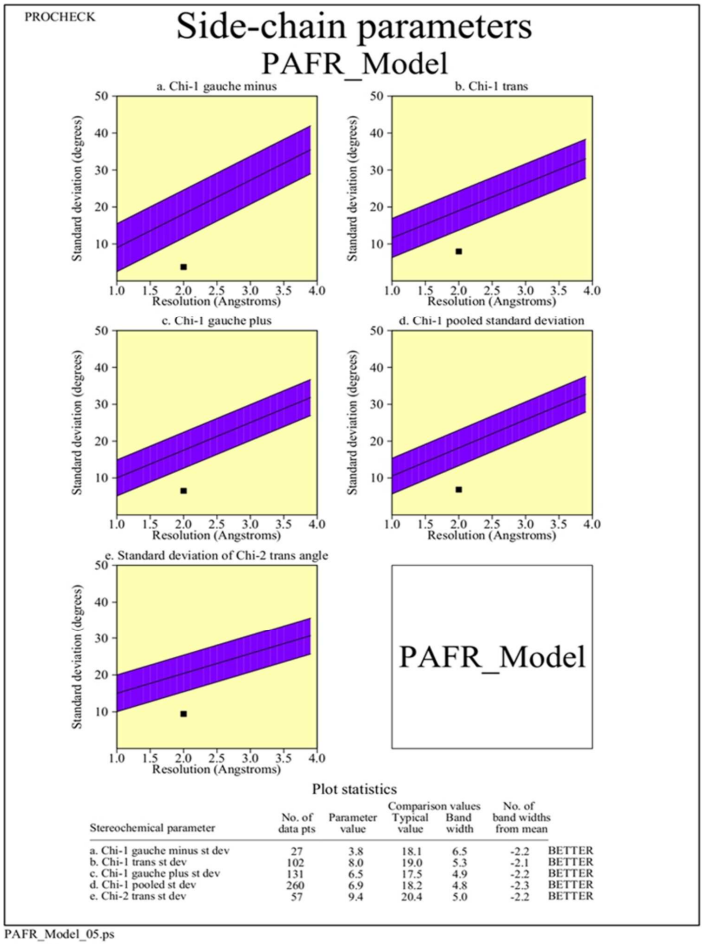

Figure S10. Analysis of the side-chain parameters of the PAFR model. In a similar way to the main-chain analysis, the side-chain analysis shows how the PAFR model (black square) compares with well-refined protein structures. This analysis evaluates five properties: (a) standard deviation values of the Chi-1 *gauche* minus torsion angles; (b) standard deviation values of the Chi-1 *trans*; (c) standard deviation values of the Chi-1 *gauche* plus; (d) pooled standard deviation of Chi-1 torsion angles; and (e) standard deviation values of the Chi-2 *trans* torsion angles.

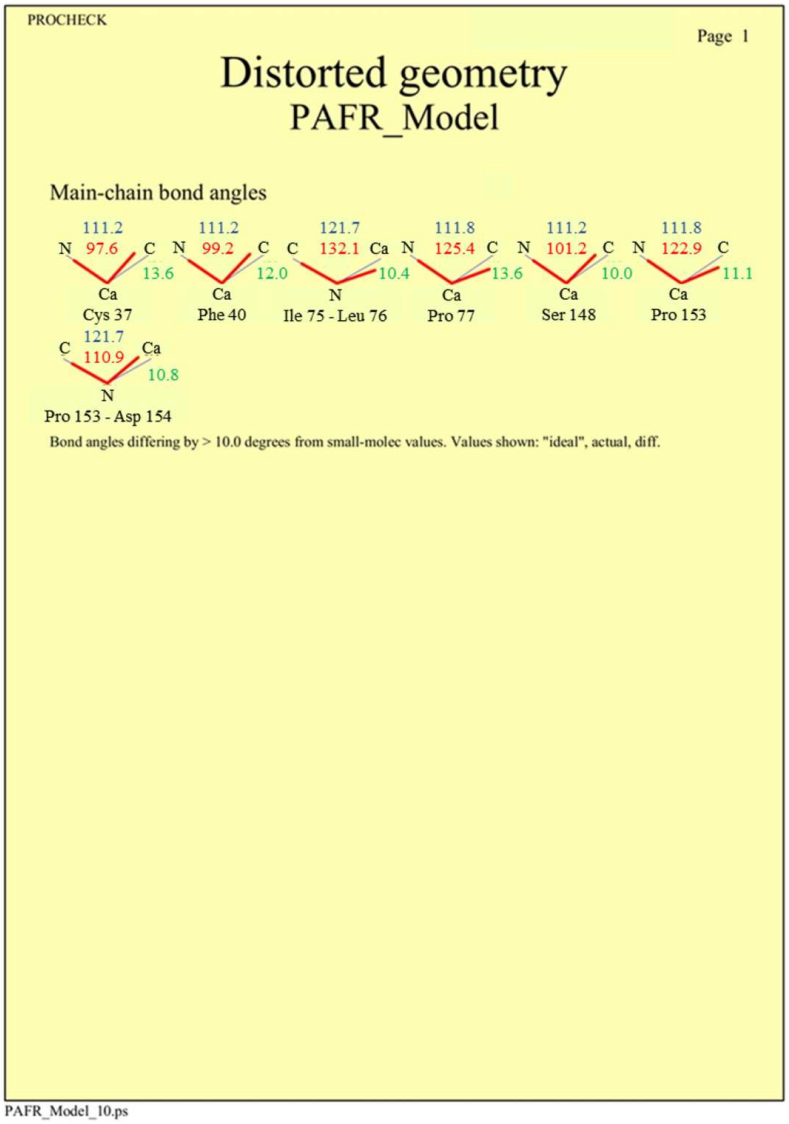

Figure S11. Analysis of geometrical distortions of the PAFR model. The parameters analyzed were: lengths and bond angles, including atoms of the main and side chains. This analysis shows the amino acid residues with distorted geometry, including their ideal values (in blue), those found in the model (in red), and the difference between these values (in green).

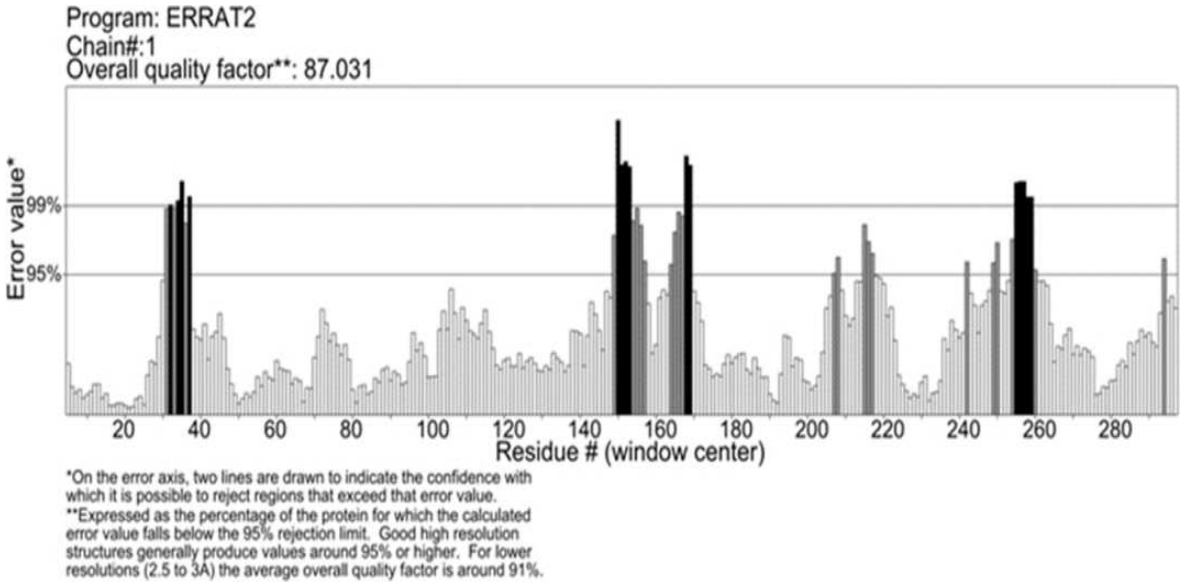

Figure S12. ERRAT analysis of the PAFR model. Errors in non-bonded atom-atom interactions of the PAFR model were verified by this analysis. The error values were plotted as a function of the position of a sliding residue in the window. An overall quality factor value of 87% was observed, thus validating the PAFR model.

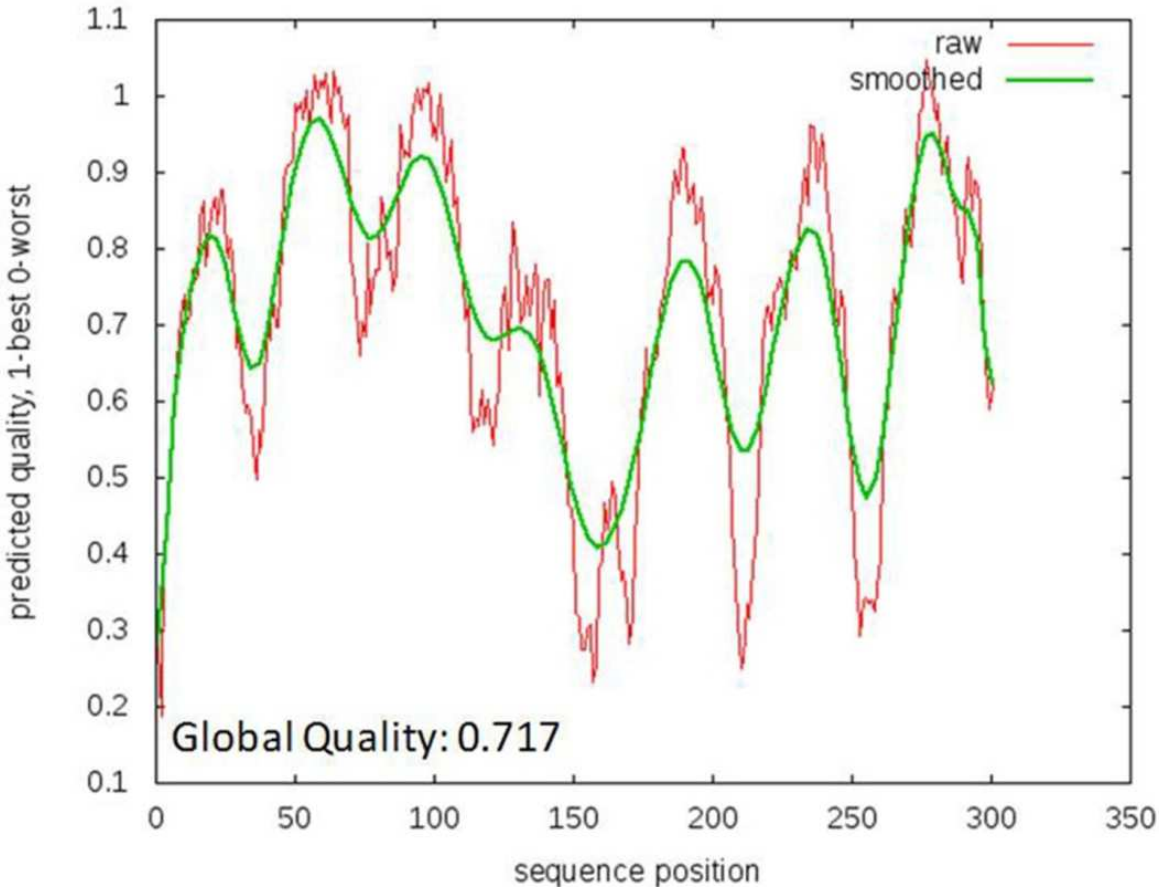

Figure S13. ProQM analysis of the PAFR model. A score was given to each residue of the protein model, which lead to a global quality factor of 0.717, which corroborates the other modelling analyses.

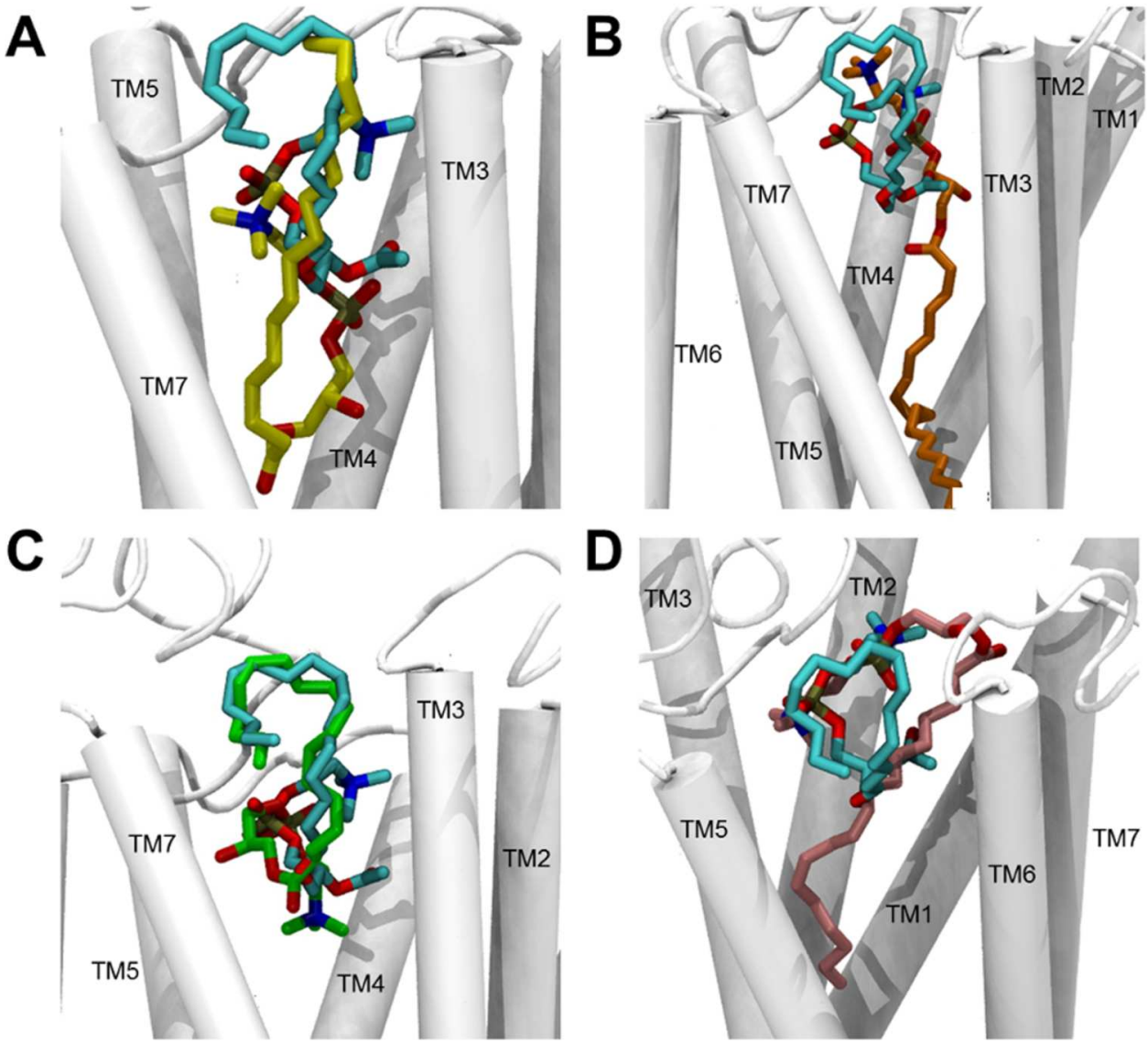

Figure S14. Comparison of binding modes of PAF and each LPC species to PAFR. (A) C16:0-PAF (cyan) and C16:0-LPC (yellow); (B) C16:0-PAF (cyan) and C18:0-LPC (orange); (C) C16:0-PAF (cyan) and C18:1-LPC (green); (D) C16:0-PAF (cyan), and C18:2-LPC (gray). Transmembrane (TM) regions are represented as white rods.

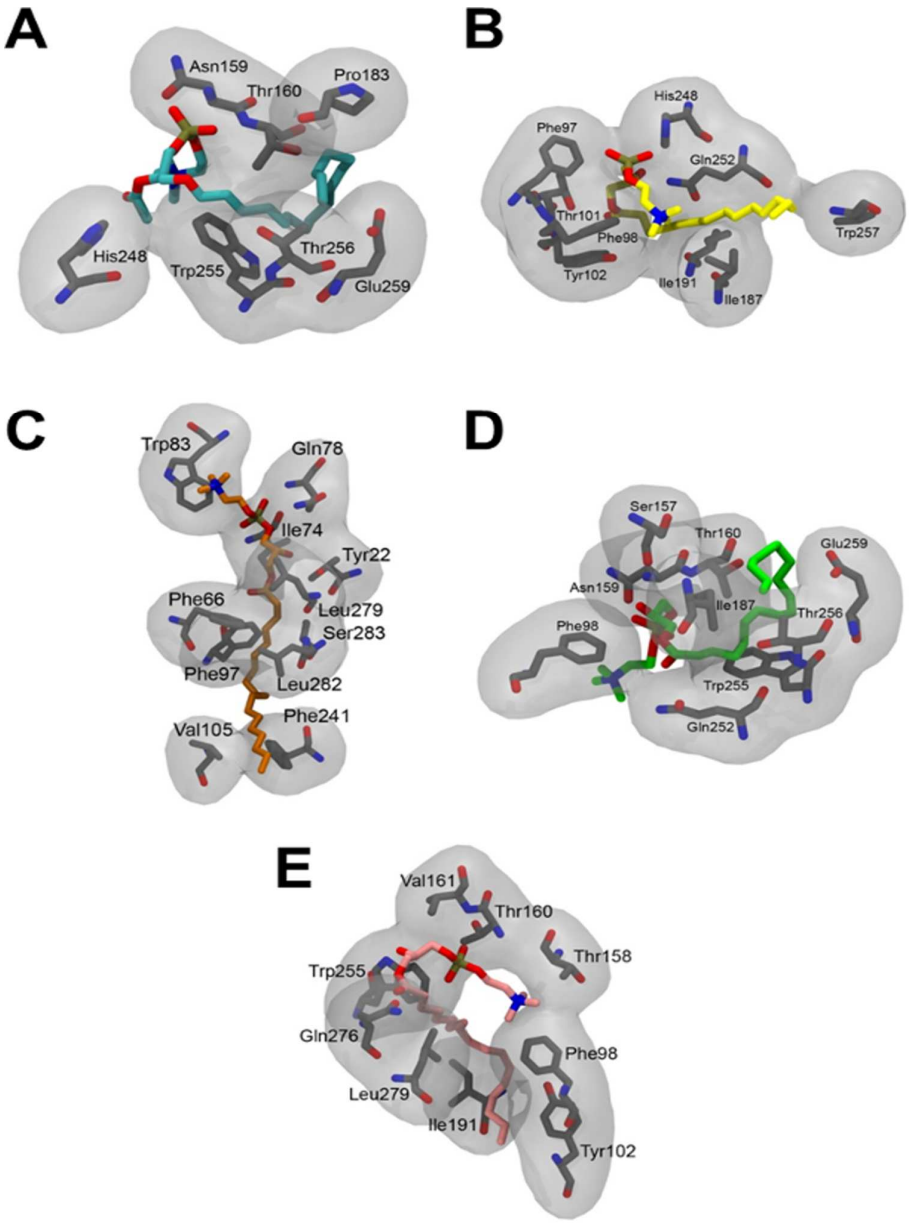

Figure S15. Unfavorable steric interactions of PAF and LPCs with PAFR. Heteroatoms are represented by different colors in structures: nitrogen atoms are shown in blue, oxygen in red, and carbon atoms of amino acids in gray. In ligands, carbon chains are represented by different colors: (A) C16:0-PAF, cyan; (B) C16:0-LPC, yellow; (C) C18:0-LPC, orange; (D) C18:1-LPC, green; and (E) C18:2-LPC, pink.

Table S1. Quantification of LPC species in extracellular vesicles (EVs) and EV-free supernatant of epimastigotes and metacyclic trypomastigote forms.

LPC species	Picomoles of LPC per 10^6 cells	LPC amount (mol^{-17}) per parasite [a, b]	Number of LPC molecules per parasite [c]
C18:2-LPC (*m/z* 526.4)			
ePellet [d]	**2.7**	0.36	2.16 x 10^6
eV2	**n/a** [e]	**n/a**	**n/a**
eV16	0.9	0.12	0.72 x 10^6
eVF	0.7	0.09	0.54 x 10^6
mPellet	0.6	0.08	0.48 x 10^6
mV2	0.8	0.11	0.66 x 10^6
mV16	**n/a**	**n/a**	**n/a**
mVF	**1.8**	0.24	1.44 x 10^6
C18:1-LPC (*m/z* 528.4)			
ePellet	**1.3**	0.18	1.08 x 10^6
eV2	**n/a**	**n/a**	**n/a**
eV16	1.0	0.14	0.81 x 10^6
eVF	0.7	0.09	0.52 x 10^6
mPellet	0.3	0.05	0.30 x 10^6
mV2	0.5	0.07	0.43 x 10^6
mV16	**n/a**	**n/a**	**n/a**
mVF	**1.9**	0.25	1.5 x 10^6

[a] The molar relative response factors (MRRF) of C10:0-LPC and LPC standards were used to calculate the amount of each LPC molecular species in Folch lower-phase fractions of *T. cruzi* .

[b] The number of parasites was determined before lipid extraction by counting live parasites in a hemocytometer. Values are means of three determinations. The standard deviation in all cases was <15%.

[c] Determined by multiplying the number of moles by the Avogadro's constant. D

[d] ePellet, Epi pellet; eV2, Epi-derived ectosomes; eV16, Epi-derived exosomes; eVF, Epi-derived EV-free supernatant or fraction; mPellet, Meta pellet; mV2, Meta-derived ectosomes; mV16, Meta-derived exosomes; mVF, Meta-derived EV-free supernatant or fraction.

[e] Not analyzed due to absence or trace amounts of the compound.

Permission to reproduce copyrighted material – PLOS Neglected Tropical Diseases

Re: RE: PLOS NTDs - Request for permission to reproduce copyrighted materials in PhD dissertation [ref:_00DU0Ifis._500U0JQMoD:ref]
PLOS Neglected Tropical Diseases [plosntds@plos.org]
You replied on 4/20/2015 10:44 AM.
Sent: Monday, April 20, 2015 10:11 AM
To: hotez@bcm.edu; Lopes, Felipe G

Hi Felipe,

Yes, Dr. Hotez is correct. You are free to republish any of our content as long as your properly cite the original article and authors. For more information please see our CC-BY license here: https://www.plos.org/open-access/license/

Please let me know if you have any other questions.

Best,
Alicia

PLOS - OPEN FOR DISCOVERY
Alicia Zuniga | Publications Assistant
PLOS Pathogens and PLOS Neglected Tropical Diseases
1160 Battery Street, Suite 100, San Francisco, CA 94111
Main +1 415-624-1200 | Fax +1 415-546-4090
plos.org

Case Number: 03902467
ref:_00DU0Ifis._500U0JQMoD:ref

---------- Original Message ----------
From: Hotez, Peter Jay [hotez@bcm.edu]
Sent: 4/17/2015
To: plosntds@plos.org;
fglopes@miners.utep.edu
Subject: RE: PLOS Neglected Tropical Diseases - Request for permission to reproduce copyrighted materials in PhD dissertation

Thanks Felipe, as far as I can tell, it's open access through creative common license and you can repurpose it as you wish - of course with attribution. But I am cc'ing PLOSNTDs to confirm, good luck! Peter

Peter Hotez, MD, PhD, FASTMH, FAAP
Dean, National School of Tropical Medicine
Professor, Pediatrics and Molecular Virology & Microbiology
Head, Section of Pediatric Tropical Medicine
Baylor College of Medicine

Texas Children's Hospital Endowed Chair of Tropical Pediatrics
Director, Sabin Vaccine Institute Texas Children's Hospital Center for Vaccine Development

President, Sabin Vaccine Institute

Baker Institute Fellow in Disease and Poverty, Rice University

University Professor, Baylor University

Co-Editor-in-Chief, PLoS Neglected Tropical Diseases

Chair, Technical Advisory Board, END Fund

E-mail: hotez@bcm.edu
Twitter: PeterHotez

Vernesta M. Jackson, Executive Assistant
Phone: 713-798-1199
Email: vernesta.jackson@bcm.edu

-----Original Message-----
From: Lopes, Felipe G [mailto:fglopes@miners.utep.edu]
Sent: Friday, April 17, 2015 5:09 PM
To: Hotez, Peter Jay
Subject: PLOS Neglected Tropical Diseases - Request for permission to reproduce copyrighted materials in PhD dissertation

Dear Dr. Hotez,

My name is Felipe Gazos-Lopes, and I'm the first author of the manuscript entitled "Structural and functional analysis of a platelet-activating lysophosphatidylcholine of Trypanosoma cruzi.", which was published on the journal "PLoS Neglected Tropical Diseases" - 2014 Aug 7;8(8):e3077. doi: 10.1371/journal.pntd.0003077. eCollection 2014.

I'm a graduate student at the University of Texas at El Paso (UTEP), and would like to ask for your permission to add this paper in full as a chapter of my dissertation (entitled "EXPRESSION AND FUNCTIONAL ANALYSIS OF LIPIDS AND GLYCOLIPIDS FROM THE MAMMAL-DWELLING STAGES OF TRYPANOSOMA CRUZI").

Thank you very much for your time,

Sincerely,

Felipe

VITA

Felipe Gazos Lopes was born in Boston, Massachusetts. The son of Ulisses Gazos Lopes and Angela Hampshire Carvalho Santos, he graduated from Escola Parque High School, Rio de Janeiro, Rio de Janeiro, Brazil, in 2002. He entered the Federal University of Rio de Janeiro in 2003, where he pursued a bachelor's degree in Biology. He joined Mario Alberto Cardoso da Silva Neto's lab in the fall of 2004, who mentored him throughout his undergraduate years. In 2009 he acquired a Master's of Science degree in Biological Chemistry at the Medical Biochemistry Institute, Federal University of Rio de Janeiro, Rio de Janeiro, Rio de Janeiro, Brazil. In the fall of 2009, he moved to El Paso, Texas, in order to pursue his Ph.D. in Biological Sciences at The University of Texas at El Paso.

Permanent address: 535 South Mesa Hills Drive,
apt# 116
El Paso, Texas 79968
fglopes@miners.utep.edu

This thesis/dissertation was typed by Felipe Gazos Lopes